Surveys in Geophysics
https://doi.org/10.1007/s10712-025-09891-x

Recent Results on Science and Innovation Related to Electrical Processes of Thunderstorms

Christoph Köhn[1] · Torsten Neubert[1] · Martin Füllekrug[2] · Ute Ebert[3,4] · Sander Nijdam[4] · Olivier Chanrion[1] · Nikolai Østgaard[5] · Martino Marisaldi[5] · Serge Soula[6] · Joan Montanyà[7] · Francisco Gordillo-Vázquez[8] · Alejandro Luque[8] · Jannis Teunissen[3] · Joachim Holbøll[9] · Alec Bennett[10] · Paul Smith[10] · Victor Lorenzo[11] · Hugh J. Christian[12] · Søren F. Madsen[13] · Diana Mihailova[14] · Jean-François Boissin[15] · Stéphane Pedeboy[16] · Laure Chaumat[17] · Matthias Heumesser[1] · Krystallia Dimitriadou[1,18] · Carolina Maiorana[5] · Simon Ghilain[2] · Zaida Gomez Kuri[6] · Adam Peverell[2] · Michele Urbani[7,11] · Thi Ny Kieu[8,20] · Andy Martinez[3] · Hani Francisco[3] · Mojtaba Niknezhad[1] · Miguel B. Teixeira-Gomes[8] · Andrea Pizzuti[2,10] · Marcelo Arcanjo[11] · Shahriar Mirpour[4] · Xue Bai[2] · Victor Reglero[19]

Received: 18 July 2024 / Accepted: 10 May 2025

Abstract
Lightning is a highly energetic electric discharge process in our atmosphere, evolving in several complex stages. Lightning is recognized as an essential climate variable, as it affects the concentration of greenhouse gases. It also threatens electrical and electronic devices, in particular, on elevated structures like wind turbines, and it endangers aircraft built with modern composite materials with inherently low electric conductivity. During the past decades, our fundamental understanding of atmospheric electricity has continued to evolve. For example, during the past 30 years, discharge processes were discovered in the atmosphere above thunderstorms, the so-called transient luminous events (TLEs) in the stratosphere and mesosphere, and terrestrial gamma-ray flashes (TGFs), accompanied with beams of photons, electrons and positrons, were observed from low orbiting satellites passing over thunderstorms. Lightning-like discharges also appear in plasma and high-voltage technology. The SAINT network was formed to bring the different research fields together. SAINT was the "Science And INnovation of Thunderstorms" Marie Skłodowska-Curie Innovative Training Network of the European Union Horizon 2020 program. From 2017 to 2021, 15 PhD students observed lightning processes from satellites and ground, developed models and conducted laboratory experiments. The project bridged between geophysical research, plasma technology and relevant industries. The paper presents a summary of the findings of the SAINT network collaboration.

Keywords SAINT · Lightning · Streamers · Leaders · Terrestrial gamma-ray flashes · Transient luminous events · Laboratory experiments

Extended author information available on the last page of the article

Article Highlights

- The SAINT network's interdisciplinary approach bridged geophysical research,plasma technology, and industry applications
- The SAINT network advanced our understanding of lightning, TLEs, and TGFsthrough ground, space observations and modelling
- Simulations and experiments elucidated streamer dynamics, plasma chemistry, dischargeinception and the emission of TGFs from the streamer-leader system inthunderclouds
- The analysis of TGFs and TLEs provided information on the properties and origin of TGFs, high-latitude TGFs as well as new results on TLEs such as associated chemistry

1 The Importance of Electrical Discharges and Motivation of Research

The atmospheric electric discharge is a fundamental process in nature that converts electric energy into ionization, radiation, chemical products and heat. Lightning is known to produce greenhouse gases like ozone O_3 (Gordillo-Vázquez and Pérez-Invernón 2021) that significantly influence the Earth's radiation balance; lightning poses a threat to lives and to our increasingly vulnerable infrastructure based on sensitive microelectronics and on advanced materials and technology where discharges can have catastrophic effects. Electric discharges are also developed and used in many branches of technology. Although studied since the time of Jaques de Romas and Benjamin Franklin (Franklin 1752) in the 18th century, much of lightning physics escapes quantification. A proof of point is the discovery that lightning can trigger electrical activity starting from the lower edge of the night time ionosphere at ∼ 80–95 km altitude (Neubert 2003), and can emit gamma-radiation (Fishman et al. 1994), antimatter and energetic hadrons (Briggs et al. 2011; Köhn and Ebert 2015; Köhn et al. 2017).

1.1 Transient Luminous Events and Terrestrial Gamma-Ray Flashes

Transient Luminous Events, first reported by Vaughan and Vonnegut (1989) as well as by Franz et al. (1990), include electrical discharges in the stratosphere (blue jets) and mesosphere (sprites) and discharges reaching from cloud tops up to the night time ionosphere (gigantic jets), as well as elves and halos in the ionospheric E layer (see Fig. 1) (Füllekrug et al. 2006) (Neubert 2003). TLEs create conductivity changes in the lower ionosphere affecting radio wave propagation, and they perturb the ozone and NO_x densities in the stratosphere and mesosphere(Gordillo-Vázquez and Pérez-Invernón 2021).

Terrestrial Gamma-ray Flashes, first reported in 1994 (Fishman et al. 1994) are bursts of hard X- and gamma-rays from thunderstorms, sometimes associated with antimatter (positrons) and neutron beams (Shah et al. 1985; Babich 2007; Dwyer et al. 2008; Chilingarian et al. 2010; Briggs et al. 2011; Köhn and Ebert 2015; Köhn et al. 2017). Energetic radiation from thunderstorms and (lightning) leaders is observed by satellite missions, from the ground, on airplanes, and from long sparks in laboratory experiments.

TLEs and TGFs are quite common and have been observed over all major thunderstorm regions of the Earth, including Europe. For TGFs, it has been debated whether the lower electric fields of km extension inside thunderclouds or the higher fields at the lightning leader tips cause the electron acceleration to relativistic energies (Dwyer et al.

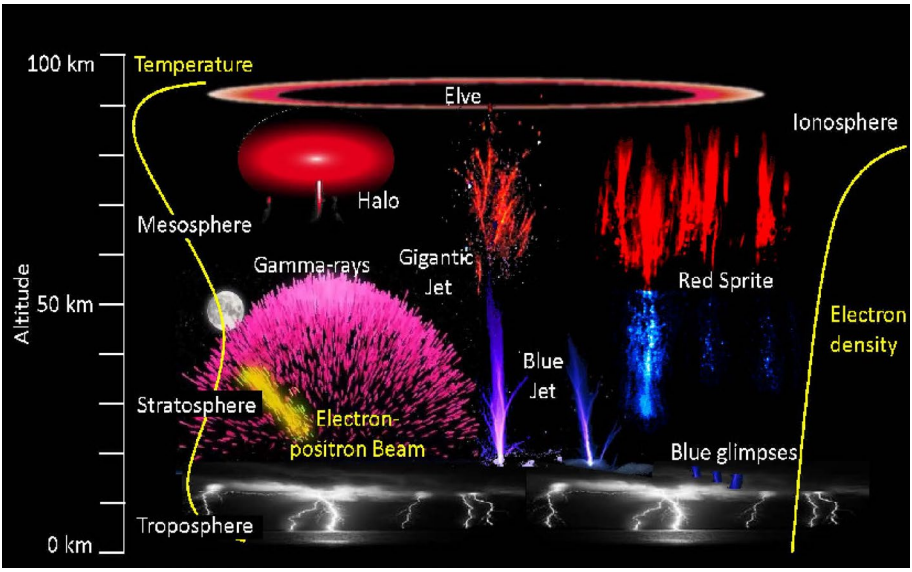

Fig. 1 An overview of the science of the SAINT project: It addresses various aspects of atmospheric electric discharges through ground observations (Sect. 2), space observations (Sect. 3), modelling (Sect. 4) and laboratory experiments (Sect. 5); figure adapted from (Neubert et al. 2019) in agreement with the CC BY 4.0 licence (`https://creativecommons.org/licenses/by/4.0/`)

2012). It was not completely known, either, whether cosmic rays play a role in seeding the runaway electron avalanches that generate the high-energy radiation, and part of the SAINT network was dedicated to deciphering the production mechanisms of TGFs through concurrent observations and simulations.

For lightning, there were mostly macroscopic engineering models for leaders and return strokes that did not incorporate features observed now with fast movie or ICCD cameras at temporal scales of nanoseconds to microseconds. But the development of microphysics-based models of the different spatial and temporal stages of lightning initiation, and streamer and leader development was making progress. The dynamic structures within lightning discharges, in particular, the streamer discharges, are similar to those in TLEs, allowing for a parallel model development, but they develop in higher air density and hence on shorter time and length scales. The top of sprites at about 80 km has an air density is about 5 orders of magnitude smaller than at sea level, and due to scaling relations (Ebert et al. 2010) the spatial and temporal scales are 5 orders of magnitude larger and thus within reach of affordable instrumentation.

Lightning observations from space and ground differ due to perspective and atmospheric absorption. The combination of multiple detectors in space and on ground allowed us to study lightning initiation and bipolar intra-cloud discharges, and to pinpoint the process generating TGFs. The discovery of energetic run-away electrons required an extension of discharge physics, and TLEs and TGFs provide a unique opportunity to study fundamental aspects of discharges in the natural laboratory of the troposphere, stratosphere and mesosphere. In addition to studying the physics of TGFs, SAINT was designed to study TLEs, both through satellite and ground observations, and thus tell us more about the origin and underlying physics of TLEs.

1.2 The Concentration and Distribution of Greenhouse Gases in the Atmosphere are Affected by Thunderstorms

Lightning is an important source of NO_x, which plays a key role for the production of the greenhouse gas ozone and thus for the climate (Schumann and Huntrieser 2007). Hence, understanding NO_x production by lightning allows understanding the possible feedback between climate change and thunderstorms (Romps et al. 2014). However, despite many attempts, including aircraft campaigns such as EULINOX and TROCCINOX (Huntrieser et al. 2002, 2007), large uncertainties remain in the quantification of lightning produced NO_x (LNO_x) because of the complexity of observations and modelling (Schumann and Huntrieser 2007; Banerjee et al. 2014; Murray 2016; Gordillo-Vázquez et al. 2019; Pérez-Invernón et al. 2022, 2023). Aircraft campaigns cannot provide continuous monitoring of LNO_x and are difficult to carry out in some regions. Nadir-viewing satellite instruments such as the Ozone Monitoring Instrument (OMI), the SCanning Imaging Absorption spectroMeter for Atmospheric CHartographY (SCIAMACHY) and the TROPOspheric Monitoring Instrument (TROPOMI) measure spectra that are employed to estimate column densities of NO_2 over thunderstorms (Ialongo et al. 2020). Several authors used OMI NO_2 measurements to estimate the LNO_x Production Efficieny (PE) in a case-based approach or systematically over different regions (Beirle et al. 2010; Marais et al. 2018), including mid-latitude regions (Bucsela et al. 2019), tropical regions (Allen et al. 2019) and the US (e.g., (Pickering et al. 2016; Lapierre et al. 2020; Zhang et al. 2020)). Satellite based measurements can help us to estimate LNO_x amounts over regions where aircraft campaigns are rare, or to systematically investigate possible relationships between the characteristics of thunderstorms and LNO_x over different geographical regions (Bucsela et al. 2019). However, the opacity of thunderclouds can strongly affect the retrieval of NO_2 (Beirle et al. 2010), while convection can transport NO_x released at the surface to the upper troposphere, where it is mixed with freshly produced LNO_x. Therefore, the use of atmospheric and radiative models in combination with NO_2 measurements is needed to estimate the NO_x production efficiency (Pérez-Invernón et al. 2022). In addition, thunderstorms entrain surface air, including water vapour, pollutants and dust particles, transporting them to the upper troposphere. There, they have longer residence times and may spread over intercontinental distances transported by the strong winds in this region. Subsequent chemical transformation might perturb the ozone concentrations and formation of aerosols affecting global climate and acid rain (Bertram et al. 2007; Jaeglé 2007). Besides ozone, water vapour is an important greenhouse gas with a large effect on climate (Solomon et al. 2010). Convectively injected into the stratosphere by thunderstorms, it increases ozone loss and UV dosage and entrains ozone-rich stratospheric air into the troposphere (a transport pathway for ozone missing in major global models) (Pan et al. 2014). The location and character of deep convection produced by global cloud models is used to infer where lightning occurs and to parameterize the greenhouse chemicals produced by lightning at those locations for distribution throughout the atmosphere (Price 2013).

A better understanding of the greenhouse gases produced by lightning will improve estimates of the effect of lightning on atmospheric chemistry in global models, which will improve forecasts of long-term changes in global atmospheric temperature and associated impacts. A prerequisite for improving estimates of the effect of lightning is to understand on a microscopic level the sub-processes of lightning that are responsible of producing the gases. Here SAINT contributed through the measurement of chemical species in electric discharges improving our understanding of discharge induced chemistry.

1.3 Lightning Protection

Lightning protection requires a new approach for exposed, complex systems such as aircraft and wind turbines, because of their size, materials, and structural complexity, their operation and location and their critical electronic systems. For example, wind turbines are now so tall that they generate upward lightning from the nacelle (housing that contains the equipment for electricity production) and/or blades to thunderstorm clouds (Montanyá et al. 2014; Sarajcev et al. 2021; Zalhaf et al. 2022). The simplified approach to upward flashes by the International Electrotechnical Commission might result in a significant underestimation of the actual number of lightning impacts. In addition, the presence of carbon-reinforced plastics (CRPs) in the blades introduces new challenges to be considered during the coordination of the blade design with the lightning protection system, for example mechanical stress resulting from the dissipation of energy caused by lightning currents in CRPs laminates. Carbon fibre composite materials are now common within the aviation industry, including cabins for the latest generation of aircraft. Their electric conductivity is generally smaller and more anisotropic than in metals, but lightning safety must remain at the same level as for fully metallic aircraft, creating new challenges for aircraft construction and subsequent testing (Mazur et al. 1984; Morgan et al. 2012).

A better understanding of lightning interactions with structures will improve the robustness of critical technologies, saving operational costs and maintaining their competitive edge in world markets. Lightning protection is fairly well understood in many applications. However, the examples above drive a need to improve current technological systems. This requires an understanding of the plasma kinetics and improved techniques for the detection of lightning initiation, development and impact which was addressed through SAINT by experiments and measurements of discharge inception as well as of lightning interaction and associated modelling.

1.4 Lightning Detection

Lightning detection systems on the ground rely on the electromagnetic (EM) radiation emitted by lightning where a group of sensors measures the waveform and a common predefined signature identifies a lightning event. Operational grade networks give the time, location, peak current and the multiplicity of strokes (Cummins and Murphy 2009). Recent advances in network techniques include denser networks with ~ 25 km baselines that measure the full lightning discharge in 3 dimensions, including intracloud lightning (Rison et al. 1999; Betz et al. 2009), and networks with long distances (~1000 km) between sensors measure global lightning activity, notably also over oceans and in less-industrialized countries without their own national networks (Abarca et al. 2010), though biased towards cloud-to-ground lightning (Holle et al. 2014) and narrow bipolar events (Liu et al. 2024), thus not allowing for a sufficient detection of total global lightning. For all networks, considerable effort goes into the determination of their sensitivities. Note that there also exist community lightning detection networks such as Blitzortung (`www.blitzortung.org`).

A technique was also developed that detects lightning optically from satellites (Christian et al. 2003). The vantage point of space gives a high detection efficiency for intracloud lightning and also captures most lightning propagating towards ground (see e.g. (Christian et al. 2003)). Optical detectors are already operative for the next generation geostationary

meteorological satellites of EUMETSAT (Rodriguez et al. 2009; Alpers et al. 2017) and NOAA (Chen et al. 2020), building on the technology of the Lightning Imaging Sensor (LIS) on the International Space Station (ISS) (Blakeslee et al. 2020). It is therefore of considerable interest to characterize the strong and weak points of lightning detection systems from ground and space (Finke 1999) and to study the potential which lies in their combination. It is also of interest to push the boundaries of current scientific knowledge further to identify underlying micro-processes of lightning and their signatures in sensitive detection systems.

A better understanding of the signatures of lightning processes in new lightning detection systems was necessary to improve the global and regional monitoring of storms and the predictions of their development where SAINT contributed through the analysis of lightning data obtained from ground and space as well as the development of new detection techniques. This will give global measurements on long timescales necessary for climate studies, and will deliver new knowledge of micro-processes (e.g. streamer processes in thunderstorms or the production of climate relevant chemicals). To harvest their full potential requires understanding the processes at a plasma kinetic level coupled with comparative studies of the new techniques (Fehr et al. 2005) (Bürgesser 2017).

1.5 Discharges in Plasma Technology and in High-Voltage Engineering

The conversion of electric energy into chemical reactants within a discharge is widely used in spark plugs of car engines and in ozone generators for disinfection (Pavlovich et al. 2013, 2014). Very actively investigated topics include plasma medicine, plasma assisted ignition and combustion (Starikovskaia 2006), plasma processing of materials and surfaces (Boulos 1991; Graves 1994; Kersten et al. 2001) and plasma assisted conversion of electric power into liquid fuel (Vadikkeettil et al. 2022; Ray et al. 2023; Sarafraz et al. 2023). In high voltage technology, corona discharges dominate energy losses along high-voltage electricity lines and they are detrimental when short-circuiting insulating layers. They are also the key ingredient in electrical circuit breakers in our electricity nets where important questions these days are how to replace the highly insulating SF_6 gas by a less polluting medium (Stoller et al. 2013) and how to design circuit breakers for possible future DC electricity nets.

A deeper understanding of the physics and chemistry of lightning processes is directly applicable to the areas of plasma technology and high-voltage engineering. Making progress requires advanced diagnostics of natural lightning and of laboratory experiments to develop new models of streamer coronas, lightning leaders and the subsequent increase of conductivity and temperature within a lightning return stroke. Better theoretical models will apply to both geophysical and engineering problems. Specifically, SAINT contributed to developing new detectors for lightning detection and models allowed to analyse the impact of wind on discharge evolution.

1.6 Numerical Models and Laboratory Experiments on Atmosphere Discharges

Electric discharges are difficult to model and to understand because they are nonlinear, far from equilibrium, and they extend over many scales in space, time and energy. Therefore, large-scale lightning phenomena are mostly approximated with macroscopic engineering models (Cooray 2003; Koshak et al. 2014), where a microphysical derivation is replaced by parametrizations. For example, for lightning propagation and strike zones on structures

such as aircraft, commonly a simple electrostatic model was adopted for an approaching leader and the evolution of the subsequent electric potential (Lalande et al. 1999). But in the past decade, physical models starting from the microscopic collisions of electrons with air molecules have progressed rapidly; they can now resolve the formation, propagation, branching and interaction of streamer discharges quantitatively in three dimensions on adaptive computational grids (Teunissen and Ebert 2018, 2017). Such models are also applicable to TLEs with their lower air densities, larger time and length scales due to their approximate scaling with density. They form the basis for modeling the high particle energies in TGFs (Liu and Pasko 2004; Li et al. 2009; Luque and Ebert 2009; Chanrion and Neubert 2010; Köhn et al. 2019; Malagón-Romero et al. 2020; Köhn et al. 2020), too.

Laboratory experiments on streamers and leaders benefited from developments in diagnostics and processing. Fast (ICCD) cameras, high-resolution spectrometers and fast oscilloscopes, combined with modern data acquisition, provide novel access to the numerous time and length scales of a discharge (Nijdam et al. 2010). Laser spectroscopy can resolve detailed spatial and temporal information on the density distribution and kinetics of a plethora of chemical species in a discharge (Ono and Oda 2008; Carbone and Nijdam 2015). The production of such chemical species is studied by techniques like Fourier transform infrared spectroscopy (FTIR) and mass spectrometry.

To improve our understanding of the multiscale processes involved in atmospheric electric discharges, SAINT coordinated studies using the newest observational instrumentation, numerical techniques and laboratory experiments. This novel approach promises better exploitation of lightning data, new advances in lightning protection strategies, and the development of new and improved models of discharge processes for technological applications.

1.7 The SAINT Network

In order to address the variety of aforementioned discharge phenomena, ranging from microscopic discharges, leaders towards the long-ranging TLEs and high-energy TGFs, the European Commission (EC) funded the Horizon 2020 Marie Skłodowska-Curie Innovative Training Network SAINT ("Science And INnovation with Thunderstorms") during the years 2017 to 2021. In the SAINT project, research groups from atmospheric science, space science and earth observation, electric discharge physics, instrumentation and scientific computing joined forces to address the scientific research objectives and technological research objectives summarized in Table 1. A high degree of multidisciplinarity and the inclusion of key industrial stakeholders made this network especially suitable for a training program in a broad spectrum of research fields including meteorology, physics, chemistry, engineering and scientific computing. It included ten academic institutions (Technical University of Denmark, University of Bath, Polytechnic University of Catalonia, University in Bergen, University of Paul Sabatier Toulouse III, Technical University of Eindhoven, Center for Mathematics and Computer Science, Institute for Astrophysics in Andalusia, Biral and DENA) and 9 industrial partners (NASA Marshall Space Flight Center, Global Lightning Protection, NOWCAST GmbH, Plasma Matters, Airbus, Météorage, Thales Services SAS, The University of Alabama in Huntsville, University of Granada) and funding for 15 PhD students who were trained to become the next generation of scientists for academia and industry. Besides engaging in the various aspects of electric discharges, the network organized various summer and winter schools to facilitate the dialog between researchers and provide directed training

Table 1 Overview SAINT's scientific research objectives (RO1–3) and technological research objectives (RO4–6)

RO1	*High-energy (0.2–40 MeV) radiation from atmospheric electric discharges:* to identify the generation mechanism(s) of TGFs; to characterize their spectral fluency distributions and their global occurrence rates
RO2	*Lightning propagation and the leader-streamer interaction:* to understand the interaction/transition between streamers and leaders in lightning propagation; to understand the effect of high-energy processes on lightning propagation; to develop computational models that couple their micro-scale kinetic physics to macro-scale manifestations
RO3	*Electric properties of thunderstorms:* to characterize the sub-processes of cloud discharges with unprecedented detail from measurements by a suite of novel sensors in space and on ground to develop and validate models of the physical processes
RO4	*Design of new tools for quantification of the chemistry of discharges:* to engineer instruments and models that enable improved characterization of the chemical reaction paths in atmospheric discharges for use in industrial applications (e.g. gas purification and ozone generation) and for quantification of the production of greenhouse gas constituents by lightning
RO5	*Design of new lightning detection approaches:* to engineer algorithms that enhance the data products from lightning detection systems in space (MTG) and on the ground
RO6	*Design of new lightning protection/mitigation strategies:* to engineer numerical models and instruments toward new designs of lightning mitigation systems for wind turbines and aircraft

to the PhD students. Schools were held in Denmark, the Netherlands, France and Spain. Except for the first school (one week only), schools consisted of two weeks whereof the first mainly consisted of a series of lectures on a topical theme (e.g. simulations or observations). The second week was organized more in a conference-like manner with presentations from students and senior staff to inform the whole network about the progress of the individual projects. Additionally, splinter as well as poster sessions were included to discuss scientific content and foster collaborations between the PhD students. All students had secondments, both in industry and with academic partners; since some of the SAINT students performed their secondments simultaneously at the same sites, this strengthened the collaboration amongst students. The PhD students, summarized in Table 2, (i) developed new scientific knowledge and insights into the physics of atmospheric discharges, (ii) developed new research models or techniques, and (iii) applied insights, models or techniques within relevant industries and agencies. The execution of the SAINT network went rather smoothly, and there were no significant obstacles. One must not forget, though, that SAINT was a doctoral training network. Hence, as aforementioned, there was a large focus on the training part, allowing less time for research as it might be the case when receiving funding from e.g. national agencies. Similarly, collaboration and secondments in industry are an essential requirement for such training programmes in order to prepare students for the labour market in Europe. This is certainly a good initiative from the European Research Council; however, also here one must not forget that the time spent at an industrial secondment lowers the time for academic research.

SAINT consisted of four different science work packages approaching open questions in atmospheric electricity through ground observations (Sect. 2), satellite observations (Sect. 3), modelling (Sect. 4) and experiments (Sect. 5). The four sections 2–5 are summarizing the results of the SAINT activities and describing the work performed in the four work packages. An overview of the SAINT publications can be found on `https://www.saint-h2020.eu/publications`.

Table 2 Overview of the PhD students of the SAINT network, together with their academic home institution

Name	Academic home institution
Matthias Heumesser	Technical University of Denmark, DK
Krystallia Dimitriadou	Technical University of Denmark, DK
Carolina Maiorana	University in Bergen, NO
Simon Ghilain	University of Bath, UK
Zaida Gomez Kuri	University of Paul Sabatier Toulouse III, F
Adam Peverell	University of Bath, UK
Michele Urbani	Polytechnic University of Catalonia, ES
Thi Ny Kieu	Institute for Astrophysics in Andalusia, ES
Andy Martinez	Centrum Wiskunde & Informatica (CWI), Amsterdam, NL
Hani Francisco	Centrum Wiskunde & Informatica (CWI), Amsterdam, NL
Mojtaba Niknezhad	Technical University of Denmark, DK
Miguel B. Teixeira-Gomes	Institute for Astrophysics in Andalusia, ES
Andrea Pizzuti	Biral, UK
Marcelo Arcanjo	DENA, ES
Shahriar Mirpour	Technical University of Eindhoven, NL

2 Ground Observations of Thunderstorms

SAINT addressed the study of electric discharges and associated phenomena through different approaches such as ground observations including the development of new equipment. Equipment for ground observations include cameras, visually recording discharges in the sky, detectors measuring in VLF (ELF) and VHF radio waves and antenna providing details about the concurrent electric and magnetic fields. During the lifetime of SAINT, we detected and analyzed several TLEs (Sect. 2.1), including the simultaneous convergence of several sprite streamers at approx. 70–80 km altitude, and TLEs for the first time observed in northern Europe. Additionally, we observed and analyzed lightning (Sect. 2.2), including superbolts. Section 2.3 addresses VHF measurements used to study high-energy emissions from thunderstorms during downward leader propagation, whilst Sect. 2.4 discusses Schumann resonances.

2.1 Ground Detection of TLEs

On July, 5th, 2017, 13 sprites were observed over northern Spain with a video camera from the Observatoire Midi-Pyrénées on the summit of Pic du Midi at an altitude of 2877 m. The camera was a low-light Watec 902 H model with 1/2" Sony ICX-429ALL ExView CCDs. Concurrent lightning data were provided by the Lightning Network (LINET). Figure 2a shows the temporal evolution of the sprite luminosity in 8 video fields for for an event producing filaments converging towards each other (Gomez Kuri et al. 2021). It illustrates two streamer regions, an upper and a lower part, separated at approx. 73 km altitude (red line). First, the upper part illuminates (F1) and subsequently the lower part illuminates (F2) initiating the convergence of these two parts (F3–F8).

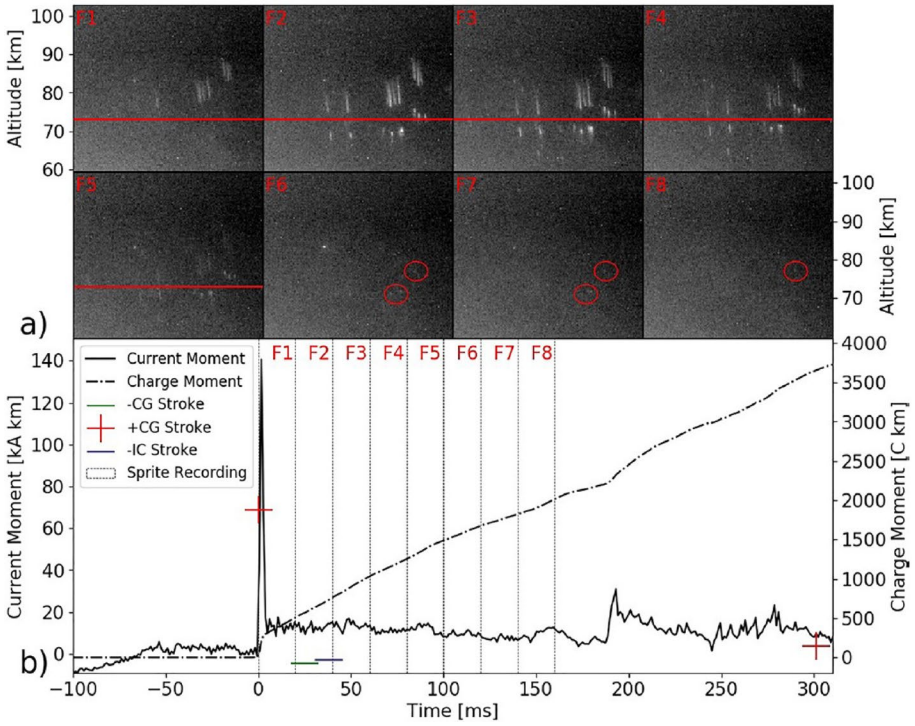

Fig. 2 **a** The temporal evolution of the sprite event luminosity over northern Spain on July, 5th, 2017 from eight 20-ms fields. The red line indicates an altitude of 73 km and the red circles identify discharge elements, still visible until the 8th field. The fields are integrated over the time intervals indicated in panel b). **b** The charge- and current moment waveforms. $t = 0$ is the time of the first causative CG stroke at 22:39:31.064 UTC. The + and - indicate the peak current (corresponding to the left axis) of CG and IC flashes, respectively, associated to the converging sprites. Figure reproduced from (Gomez Kuri et al. 2021)

The average velocity of the approaching streamers was $\sim 0.8 \cdot 10^5$ m s^{-1} in the upper part and $1.1 \cdot 10^5$ m s^{-1} in the lower part.

Figure 2b shows the corresponding current- and charge-moment of the causative lightning flash indicating a sudden peak at the onset of the sprite activity at 22:39:31.064 UTC. At the onset of the sprite activity, the current moment is substantial with a value of approx. 140 kA km of the continuing current which ends 320 ms after the return stroke of the sprite-parenting CG stroke (large red plus at 69 kA). The charge moment continues to increase during the event, suggesting that a high electric field is maintained in the mesosphere during the whole process (Gamerota et al. 2011).

The underlying assumption is that the main source of electrons forming a current moving to the upper region is detachment from negative ions in regions of continued background electric field. We suggest that the electron current from the ambient atmosphere (J_e^{ambient}) tends to dissipate the overall positive space charge of the lower tip, while the electron current from the tip upwards in the filament channel (J_e^{filament}) tends to enhance the overall space charge. As the tip continues to glow, the electric field and the overall positive space charge in the tip are maintained making the luminous region migrate upward.

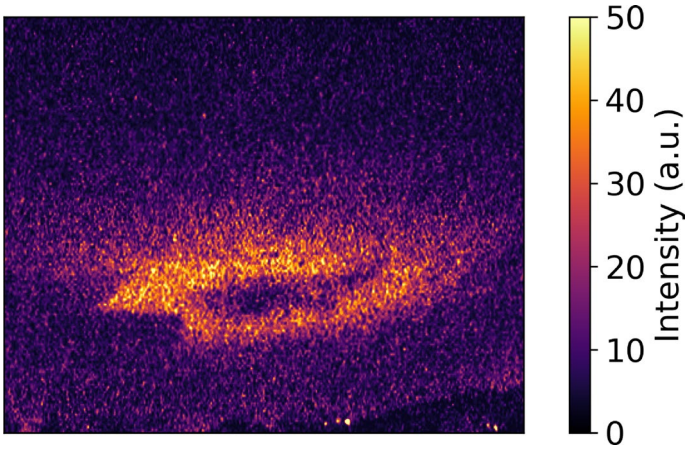

Fig. 3 The first elve ever detected from the UK by a low-light camera installed at the University of Bath. The CG stroke (– 750 kA) responsible for this optical emission occurred at 23:12:51.8 UTC on December, 19th, 2020, located close to the northwest coast of France (≈ 400 km away from the camera). Figure reproduced from (Pizzuti et al. 2022)

In contrast to such sprite observations in France, Spain and Columbia, a rare Mesoscale Convective System (MCS) producing 23 sprites was observed in the UK in 2017 (Pizzuti et al. 2021), displayed in Fig. 3. Most of the sprites occurred during a local minimum in the -CG flash rate and prior to the transition between the mature and dissipating stage of the storm (Fig. 4). The sprite-parent positive cloud-to-ground strokes exhibited an exceptionally high peak current average value of +170 kA.

2.2 Ground Detection of Lightning

During the lifetime of SAINT, instrumentation for long baseline interferometry was developed (Peverell 2022) to detect lightning signals from large distances compared to the baseline of the detector array, and at much longer wavelengths than the baseline. Work with km scale baselines in VLF has been conducted with radio signals from lightning (Füllekrug et al. 2016), and transmitters (Mezentsev and Füllekrug 2013; Füllekrug et al. 2015; Fan et al. 2018). The findings of these works could be achieved by developing deployable (briefcase-sized packages when stowed), sensors in the ELF-MF band, to be transported to an area of interest and set up for remote sensing. Operating at 0–400 kHz, an array of 6 sensors was deployed to a lightning rich environment in northern Colombia (see Fig. 5a) and used to measure azimuthal angles of lightning with sub-wavelength scale baselines of around 600 m.

The detection of lightning is shown in Fig. 5b, mapped according to direction from the sensor array. The distribution is consistent with expected strong lighting activity in the Catatumbo basin of Central Colombia, and the Maracaibo region of Western Venezuela, as viewed from the North of Colombia (Santa Marta). Storms over the ocean to the West can also be seen as regions of less intense event density on the color coded distribution.

As described by Stock et al. (2014), small differences in the arrival time of pulses at separate array stations determine the incoming wave angle, with the direction in this case calculated in a similar way to that used by Mezentsev and Füllekrug (2013). We

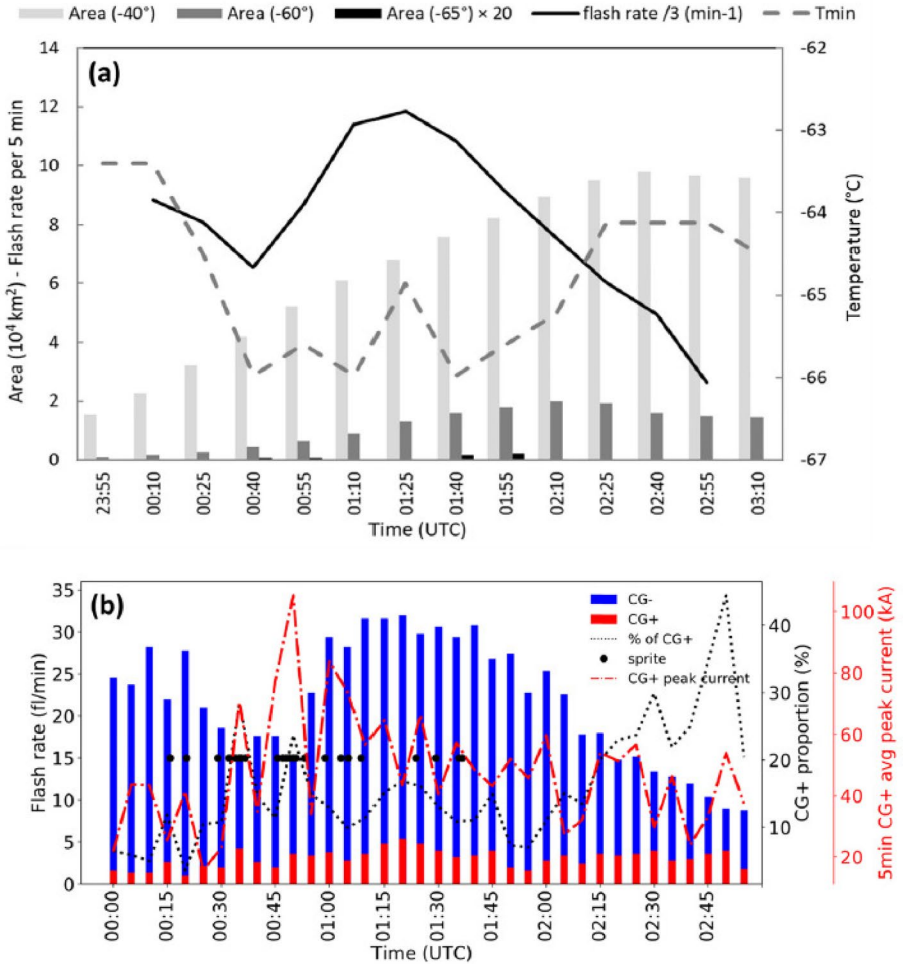

Fig. 4 Storm structure and lightning activity around sprite occurrence above England at ~ 00:15 UTC on May, 27th, 2017. **a** The minimal cloud top temperature (CTT) T_{min}, areas with CTT < −40° C, < −60° C and < −65° C and the flash rate (solid black line) as a function of time. **b** The CG flash rate for different polarities (blue: negative, red: positive) as well as the ratio of +CGs (black dotted line) and the average peak current of +CGs (red dashed line). The black circles indicate the time of observed sprites. Figure reproduced from (Pizzuti et al. 2021)

would expect a normal distribution centered on zero to account for random noise, with the width a measure of the precision of the calculations. Methods of matching the waveform shape of the relevant timeslice of the pulse of interest were applied, first using cross-correlation as described in (Peverell 2022), and also for comparison by applying complex analysis techniques to the waveform to infer phase information for each sample, in a method adapted from Füllekrug et al. (2016). The sample phase method showed a more predictable and normally distributed shape of the azimuthal angles, but with a clear offset, whereas the cross-correlation method showed a distorted distribution, but more accurately centered.

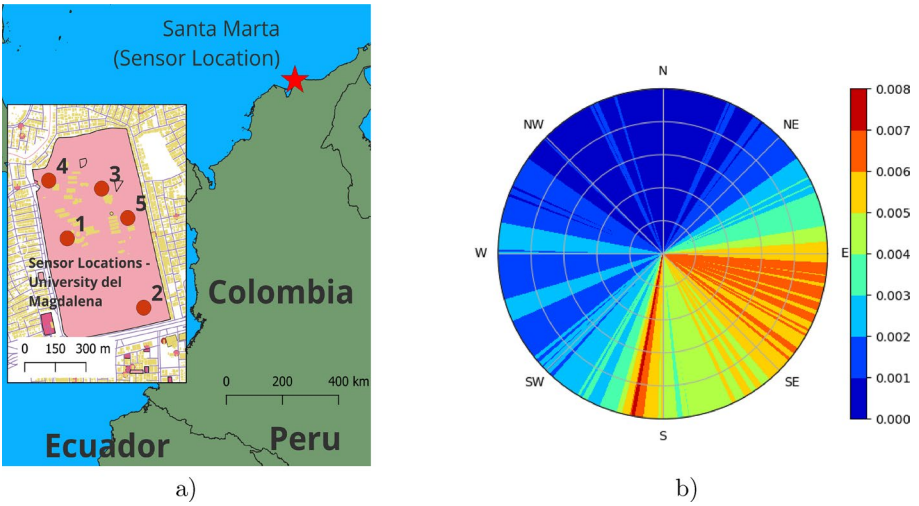

Fig. 5 **a** Geographic location of array sensor deployment on country scale and university campus scale (inset). **b** Normalised distribution of detected angles of lightning event bearings as calculated from an ELF/VLF small baseline array in northern Colombia. The color code gives the fraction of lightning events relative to the total number of lightning events. Figure adapted from (Peverell 2022)

Various studies highlighted that the most intense lightning with large peak currents on Earth typically occurs in areas that experience significantly less lightning activity than the major equatorial lightning centers, and surprisingly during the cold season of the northern hemisphere. One of such superbolt (lightning with approx. 10^6 J per stroke (Efraim et al. 2023)) hotspots is found in the northeast Atlantic region (Holzworth et al. 2019). Figure 6 demonstrates the first detailed analysis of superbolts in this region, in a domain centered in the UK (Pizzuti et al. 2022); it shows details about the climatology of superbolts in the area for the 10-year period from 2010 until 2020.

2.3 High-Energy Emissions in Coincidence with VHF Interferometer Lightning Mapping

To investigate the correlation between high-energy emissions and cloud-to-ground lightning propagation, a broadband VHF interferometer (20–80 MHz) capable of mapping lightning propagation was developed and built during the SAINT project (Urbani et al. 2021, 2022), which is the first of its kind to be built and installed in Europe. Thanks to the interferometric processing technique called the window-based cross-correlation method (Stock et al. 2014) this instrument allows mapping lightning propagation with the highest temporal resolution, on the order of nanoseconds. This feature makes it ideal for investigating the development of lightning flashes on a very rapid temporal scale and studying the physical processes that occur simultaneously with lightning propagation. With a coverage radius of a few tens of kilometers and an omnidirectional field of view, it enables the observation of fast processes such as lightning initiation, recoils, or lightning attachment, even when they occur inside clouds.

After a few measurement campaigns in the Pyrenees (Montanyà et al. 2014), it was realized that the probability of coincidentally observing high-energy emissions on the ground

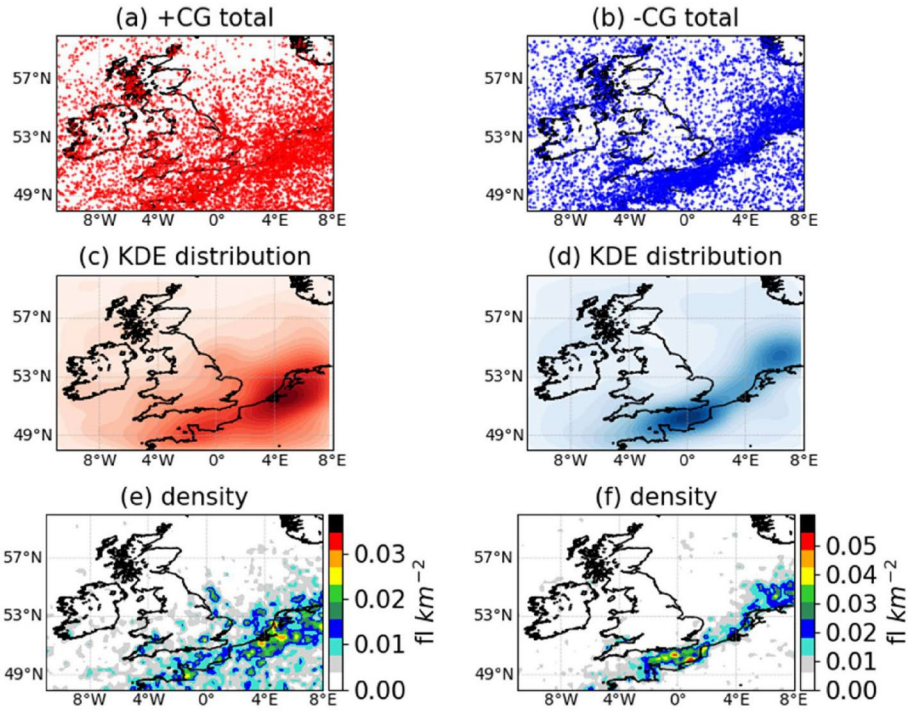

Fig. 6 Overall distribution of superbolts measured by Météorage (left: positive, right: negative). **a**, **b** Scatter plot of superbolt coordinates; **c**, **d** corresponding probability densities (0.25° resolution), determined by the kernel density estimation (KDE); **e**, **f** superbolt flash density map (with a spatial resolution of 0.25° × 0.25°). Figure reproduced from (Pizzuti et al. 2022)

and obtaining a good image with the interferometer was very low (about a couple of events per year). For this reason, it was chosen to plan a measurement campaign in a location with a higher flash rate to maximize the chances of getting good data. Thanks to the UPC (Polytechnic University of Catalonia) research contacts, it was possible to plan a measurement campaign in north-central Colombia in 2019 and 2020. Two interferometers were installed inside the coverage area of the Colombia Lightning Mapping Array (CO-LMA), previously installed by the UPC Lightning Research Group around the city of Barrancabermeja, together with two NaI(Tl) high-energy detectors and an electric field antenna (López et al. 2019; Urbani et al. 2021; Montanyà et al. 2021).

Multiple high-energy emissions were detected in several natural lightning strikes simultaneously with the mapping of the VHF sources located by the broadband interferometer (Fig. 7) (Urbani et al. 2021). X-ray bursts were detected in the last 1 ms before the return stroke, and the energy spectrum was within 1 MeV for the vast majority of the detection, except for a few instances registering a few MeV (likely due to pileup phenomena within the temporal resolution of the detector 0.5 μs).

All the X-ray bursts were detected within an area delimited by a radius of about 1.2 km, and almost every negative CG in that area produced X-ray bursts. These observations and other considerations regarding the analysis of these events suggest that the high-energy emissions in lightning are more common than what has been expected and the exponential

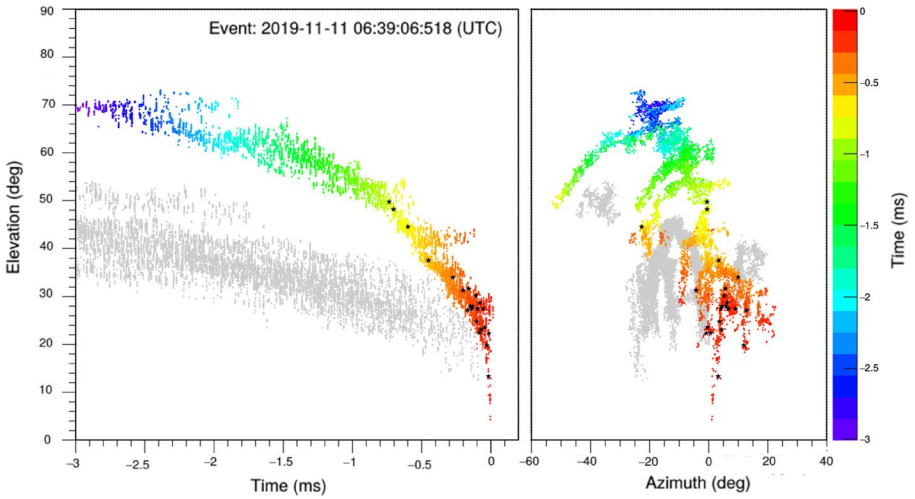

Fig. 7 Simultaneous measurements of a negative downward leader and high energy emissions. The leader propagation is colored by time and the correspondence between VHF sources and X-rays emissions is marked with black stars. Figure adapted from (Urbani et al. 2021)

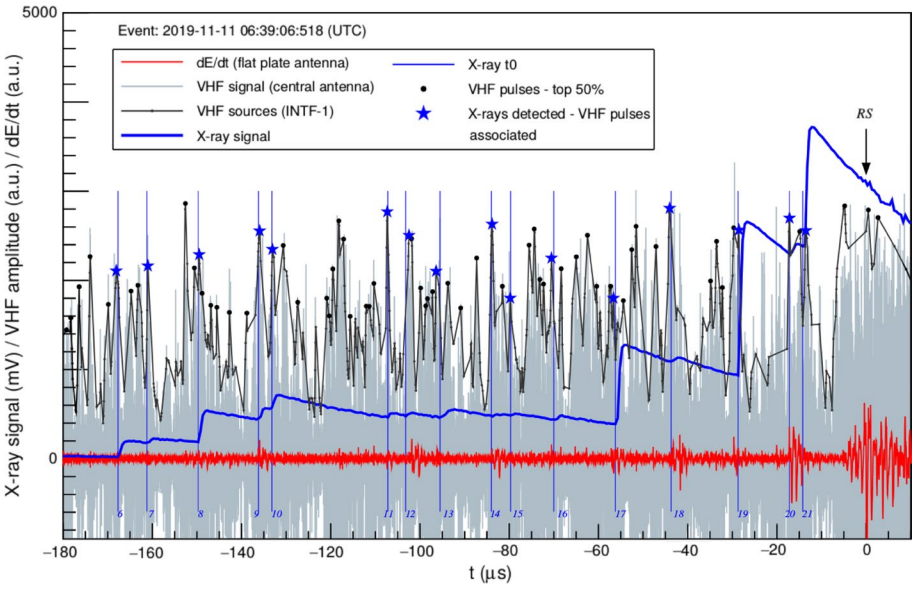

Fig. 8 Temporal correspondence between the X-ray pulses (depicted by blue lines and labels) and the most intense VHF pulses in the last 180 microseconds before the return stroke of the flash at 2019-11-11 06:39:06. The correspondence is marked with blue stars. Figure adapted from (Urbani et al. 2021)

absorption in the atmosphere, especially at low altitudes, plays a crucial role in limiting their detection.

A strong temporal correlation was observed between the high-energy emissions and the most intense VHF pulses during the downward propagation of negative leaders

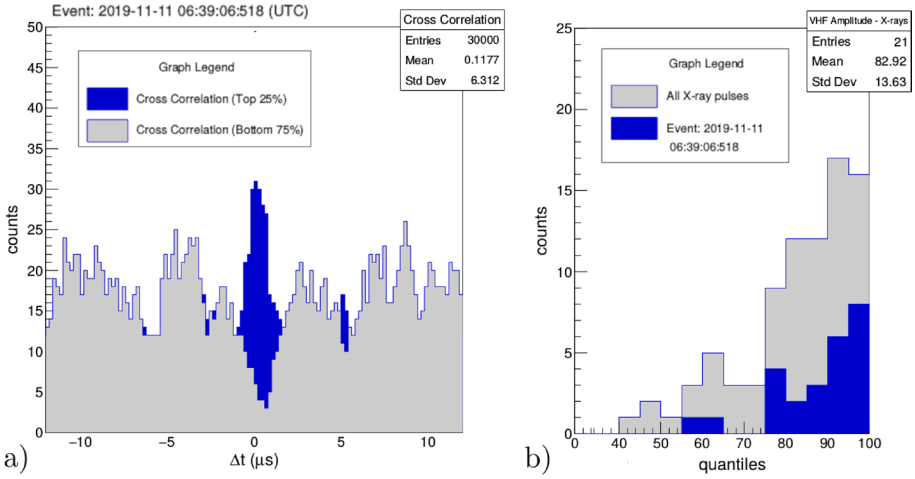

Fig. 9 **a** Temporal cross-correlation analyses between the X-ray time-of-arrival (t_0) and both the top 25% of the most intense VHF pulses and the bottom 75% of less intense VHF pulses. In both cases, an uncertainty of ± 0.5 μs on t_0 was considered. **b** Distribution of the VHF sources associated with X-ray emissions. The VHF amplitude is expressed in quantiles to facilitate the comparison between different events. Figure adapted from (Urbani et al. 2021)

(Figs. 8, 9). This correlation is statistically significant; therefore it is possible to associate specific VHF sources to the corresponding high-energy emissions and locate them during the downward leader propagation.

Furthermore, it emerges from the data that the emission of X-ray bursts in descending leaders can be localized in different branches of the descending leader, even hundreds of meters apart. This suggests that the conditions for high-energy radiation emission can easily occur. The mechanism giving rise to them is the relativistic runaway of electrons (Dwyer et al. 2005; Gurevich et al. 2007), likely occurring when the streamer bursts precede the leader step (Köhn et al. 2020). These high-energy observations associated with downward leader development can be particularly interesting and complementary to the study and understanding of terrestrial gamma-ray flashes. Although the geometry is inverted and the atmospheric density is different, the implications of this study suggest that high-energy emissions are likely a common phenomenon in lightning. However, many questions remain open regarding their frequency, energy, and intensity, as well as the occurrence of additional physical phenomena associated with them.

Despite the main goal of the research campaign conducted in Colombia being the study of high-energy radiation from cloud-to-ground lightning, the analysis of the collected data also revealed a rare observation of multiple positive strokes sharing the same channel to ground (Urbani et al. 2022). For the analysis of these flashes, an advanced data processing technique called "quasi-3D conversion" is utilized, which combines the high resolution of the interferometer with the three-dimensional accuracy of the LMA (Stock et al. 2014). The optimal positioning of the instrument relative to the flash, combined with its simultaneous detection using the LMA, enabled an unprecedented analysis of the mechanisms underlying this phenomenon. The analysis provided a detailed description of the flash propagation mechanism and enabled the first ever comparison of the characteristics and VHF signatures of two downward positive leaders sharing the same channel to ground (Urbani et al. 2022) .

2.4 Long-Term Observations of Schumann Resonances at Portishead (UK)

We extended our field of application to other areas of research in atmospheric electricity, such as the Schumann resonances (SR) recorded at ELF frequencies (< 50 Hz) (Pizzuti et al. 2021). The introduction of a new signal processing technique enables the extraction of such Schumann resonances in fair weather and separated from lower frequency sources of displacement current (i.e. space charge). This technique has been applied to 5 years of data (2015–2020) collected in an urban environment in south-western England for the first time. Analysis of this data set confirms diurnal and seasonal trends in SR intensity that agree with trends found previously elsewhere, but also presents new evidence of a potential link between inter-annual changes in SR intensity and the variability of global climate drivers, such as ocean surface temperature. Finally, because the measurements were obtained at a site that urban noise made far from ideal, it is possible to examine whether variations in man-made noise between working days and weekends affected SR measurements.

3 Space Observations of Thunderstorms

After scientists discovered TLEs and TGFs, it became apparent that several different scientific fields were required to understand the physical processes, including meteorology, cloud charging, discharge physics, chemistry, and nuclear physics. It also became clear that new sensors and a new generation of simulation tools and models were needed. In response to these challenges, the European space science community proposed two space missions for thunderstorm research that both were selected: ASIM with ESA (Neubert et al. 2019) and TARANIS (Tool for the Analysis of RAdiation from lightNIng and Sprites) with the French Space Agency CNES (Centre National D'Etudes Spatiales) (Spizzi 2018). ASIM was launched to the International Space Station (ISS) on April, 2nd, 2018, and has functioned successfully since then. Unfortunately, the launch of TARANIS with the Vega rocket on November, 16th, 2020 failed. The two missions were complementary, so the TARANIS loss was a loss to the entire community.

Data from the ASIM experiment on the ISS are in the focus of the SAINT studies of space observations. The ISS coverage is approx. ±51° latitude and suited to measure lightning, TLEs, and TGFs, which predominantly occur in the equatorial region. ASIM is the first payload with instruments dedicated to simultaneous measurements of lightning, TLEs, and TGFs. It has three photometers that measure in the bands 337 nm with 4 nm bandwidth (PHOT1), 180-235 nm (PHOT2), and 777.4 nm with 5 nm bandwidth (PHOT3). The photometers sample at 100.000 kHz. It also has two cameras at 337 nm with 5 nm bandwidth (CHU1, CHU = Camera Head Unit) and 777.4 nm with 3 nm bandwidth (CHU2). The bands are sensitive to streamer and leader emissions, the fundamental modes of lightning. The cameras have 1000 x 1000 pixels and run at 12 frames per second. The photometers and cameras have an 80-degree diagonal field of view and are oriented towards the nadir, giving approximately 400 x 400 m spatial resolution on the ground. The optical instruments only observe during the night (Chanrion et al. 2019). TGFs are measured by a low-energy detector sensitive to photon energies from 20 to 400 keV and a high-energy detector sensitive to energies from 200 keV to above 20 MeV. The low-energy detector is pixellated with a coded mask in front that allows identification of the direction of photon bursts from point sources. The low-energy detector operates at night, and the high-energy

detector operates day and night. The two detectors are oriented towards the nadir (Østgaard et al. 2019b).

The optical instruments are combined in the Multispectral Modular Imaging Array (MMIA) and the X- and gamma-detectors in the Modular X- and Gamma-ray Detector (MXGS). The baseline mode of operation is the "trigger" mode, where the instruments run continuously. The onboard trigger software identifies flashes and stores data corresponding to a period from before to after the trigger. The MMIA and MXGS cross-trigger, so all instrument data corresponding to a trigger are saved for download.

The LIS (Lightning Imager Sensor) instrument on the ISS (NASA, February 2017 to November 2023) measured lightning radiation at 777.4 nm in a 1 nm band at ~ 4 km spatial resolution and 2 ms temporal resolution. It measured day and night (Blakeslee et al. 2020). The common band of LIS and ASIM (777.4 nm) allowed for direct data comparisons between the two instruments (Köhn et al. 2024).

TGFs were observed in the past by instrumentation designed for observation of astrophysical objects, e.g., AGILE (Astro-Rivelatore Gamma a Immagini Leggero) (Marisaldi et al. 2010; Tavani et al. 2011), RHESSI (Reuven Ramaty High Energy Solar Spectroscopic Imager) (Cummer et al. 2005; Smith et al. 2010) and Fermi (Briggs et al. 2010) that have provided a catalogue of observed TGFs. However, the sensors and their trigger logic were not optimized for TGF observations. Here, ASIM is unique. The MXGS is the first space detector designed to measure TGFs, and the combination of the MMIA and MXGS modules allows us to understand the relationship between lightning (optical), TLEs (optical), and TGFs. ASIM is also unique by observing thunderstorms at the closest distance accessible from space (400 km), by sampling the optical radiation from lightning processes at the highest frequencies to date from space (100.000 kHz), and in a band that is sensitive to streamer discharges (337 nm). The new features of ASIM have led to discoveries, particularly regarding TGFs (Sects. 3.1-3.3), blue streamer discharges from the top of thunderstorms (Sect. 3.4) and sprites above thunderstorms (Sect. 3.5). The following subsections describe the studies in these areas conducted during SAINT.

3.1 TGF Observations by AGILE and ASIM

Since SAINT started in 2017, but ASIM had not been launched before 2018, data of the previous mission AGILE were analysed (Lindanger et al. 2020; Maiorana et al. 2020). AGILE (Tavani et al. 2008) is a mission of the Italian Space Agency dedicated to high-energy astrophysics, launched in 2007 and de-orbited in February 2024. Although AGILE reported observation of TGFs since 2010 (Marisaldi et al. 2010), a major change in the onboard configuration in 2015 resulted in a ten-fold increase in TGF detection rate (Marisaldi et al. 2015). At the time of start of the SAINT project there were almost two years of unexplored TGF observations. Analysis of these data resulted in the 3rd AGILE TGF catalog, published in two companion papers (Lindanger et al. 2020; Maiorana et al. 2020) and comprising more than 3300 TGFs, also available online[1] and available to the scientific community. Figure 10 shows a world map distributed of all TGFs in the new AGILE catalogue (Maiorana et al. 2020). TGFs are clearly distributed around three main chimneys in Central/Southern America, Central Africa and South East Asia (Inan et al. 2006; Carlson et al. 2012) with some events being over

[1] https://www.ssdc.asi.it/mcal3tgfcat/

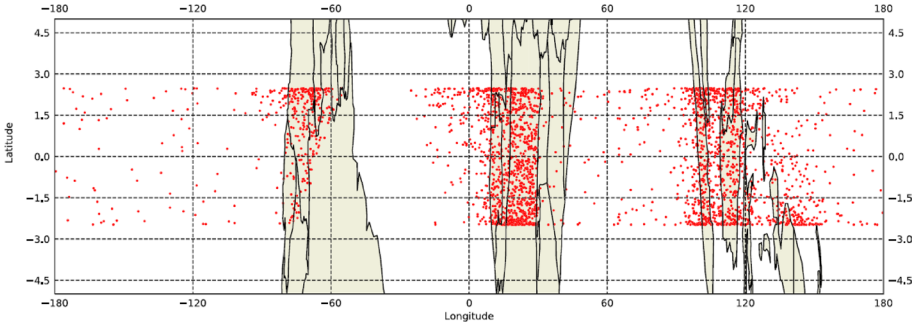

Fig. 10 An example of TGFs measured by AGILE. Figure reproduced from (Maiorana et al. 2020). The shaded areas denote areas of Central/Southern America, Central Africa and South East Asia. Red dots are the satellite footpoints at detection time (±2.5° in latitude due to orbital inclination) but TGFs can be detected up to about 800 km radial distance. The maximum/minimum latitude observed by AGILE is ±10°

the Ocean. In Fig. 10, the cutoff in TGF detections at ±2.5° latitude, as well as the larger detection density at these cutoff latitude values, is due to the low orbital inclination of AGILE. The empty area over Southern America corresponds to the South Atlantic Anomaly (SAA), where AGILE did not take measurements, also explaining the smaller number of TGFs in that region. The analysis of data from various missions before 2018 gave us sufficiently much experience to study data provided by ASIM, the first mission dedicated to study the relation between lightning, TLEs, TGFs and associated discharge phenomena.

Figure 11 shows the cumulative number of TGFs during the 10 months of ASIM operation from June 2018 until April 2019 as well as their global distribution (Østgaard et al. 2019a). Panel (a) shows that 217 TGFs were measured during that period amounting to approx. 0.7 TGFs per day; panel (b) shows that these TGFs are distributed around the equator with the three main chimneys in Central/Southern America, Central Africa and South East Asia (Inan et al. 2006). For an example TGF on June, 21st, 2018, Fig. 12 shows concurrent measurements by ASIM and by the Fermi satellite, one of the missions dedicated to study gamma-rays from outer space, but suitable enough to also detect TGFs. It generally illustrates a good agreement between ASIM and Fermi measurements, but also that ASIM provides more data points and thus a more detailed view on the temporal evolution of such a TGF. Both ASIM and Fermi show the main occurrence of photons at approx. $t = -2.2$ ms and $t = 0$ (relative timing); however, ASIM provides significantly more data points between the two main signals. Since the energy channel is equivalent to the deposited photon energy, this indicates that the photons not or hardly detected by Fermi have similar energies as in the two main peaks, although being less abundant. Panel (b) and (d) compare the (time binned) number of photons as a function of time. Whilst there are almost no photons detected by Fermi in the period between ≈ -2 ms and ≈ -0.5 ms, there is a clear, albeit small signal measured by ASIM. Similarly, Figure 13 shows the temporal evolution of a multipulse TGF (Østgaard et al. 2019a), pulses of TGF photons occurring shortly after each other. Panel b) shows the number of photons binned into time windows of 50 μs. All the subpulses with clearly visible peaks are separated by approx. 2 ms with an decreasing peaks of the photon number. Interestingly, although the photon number decreases, panel a) shows that the energies (equivalent to the energy channel number) are not necessarily

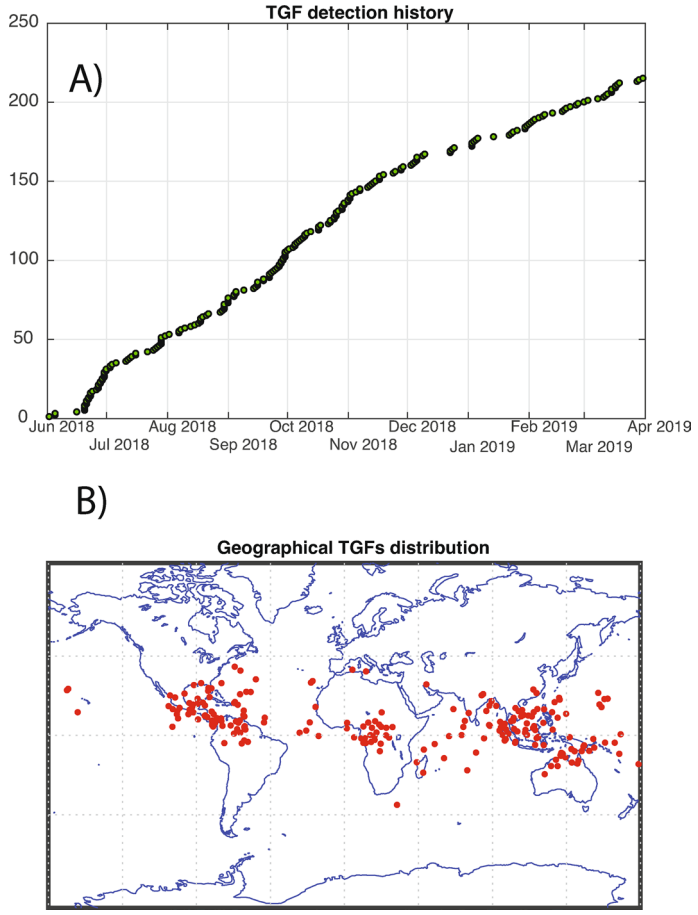

Fig. 11 **a** The cumulative distribution of the observed number of TGFs versus time for the first 10 months of the ASIM mission from June 2018 until April 2019. **b** Geographic location of these TGFs. Figure reproduced from (Østgaard et al. 2019a)

less for later pulses, but in turn can even be higher for earlier sub-pulses, see e.g. the red dot after ≈ 6 ms. ASIM has thus given us the opportunity to study multipulse TGFs in unprecedented detail.

The TGFs shown in Figs. 10 and 11b occurred mainly in equatorial and tropical regions, at longitudes matching the well-known lightning chimneys. Although a few TGFs were reported at higher latitudes up to 37° latitude (Smith et al. 2010; Gjesteland et al. 2015), no TGF observations were possible at still higher latitudes because of the low orbital inclination of the satellites with TGF detectors. ASIM data from the ISS, which had an orbital inclination of 51°, provided the first opportunity to search systematically for TGFs at middle latitudes (Maiorana et al. 2021). We observed 14 TGFs detected by ASIM between June 2018 and August 2020 in both hemispheres; all were in the latitude bands between 35° and 51°, see Fig. 14. The associated storms show strong convection, but not extreme or unusual characteristics. TGFs at mid latitudes are rare, but this rarity appears to be mostly due to gamma-ray absorption in the atmosphere due to a lower tropopause height than in

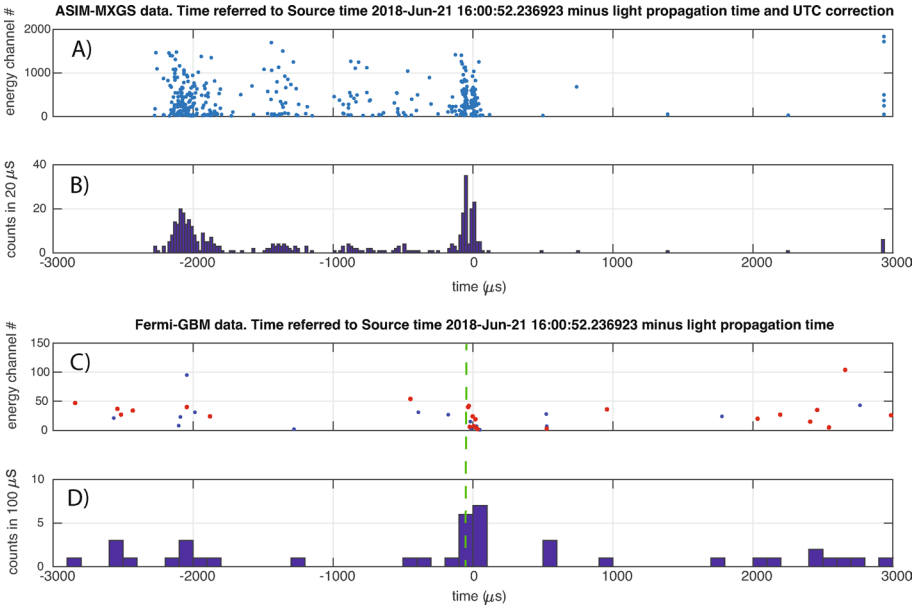

Fig. 12 The simultaneous observation of a TGF over central Africa by ASIM and Fermi on June, 21st, 2018. **a** The MXGS HED energy channel counts as a function of time. **b** MXGS HED counts in 20 μs bins. **c** Fermi BGO counts as a function of time. Red is BGO 1 and blue BGO 2. **d** Fermi GBM BGOs counts in 100 μs bins. The green dashed line in panels **c** and **d** is the time of a lightning stroke detected by the Worldwide Lightning Location Network (WWLLN) and was found to be simultaneous to within 13 μs of the Fermi measurements when propagation time is accounted for. Figure reproduced from (Østgaard et al. 2019a)

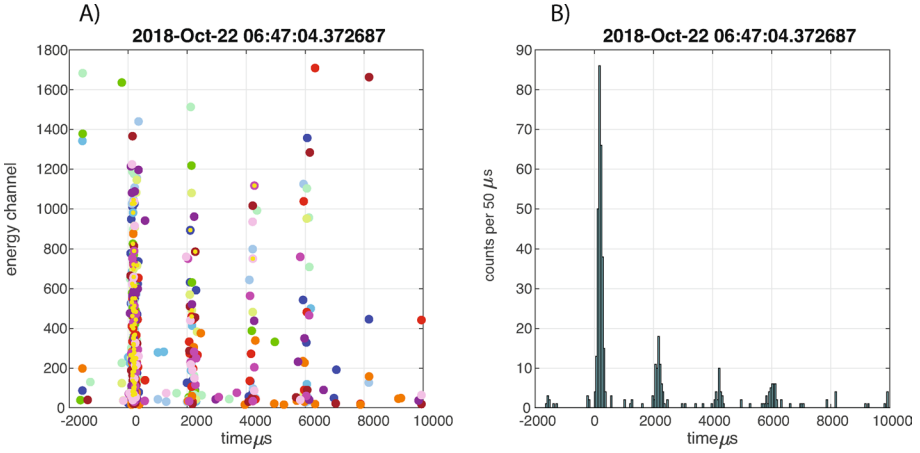

Fig. 13 A multipulse TGF observed by ASIM outside the West African Coast on October, 22th, 2018. **a** MXGS HED energy channel counts as a function of time (the color code identifies the individual detectors). **b** The counts binned into time windows of 50 μs as a function of time. Figure reproduced from (Østgaard et al. 2019a)

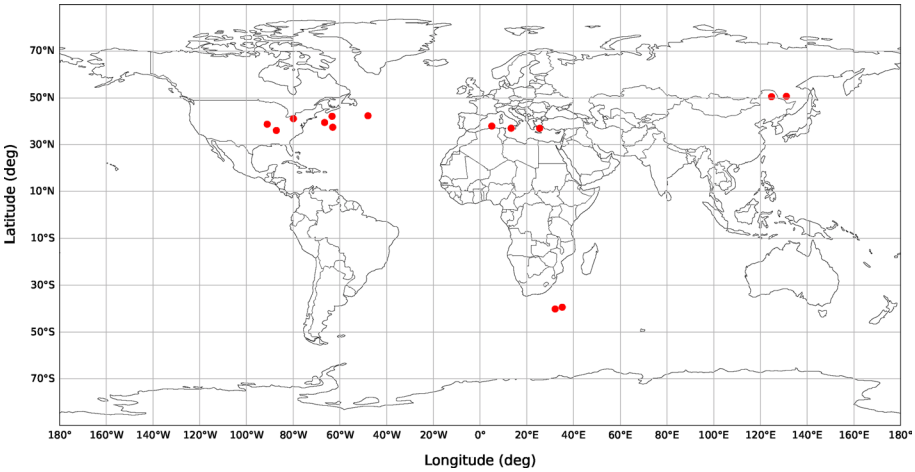

Fig. 14 The location of 14 TGFs detected between 35° and 51° latitude. Figure reproduced from (Maiorana et al. 2021)

the tropics. When this effect is taken into account, the TGF-to-lightning ratio at mid latitudes is typically lower, but marginally agrees with that observed in tropical regions. It also shows that the ASIM TGF-to-lightning ratio in tropical regions is comparable to previous results obtained by other space missions (Smith et al. 2010; Briggs et al. 2013).

ASIM and SAINT paved the way for future observations of gamma-ray flashes not only from space, but also from aircraft in the vicinity of thunderstorms. Amongst these, the most recent one is the ALOFT ("Airborne Lightning Observatory for FEGS and TGFs") mission (Østgaard et al. 2023a), dedicated to terrestrial gamma-ray flashes and gamma-ray glows (Parks et al. 1981; McCarthy and Parks 1992; Wada et al. 2019) from thunderstorms. Results of this mission show as a matter of fact that bursts of gamma-rays are more common than previously thought (Marisaldi et al. 2024), but that many are too weak to be detected at satellite altitudes due to atmospheric absorption (Østgaard et al. 2023b; Sarria et al. 2023; Bjørge-Engeland et al. 2024).

3.2 Simultaneous Observations of TGFs and Lightning

ASIM is the first mission that enables analysis of correlations between lightning activity in the cloud measured by the MMIA and the X- and gamma-radiation measured by the MXGS, such that the nature of the TGF generation mechanism can be explored. One proposed mechanism holds that free electrons are accelerated to high energies up to tens of MeV in an impulsive electric field in a 10-100 m-region around a lightning leader tip (Heumesser et al. 2021; Babich et al. 2017). In this case, a TGF should be associated with an optical pulse, provided the photon flux from the source is not reduced below the detection threshold by cloud scattering and absorption. Another mechanism suggests that electrons are accelerated in a kilometer-scale field in the clouds and that observed flux levels are reached through feedback whereby antimatter positrons created by pair production and back-scattered X-rays seed additional avalanches (Dwyer 2003; Dwyer et al. 2008). In this case, we would expect modest levels of optical emissions.

During the first 17 months of observations, 69 TGFs were observed during the night time and within the FOV of MMIA. All were accompanied by optical pulses and were analyzed by Heumesser et al. (2021). Figure 15 shows two examples of MMIA signals in the three photometers on a time axis where $t = 0$ is the TGFs' onset time. Considering models of light propagation through thunderclouds (Koshak et al. 1994; Light et al. 2001; Soler et al. 2020), the MMIA signals as a function of time t can be fitted to (Soler et al. 2020)

$$\sqrt{\frac{\tau}{\pi(t-t_0)^3}}\exp\left(2\sqrt{\nu\tau}-\frac{\tau}{t-t_0}-\nu(t-t_0)\right) \tag{1}$$

where t_0 is the source time of the TGF photons, τ is the characteristic diffusion time and ν is the absorption rate (Heumesser et al. 2021). We used this equation to determine the source time of the first TGF photon (dashed green line in Fig. 15) which occurs at the onset of streamer and leader activity.

The optical pulses have onsets close to the onset of the TGFs. It was concluded then, that the observations favored the leader tip mechanism, although a contribution from the feedback mechanism could not be excluded (Köhn et al. 2017).

A question discussed by Heumesser et al. (2021) was whether the TGFs come before or after the optical pulse onsets. It was concluded that the accuracy of the timing was not sufficient to answer this question. The absolute timing (needed for correlation with ground observations) was around 25 ms and could be reduced to 5 ms in most cases. More important is the relative timing between MMIA and MXGS. The UV photometer measures elve emissions in the lower ionosphere. Elves are horizontally stratified expanding rings of emissions generated by the electromagnetic (EM) field of a lightning leader current pulse (Fukunishi et al. 1996; Barrington-Leigh and Inan 1999; van der Velde and Montanyá 2016). The EM radiation is unaffected by cloud scattering and the UV pulse serves as a

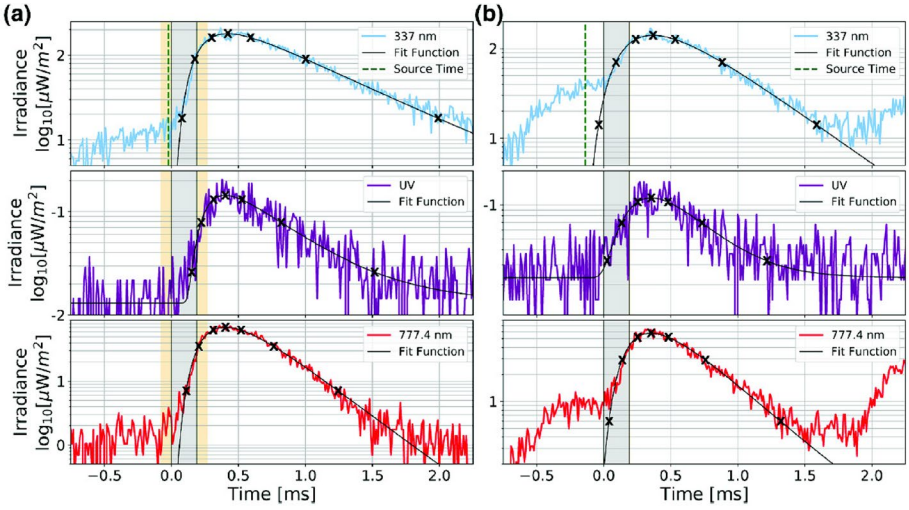

Fig. 15 Two examples of MMIA signals in 337 nm (top), 180-230 nm (middle) and 777 nm (bottom) band associated to TGFs; $t = 0$ is the TGFs' onset time. The gray shaded region marks the duration of the TGF; the orange shaded region the respective time uncertainties of the measurement ($\pm 80\ \mu$s in panel a and $\pm 5\ \mu$s in panel b). The black solid line represents the fit to Eq. (1) providing the source time t_0 (dashed green line). Figure reproduced from (Heumesser et al. 2021)

marker of the source current onset after time-of-travel corrections. The relative timing was 80 μs reduced to 5 μs halfway through the observation period due to a software update. These are relatively large errors compared to the TGF pulse duration, which was 10–50 μs.

Additional uncertainties in the relative timing come from pre-activity that could extend from a few ms to a few 10 s of ms before the main pulse onsets. The definition of the pulse onsets was an estimate from a function that accounts for delays and absorption in the clouds (Soler et al. 2020; Luque et al. 2020). Summarizing these effects, methodical errors in the onset time added a further 30–40 μs uncertainty.

It was concluded by Heumesser et al. (2021) that there was a consistently high amplitude signal in the blue (337 nm) band, on average exceeding the red (777.4 nm) band by more than a factor 2, suggesting a high level of streamer activity (blue) relative to leader activity (red). Based on this, they suggested a scenario where the optical and TGF emissions are generated as the atmosphere of the region ahead of a leader tip breaks down in a flash of streamers, leading to a high energy current source in line with the model proposed by Köhn et al. (2020), see Sect. 4.4 for details.

Fitting the optical pulses with the cloud scattering function, Heumesser et al. (2021) estimated the source depth in the clouds under assumptions on the cloud particle density (2.5×10^8 m^{-3}) and particle radii (15 and 20 μm). It shows that the source depth is 2–4 km below the cloud tops.

More sophisticated studies of TGFs and the respective optical pulses using ASIM data were later performed by Skeie et al. (2024) and Lindanger et al. (2022). Using the measured TGF durations and the time between the onset of the TGFs and optical pulses, they found that the TGF onsets are before or at the same time as the optical pulses; also they observe that longer lasting TGFs tend to have longer delays between the onsets of optical and gamma-ray emission. Using additional radio measurements, the lightning activity, that is associated to TGFs, was found to be enhanced in an interval between 150 and 750 ms after trigger time. This is a characteristic property of a significant fraction of flashes following a TGF event.

3.3 Simultaneous Observations of TGFs and Elves

When ASIM was first conceived, the origin of many forms of TLEs was unknown. Because TLEs and TGFs were discovered within a few years of each other in the early 1990 s (Fishman et al. 1994) (e.g., Sentman, Wescott, Fishman references), it was thought that they might be related, which seemed logical at the time because the flux of photons in TGFs was considered so high that the source was likely to be high in the atmosphere where atmospheric scattering is small (Fishman et al. 1994; Sentman et al. 1995; Wescott et al. 1995). While it was realized over time that the source of TGFs is located at lower altitudes, when more observations became available (Dwyer and Smith 2005), exploring this aspect with ASIM was still of interest.

One of the first studies on this topic reported an event in which an elve followed a TGF (Neubert et al. 2020). As discussed by Heumesser et al. (2021), this is not uncommon, but represents a discovery nonetheless, underscoring the relationship between impulsive lightning currents and TGFs. Figure 16 shows the pulses detected by the three photometers and the low-energy (LED) and high-energy (HED) detectors of MXGS. The event had a relatively large UV signal (the elve), and the MXGS photons measured by the LED were sufficient to estimate the TGF source location in the storm clouds. Neubert et al. (2020)

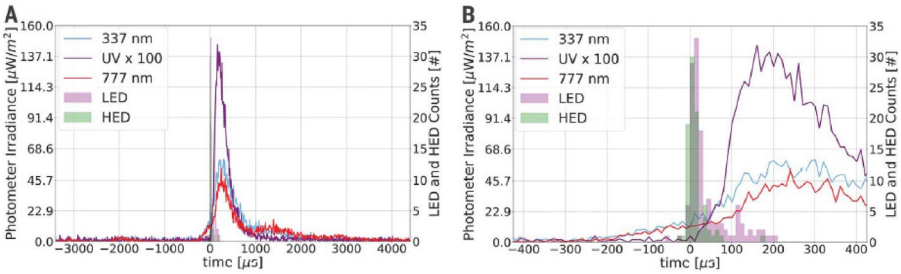

Fig. 16 Data signal for a TGF accompanied by an elve: The TGF trigger time is at $t = 0$, corresponding to 13:01:33.100080 UTC. **A** Photometer (left axis) and X-ray and gamma-ray (right axis) measurements around the time of the event. The UV photometer measures 180 to 230 nm and is multiplied by 100 to show on the same scale as the optical photometers. **B** The same data as in **A** zoomed in further at the time of the TGF. Figure reproduced from (Neubert et al. 2020)

found that the optical pulse originated from the same storm section as the TGF and that the two were co-located within the error estimates of their geolocation.

The scenario proposed for the observation is shown in Figure 17. It was suggested that the optical pulse was from an upward intra-cloud lightning flash (IC) that generates the TGF flash and an electromagnetic pulse (EMP), which excites the elve. These findings were later substantiated by Bjørge-Engeland et al. (2022) who performed a study of 17 TGFs accompanied by elves. Østgaard et al. (2021) report on the simultaenous measurements of lightning, TGFs, elves and an energetic intracloud pulse (EIP) where the lightning leader producing the terrestrial gamma-ray flash is associated to an EIP that triggered an

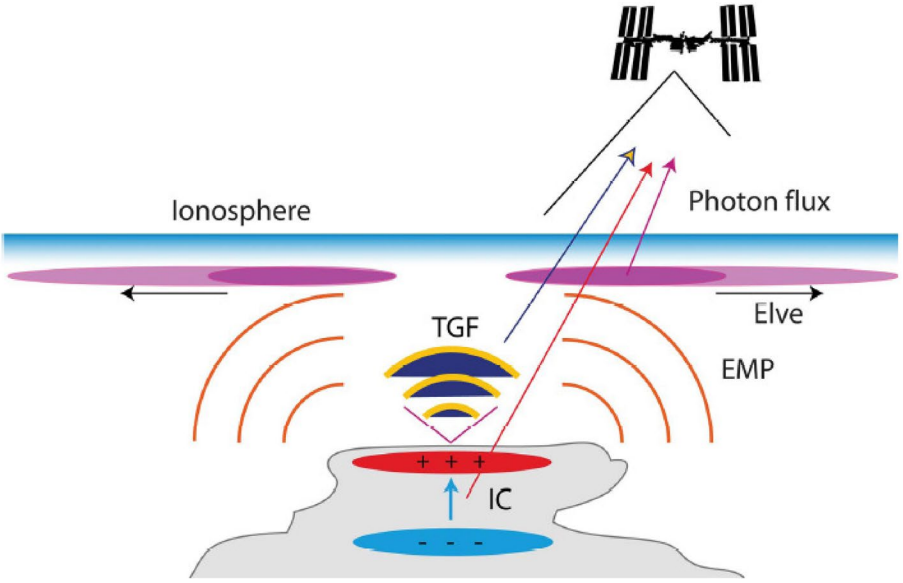

Fig. 17 An intra-cloud (IC) lightning event generates a TGF and electromagnetic pulse (EMP) which in turn excites expanding waves of UV emission in the lower ionosphere (elve). TGF and UV emissions are observed by ASIM on the ISS (arrows). Figure reproduced from (Neubert et al. 2020)

electromagnetic pulse exciting an elve. The authors speculate that not only the current in the lightning channel, but also the TGF current contributed to the EIP.

3.4 Observations of Blue Jets and Blue Streamer Discharges

ASIM was preceded on the ISS by an experiment, THOR, conducted in 2015 by the Danish ESA astronaut Andreas Mogensen. He used a conventional Nikon color camera to observe thunderstorms during ISS overflights. His recordings revealed copious activity of small, localized blue flashes at the cloud tops (Chanrion et al. 2017). Few observations were taken because his time on the ISS was limited to 10 days. With some anticipation, ASIM was installed on the ISS with its specialized instruments including measurements at 337 nm (blue). We were not surprised: ASIM often detects blue flashes that seem quite common. The fact that they are almost exclusively observed in the blue band leads us to conclude that they are blue streamer discharges.

One event stands out and was analyzed by Neubert et al. (2021): Five blue streamer flashes were observed during the overflight of a storm near the island of Nauru in the Pacific Ocean, and one of these appeared to stimulate a pulsating blue jet reaching the stratopause. Figure 18 shows the photometer signals of one of the blue flashes. The blue signal has a very fast rise time, peaking in one sample, or 10 μs. It suggests that the source is at the cloud top, where the photon propagation is not influenced by scattering in cloud particles. The UV signal is delayed and was interpreted as a signal from an elve generated in the discharge process. A red signal that would be from leader emissions is absent.

One of the flashes stimulated the pulsating blue jet, shown in Figure 19. The top panel (a) is now on a timescale covering 400 ms and shows a blue photometer signal that appears to have two main pulses. The middle panel (b) shows the corresponding camera images, also in the blue (337 nm). The signal is extended in the opposite direction of the arrow that points towards the nadir location of the ISS. Because of fortuitous viewing geometry, with the event at some distance from the ISS nadir ground location, the blue jet could be identified and its altitude determined. The red photometer signal remains in the noise level except at the blue pulse onsets, suggesting that the blue jet

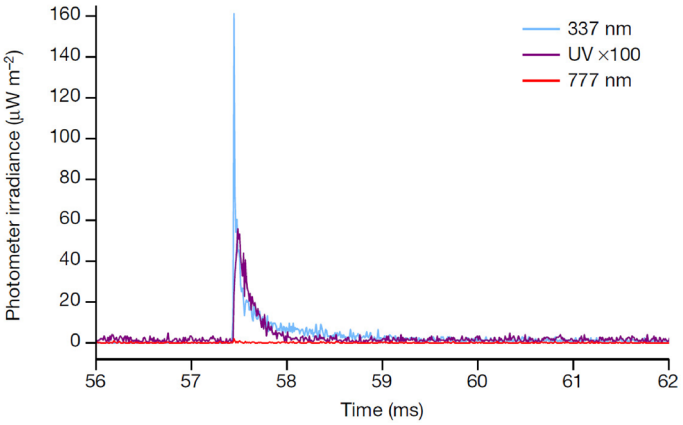

Fig. 18 Photometer signal of a blue flash with an elve. Figure reproduced from (Neubert et al. 2021)

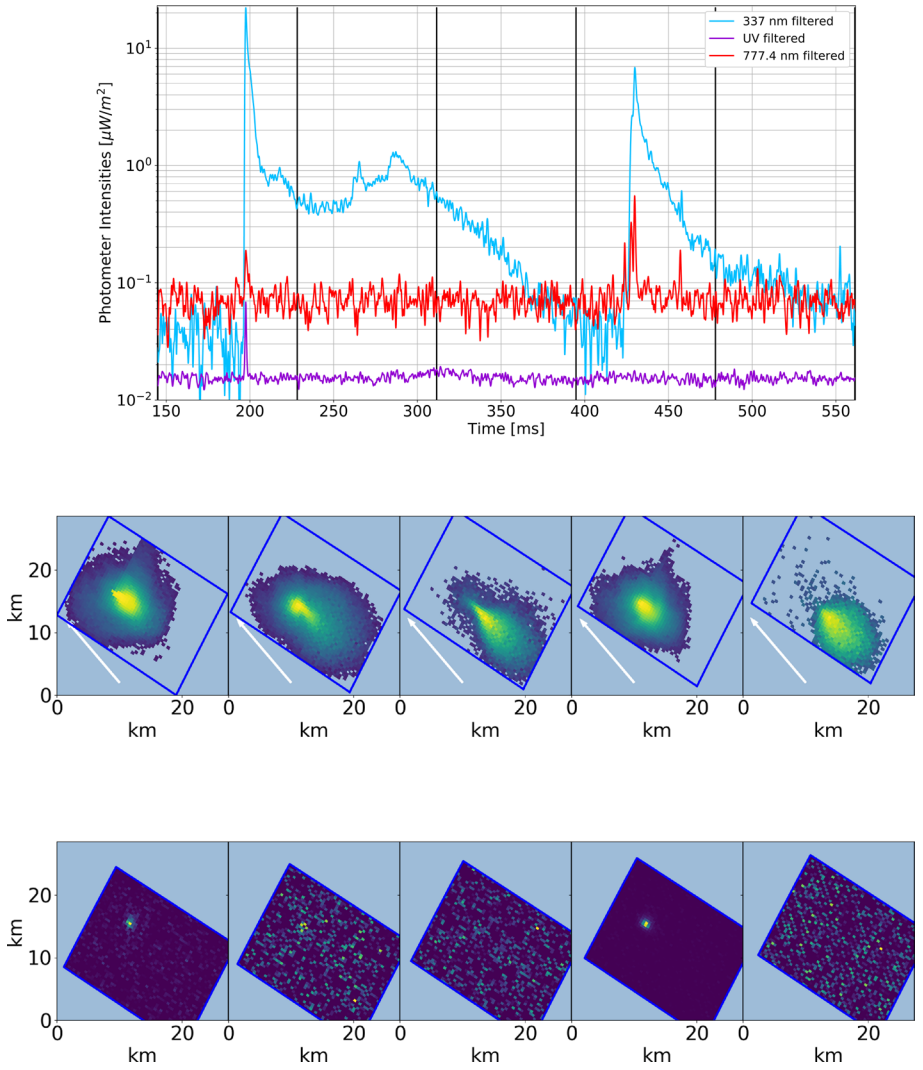

Fig. 19 **a** The photometer signals of blue jets are on a logarithmic scale, 30-point Gaussian filtered. Vertical lines mark the camera image exposure periods. $t = 0$ corresponds to February, 26th, 2019 at 15:11:06.000 UTC. **b** The consecutive camera images in the blue band (337 nm), given on a logarithmic scale adjusted to the maximum pixel value of each image. **c** The images in the red band (777.4 nm) are on a linear scale. The images are projected to an altitude of 16 km. The geographical box of the projections is identical for the two camera images. White arrows point towards the direction of the ISS. Figure reproduced from (Neubert et al. 2021)

primarily is made of streamers. The bottom panel shows the signal in the red leader band. The signal is localized to a few pixels, primarily emitted at the onset of the two jet pulses (Fig. 19a).

In their discussion, Neubert et al. (2021) suggested, consistent with earlier findings from the ISUAL experiment (Imager of Sprites and Upper Atmospheric Lightning) (Chou et al. 2018; Liu et al. 2018), that the fast blue discharges with rise times of a few

tens of μs are associated with Negative Bipolar Events (NBEs), commonly observed in the electromagnetic spectrum at the top of clouds (Wu et al. 2012).

The interpretation of the UV signal as from an elve is supported by ground-based observations of elves associated with NBEs (Marshall et al. 2015) and with a model of the high-amplitude current pulses carried by streamer corona discharges (Cooray et al. 2020). NBEs are known to stimulate lightning (Rison et al. 2016), and now also blue jets, as documented by ASIM.

The correlation of blue corona discharges with severe convection suggests that the discharges tend to originate in developing or mature cloud cells, also suggested by NBE observations (Wu et al. 2012; Karunarathna et al. 2015). To explore this aspect further, Dimitriadou et al. (2022) analyzed blue corona discharges detected by ASIM in two convective cells of the same thunderstorm but in different phases of convection. The storm was in northwestern Australia and generated a multitude of blue discharges, some with the fast rise times of a few tens of μs that signify they are from the top of the clouds and some with longer rise times that indicate they are at some depth within the clouds. They selected the 14 fast pulses observed during the overflight for analysis. An example of a discharge is shown in (Fig. 20). The bottom panel shows the images in 337 nm (blue) and 777.4 nm (red), corresponding to the photometer signals in the top panel (12 frames per second = 83.3 ms per frame). Lightning shows up as two wider spots in both images and the blue activity as a focused spot in the blue (left) image, signifying discrete, blue emissions at the cloud top. Recent space-based optical and electromagnetic observations of high-altitude blue discharges have enabled independent estimates of their altitude with improved accuracy. By combining ASIM photometric data with skywave propagation modelling from ground-based electric field measurements, Bai et al. (2023) constrained blue discharge altitudes to between $10.9 - 16.5$ km from optical analysis and $16.0 - 18.8$ km from electromagnetic analysis. These findings are consistent with cloud-top heights derived from infrared satellite data and highlight the potential for overshooting convection to influence discharge formation. Such measurements refine emission profile characterisation and enhance understanding of the role these discharges play in upper tropospheric chemistry.

The cloud cell altitudes were constructed from observations by the Himawari geostationary satellite and an atmospheric-sounding profile taken at Darwin Airport. The discharges occurred in both types of cloud cells, with 11 occurring in the developing cell reaching 16-17 km altitude and 3 occurring in the collapsing cell at lower altitudes. The observations suggest that blue cloud-top discharges are not exclusive to developing and mature cells with the highest cloud tops. A more detailed analysis of the collapsing cell based on coincident radar observations suggests a connection to high concentrations of ice hydrometeors and convective sub-regions.

The GLD360 ground-based lightning system detected most discharges, indicating rapid breakdown processes with high currents of up to ~100 kA. Furthermore, UV pulses follow 7 of the 14 discharges interpreted as elves demonstrating the complex interactions of thunderstorm activity with the broader atmospheric environment. A more thorough analysis is provided in (Dimitriadou 2021).

3.5 Observations of Sprites with ASIM

The method for searching sprites in MMIA observations is based on GLD360 lightning data detected from ground. We filtered for the positive CG strokes associated with the 500,000 UV events worldwide (events with CHU1 (337 nm bandwidth) to CHU2 (777.4

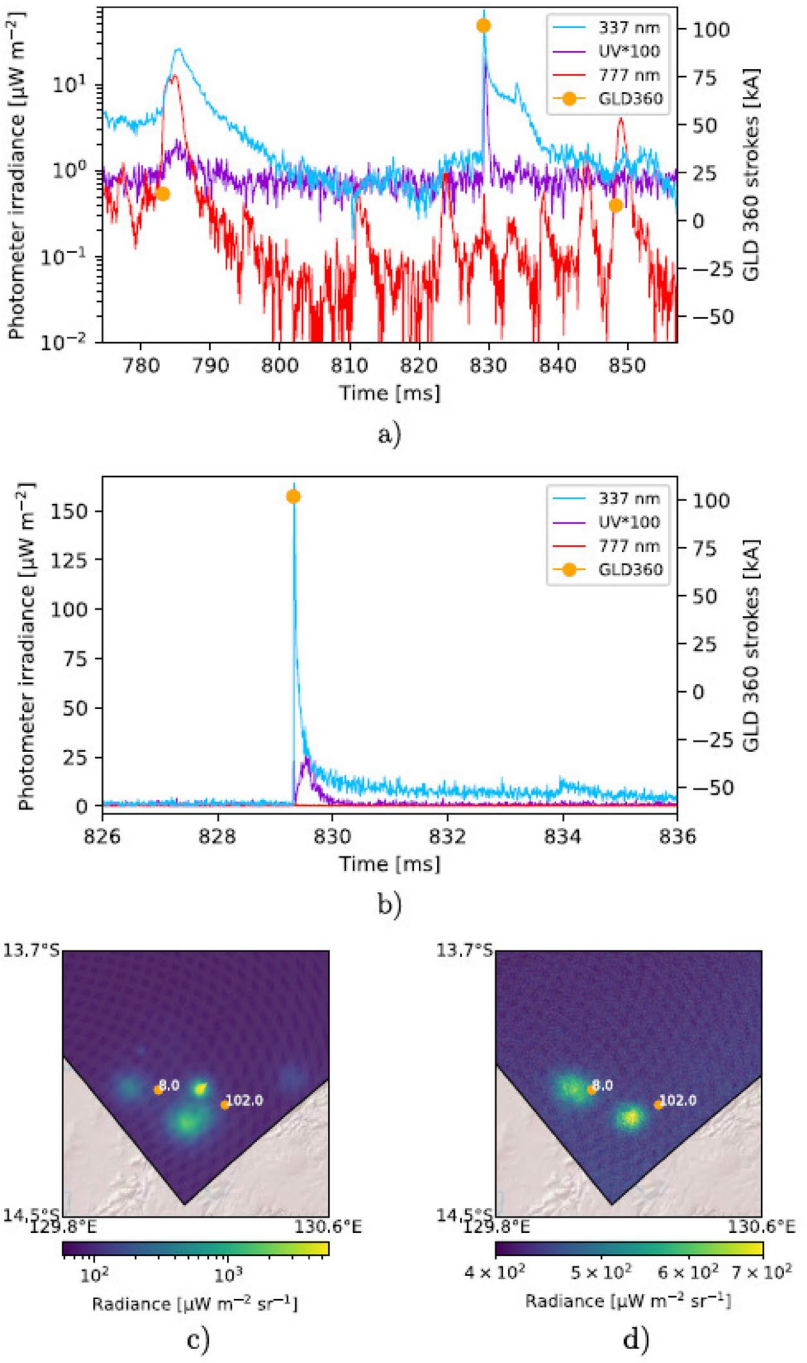

Fig. 20 Blue corona discharge in a developing cell: **a** Photometer signals in the 337 nm (blue), 180-230 nm (vacuum UV), and 777 nm (red) band. Concurrent GLD (Global Lightning Detection) strokes are plotted on top. $t = 0$ indicates January, 30th, 2019, 17:02:48.525 UTC. **b** Photometer signals around the blue corona discharge. **c**, **d** 337.0 nm (**c**) 777.4 nm (**d**) MMIA camera images projected at an altitude of 16 km. GLD strokes occurring within the integration time are displayed as orange dots. Figure reproduced from (Dimitriadou et al. 2022)

nm bandwidth) ratios > 2). The filtering was performed by selecting a 3° × 3° area centered at the sub-ISS point and within 1 s before and after the maximum peak in PHOT3 which resulted in about 9000 events. Subsequently, these were filtered for all events where the peak in PHOT2 occurred any time after the highest peak in PHOT3 and where the peak current of the CG stroke was larger than 20 kA to minimize contamination by intracloud flashes. The first confirmed sprite observation from the ASIM cameras was obtained with this method on October 7th, 2019. More tests are necessary to better validate the method.

This event occurred over the Dulombi-Boe National Park in Guinnea-Bissau. The flash started at 21:53:16 UTC including a positive CG stroke at 21:53:16.999 with a peak current of 21 kA. Then, a second stroke with a peak current of 41 kA at 21:53:17.547 UTC occurred (Fig. 21). This stroke produced the usual 777.4 and 337 nm signals, however it was followed by two strong far ultraviolet (FUV) peaks (in PHOT2): one 7.5 ms and the other 16.5 ms after the peak 777.4 nm luminosity of the stroke. The flash luminosity of the +CG stroke evidences the difference in the scale of luminosity in PHOT2 between the stroke and the sprites. These are the signatures of sprites in photometer measurements as these wavelengths are strongly absorbed in air; therefore they must come from a high altitude and they are not accompanied by any 777.4 nm signal.

The camera images for two frames are shown in Fig. 22 where the top row are the images in 337 nm, the middle row are the images in 777.4 nm and the final row shows the log of the ratio between the previous two images. A close inspection of the ratio image for frame 9 (left) reveals a faint filamentary structure at about 11.9° N, 14.55° W (indicated with the red circles). This structure presents several elongated and thin elements different from the scattered luminosity of the cloud illuminated by the flash. Its shape is characteristic of wishbone sprites observed from the ground with tendrils streaming up from the main body (Bór 2013). Furthermore, in frame 10 (right) there are sets of filaments clearly visible in CHU1 (337 nm band) which do not appear in the 777.4 nm band, that resemble column sprites with lower tendrils (Bór 2013). The two sprite elements are shown with the red circle south west of the brightest

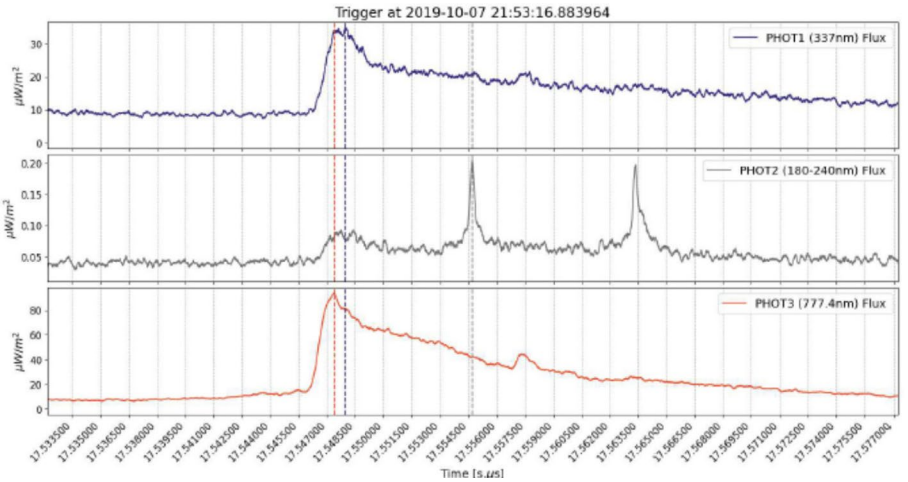

Fig. 21 The data of the 3 photometers associated with the lightning stroke with a peak current of 41 kA at 21:53:17.547 UTC. The dashed lines indicate the timing of the highest value of the photometer signal in the corresponding color, i.e. the blue one for PHOT1 and the orange one for PHOT3. Figure adapted from (Gomez Kuri 2021)

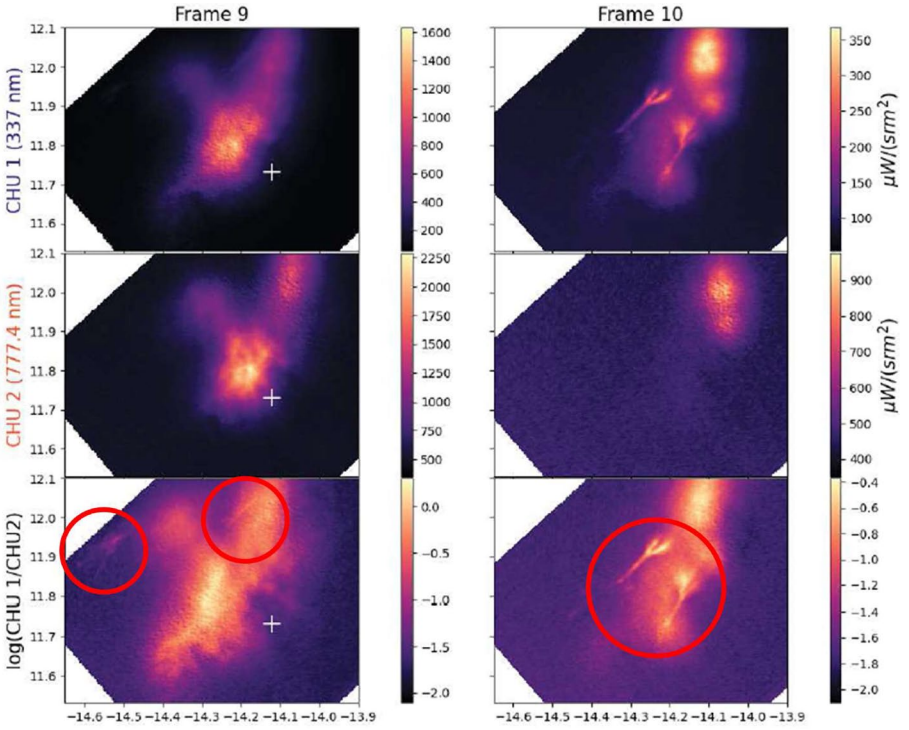

Fig. 22 The CHU camera images of the frames 9 and 10 (including the stroke and the sprite signals, respectively). CHU1 (CHU2) is the camera in 337 (777.4) nm wavelength, and lastly the log of the ratio between the two is displayed. The y-axis shows the latitude, ranging from approx. 11.6° to 12.1° N; the x-axis shows the longitude ranging from approx. 14.6° to 13.9° W. This region is located in western Africa. The colorbars show the intensity in CHU1 and CHU2 (first two rows) as well as their ratio (last row). The location of the lightning stroke associated to this event is marked with a plus sign. The sprite event is marked by a circle. Figure adapted from (Gomez Kuri 2021)

luminosity of the stroke which is centered at 12° N, 14.1° W in the ratio image. Structures like these have not yet been found in other MMIA observations. As within the previous frame, the sprites here are visible in CHU1 even though there is no signature in the photometer data (see Fig. 21) also invisible in Fig. 31). An explanation to this is that there is a continuing current in the stroke channel producing luminosity in photometers 1 and 3, but the luminosity in 337 due to the stroke is higher than that emitted by the sprites (which would be visible in the 337 nm band, but not in the 777.4 nm band; note the scale in Fig. 22). These observations are made at a relatively low angle as the ISS is about 200 km northeast from the location of the flash as shown in Fig. 22, which explains the shape that is observed. Note that this sprite is barely visible in the CHU1 image as the scale of the luminosity includes that of the bright flash, whereas the log of the image shows this feature.

4 Modeling and Scientific Computing

Observations in nature (Sects. 2 and 3) and experiments in the laboratory (Sect. 5) determine light or electromagnetic waves or energetic radiation, but in most cases they do not give direct access to the local distribution of electric fields or to density and energy distributions of free electrons, ions or excited molecules. Such complementary information can be gained from simulations, in particular, if they are validated, i.e., if their predictions on the emission of light etc. agree reasonably with observations. A simulation can also demonstrate physical mechanisms in general, and it can predict phenomena, that have not been observed yet.

Within the SAINT network several microphysics based models were used. A major task was to bridge the gap from molecular input (like energy dependent cross sections of electron molecule collisions) to macroscopic predictions. The models were applied to electric discharges and extended to new phenomena, parameter regimes and to new computational techniques. A substantial amount of work was devoted to streamer discharges that occur during the early stages of a gas discharge, and that are stabilized by the nonlinearity of space charge effects.

The present modeling section is organized in 4 subsections: 4.1. new results on single axially symmetric streamers, 4.2. interacting and branching streamers, 4.3. streamers in inhomogeneous and moving air, and 4.4. modeling of terrestrial gamma-ray flashes.

4.1 Modeling Single Streamers

Microphysics based streamer models start from the motion of free electrons in electric fields and from their collisions with gas molecules that are treated as a background. Emission of photons from excited molecules and ionization of molecules by these photons is another essential mechanism, in particular in air. Electrons and photons can either be treated as particles (taking their discrete nature into account), or they can be approximated as densities. If they are treated as densities, we get a so-called fluid model, which we call classical fluid model in the case of the local field approximation (LFA) (Nijdam et al. 2020). LFA is used in all fluid simulations in this section; only for stagnating streamers will corrections be discussed.

Single streamer discharges in homogeneous electric fields mostly can be approximated as axially symmetric, therefore they can be modeled with only two spatial coordinates, a radial and a longitudinal one, denoted as r and z. On the other hand, streamers can destabilize and branch, in which case at least the photons need to be treated as discrete (Bagheri and Teunissen 2019; Wang et al. 2024), and the simulation needs to resolve phenomena in full three spatial dimensions. To model electron runaway and highly energetic radiation, the statistical evolution of electron need to be resolved with a particle model as well.

In recent years, different particle and fluid codes for single positive streamers in air have been bench-marked against each other. First, implementations by 6 different groups of the fluid model in axial symmetry were bench-marked and discussed in (Bagheri et al. 2018). Second, fluid models treating the ionizing photons either as a density or as discrete particles agree for propagating streamers (Bagheri and Teunissen 2019). Third, the solutions of particle models (PIC-MCC) and fluid models for the electron dynamics both in axial symmetry and in full three spatial dimensions also agree well (Wang et al. 2022), as long as the

cylindrical symmetry is not broken. In case of broken symmetry, indeed axially symmetric models lose their validity.

It should be noted that negative streamers were not investigated on an equal level with positive ones, because many investigations were motivated by technical applications where positive streamers are more relevant, because they emerge and propagate more easily.

This progress in implementation and bench-marking different streamer simulation approaches has formed the basis for further studies of the physical properties of single streamers within the SAINT project, as described below.

4.1.1 The Properties of Steady Streamers

Most simulations of single streamers show an accelerating head with growing radius. The head leaves a weakly ionized channel behind. Such simulations can be preformed relatively easily nowadays (Bagheri et al. 2018).

However, if the background field is substantially weaker, streamers accelerate less, or they propagate steadily, or they slow down and stop. An example of an accelerating and a steady positive streamer is shown in Fig. 23. The medium is dry air under normal conditions. On the right half of the Figure, 4 time steps in intervals of 17.5 ns are shown of an accelerating streamer in an electric field that equals about half of the breakdown field. The radius of the streamer head increases while it is propagating, and there is a

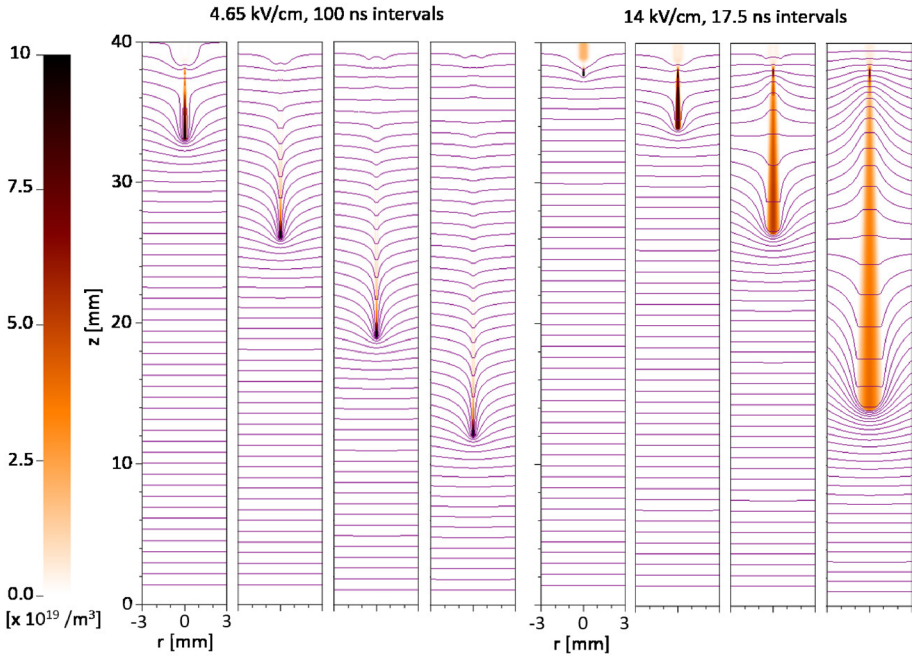

Fig. 23 Steadily propagating streamer (left) and accelerating streamer (right). The steady streamer propagates in a field of 4.65 kV/cm$\approx 0.15E_k$ and is shown in time intervals of 100 ns, the accelerating streamer propagates in a field of 14 kV/cm$\approx 0.44E_k$ (where $E_k = 3.2$ MV m^{-1} is the classic breakdown field at standard temperature and pressure) and is shown in time intervals of 17.5 ns. Shown are the electron density and the equipotential lines. Figure reproduced from (Francisco et al. 2021)

substantial electron density (color-coded) along the whole length of the channel. The equipotential lines indicate the electric field distribution and therefore also the charge distribution: there is a growing positive charge at the streamer tip, and a growing negative charge at the back.

The left half of Fig. 23 shows a steady streamer. The background electric field is only about one sixth of the breakdown field, and the time step between the panels is as large as 100 ns. There are important differences compared to the accelerating streamer:

• The streamer propagates with constant velocity. Its radius and overall shape, including the back part, do not change within a co-moving frame.

• The electron density largely disappears at some distance behind the streamer head due to attachment and recombination.

• The equipotential lines become quite straight again at some distance behind the streamer head, so there is no substantial charge left behind.

As a consequence of these observations, steady streamers carry a fixed amount of positive charge in their front part and only negligible charge at their back part. They lose conductivity at the back, and they leave an equal amount of positive an negative ions behind on their trace. Therefore from a sufficient distance a steady streamer resembles a positively charged monopole located approximately at the head.

The transition from accelerating to steady propagation was first found in a study of the effect of enhanced electron attachment rates in the ionized steamer channel, in the context of discharges in insulating gases for high-voltage engineering (Francisco et al. 2021). But then the same transition from accelerating to steady motion was found in air as well when the background field was varied while the electron loss rate was kept fixed (Francisco et al. 2021).

The observation of steady propagation initially led us to conclude in (Francisco et al. 2021) that the background field of 4.65 kV/cm is the stability field in air at ground pressure. The existence of a stability field was postulated at least 60 years ago, if we use the definition of a streamer propagating with constant velocity and shape. Meanwhile the stability field has become a general concept in high voltage engineering and lightning research. For other definitions of the stability field and their discussion, we refer to (Francisco et al. 2021).

However, more recent studies (Li et al. 2022) have shown that the stability field in a given gas composition is not unique. Rather the steady propagation depends both on the background field and on the streamer radius; the larger the radius, the smaller the background field in which the streamer can propagate steadily. Numerical evidence for these statements on positive streamers in air is given in (Li et al. 2022), and some properties of steady streamers with velocities ranging from 3×10^4 to 12×10^4 m/s are elaborated in that paper.

The same multiplicity of steady solutions was found for negative streamers as well (Guo et al. 2022). But the lowest background field in which a negative streamer was found to propagate steadily, was 9.19 kV cm^{-1}, while steady positive streamers would propagate in a background field as low as 4.05 kV cm^{-1}. The properties of steady negative and positive streamers differ substantially also in other respects. For example, for steady negative streamers, the ratio between streamer velocity and maximal electron drift velocity ranges from about 2 to 4.5, and can never drop below 1 (Nijdam et al. 2020), whereas for steady positive streamers this ratio ranges from about 0.05 to 0.26 (Li et al. 2022; Guo et al. 2022).

Steady streamers do not depend on time when analyzed in a co-moving coordinate system. Therefore error control in model reduction is easier to achieve. First steps in this direction are taken by Bouwman et al. (2023) where the space charge layer is integrated

out, and a new and better approximation for the electron density behind the ionization front is found. Further steps in this direction are presently being taken.

4.1.2 Stagnating and Fading Streamers

Steady streamers are easier to parameterize than those with changing shape and velocity, and they can serve as a proxy for analytical model reduction. However, they are dynamically unstable, hence they easily accelerate or slow down (Li et al. 2022). In that sense they are like a separatrix between different asymptotic behaviors. Simulations of the slowing down and stopping of single positive streamers are numerically challenging, and progress was made during the SAINT project both by the DTU and by the CWI group. In the following, we use the term “stagnation" for the stopping of positive streamers, and “fading" for negative streamers.

Niknezhad et al. (2021) observed the unstable behavior of the positive streamer head when it propagated away from the anode toward its stagnation: The electric field diverged while the streamer was slowing down. A similar behavior has been reported in multiple numerical studies of positive streamers (Pancheshnyi and Starikovskiy 2004; Starikovskiy et al. 2021; Francisco et al. 2021). In (Niknezhad et al. 2021b), we proposed that this behavior arises from the local field and density assumption on the drift-diffusion equation. Using an extended model which takes the non-local nature of the ionization source term into account will lead to a stable and physical behavior.

We simulated a positive streamer in air using two different models, one using a drift-diffusion model with local field approximation and the other using an extended description of the ionization term (Niknezhad et al. 2021b). Fig. 24 shows the electric field at the streamer tip as a function of streamer length (top) and the electron density profile along the streamer axis at different time instants (bottom) for both the local and the extended

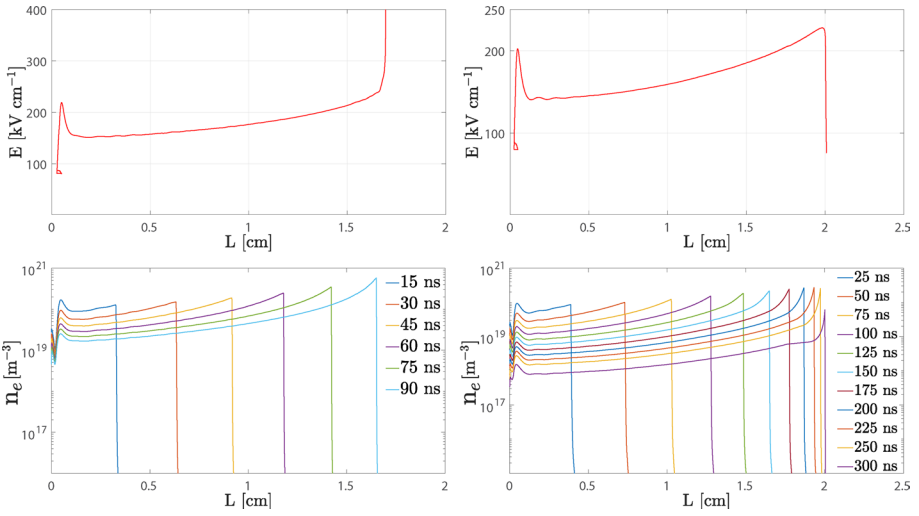

Fig. 24 Streamer tip electric field vs. streamer length (top) and the electron density profile at different instants in time (bottom) for the local model (left) and the extended model (right). Figure reproduced from (Niknezhad et al. 2021b) in agreement with the CC BY 4.0 licence (`https://creativecommons.org/licenses/by/4.0/`)

model. The extended model results in a decelerating positive streamer where the electric field remains bounded and eventually fades away. However, the local model leads to an unbounded and nonphysical electric field in the streamer tip. Therefore, we recommended using models with higher moments of Boltzmann equation for accurate modeling of positive streamer stagnation.

The positive streamer simulation using the extended model showed that as the streamer propagates away from the anode, its diameter reduces and the streamer velocity continuously decreases. A very interesting observation was that the trend in the decrease of the streamer diameter reverses when the streamer velocity lowers to values close to that of the positive ions in the streamer tip. The streamer charge layer then starts to widen and the streamer radius grows which leads to a drop of the streamer tip electric field and the eventual stagnation of the streamer. This highlights the important role of the positive ion motion in the stagnation process of the positive streamers and why the assumption of immobile ions needs to be relaxed to model the positive streamer stagnation accurately.

The problem of diverging fields at the heads of stagnating streamers was also analyzed at CWI in (Teunissen 2020; Li et al. 2022). Within the local field approximation, nonphysical effects can occur when there is diffusion parallel to the electric field. In particular, the electron energy is then erroneously determined by the local field, and does not correspond to the electron's previous path within the configuration of the electric field. Several methods to avoid this artifact were compared in (Teunissen 2020) where an earlier approach (Soloviev and Krivtsov 2009) was compared with two new approaches. All methods could prevent the numerical issues arising in one-dimensional tests. A correction factor as given in (Soloviev and Krivtsov 2009; Teunissen 2020) was then used for the studies of stagnating positive streamers in (Li et al. 2022), and it prevented the divergence of the field.

When negative streamers slow down, a very different dynamics occurs: rather than diverging, the field maximum at the streamer tip decreases in time (Guo et al. 2022). This is because the space charge layer around the head here consists of electrons rather than positive ions. The existing electrons at the tip of a negative streamer keep running forward and outward from the tip, even if the impact ionization decreases due to a decreasing electric field. The negative streamer then loses focus and fades away.

4.2 Interacting and Branching Steamers

Simulating streamer discharges is computationally demanding, especially when cylindrical symmetry is not applicable and a full three-dimensional representation of the system is required. Simulations in homogeneous media are presented in the present subsection, and streamers in inhomogeneous and moving media in the next section.

4.2.1 Studying the Collective Behavior of Streamers with a GPU-Based Code

Over the past decade many computationally demanding applications have shifted towards using general-purpose Graphical Processing Units (GPUs). For suitable tasks, GPUs provide a higher level of parallelism compared to conventional Central Processing Units (CPUs), leading to more scalable codes that leverage recent advances in hardware. However, adapting Adaptive Mesh Refinement (AMR) codes to GPUs has been challenging in many cases.

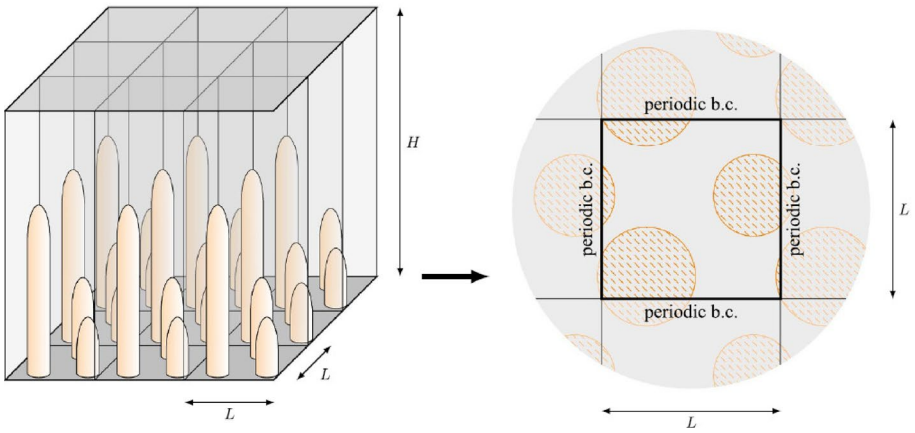

Fig. 25 Configuration for the study of dense streamer fronts employed by (Teixeira-Gomes et al. 2023). The front is modeled as an infinite array of identical square cells, each containing several streamers. Thus an infinitely extended front is reduced to a single cell with periodic boundary conditions (b.c.) on its four sides. Figure reproduced from (Teixeira-Gomes et al. 2023) in agreement with the CC BY 4.0 licence (`https://creativecommons.org/licenses/by/4.0/`)

Within the framework of the SAINT network, we developed a new (fluid-based) AMR streamer code that runs on GPUs. The code was introduced in (Teixeira-Gomes et al. 2023), where it was applied to explore the collective dynamics of dense streamer fronts. Consider a large number of streamers propagating in parallel. While neighboring streamers exhibit strong interactions, the influence of distant streamers can be largely disregarded. Therefore we model the system as an infinite array of identical cells, each containing a manageable number of streamers (see Fig. 25) and satisfying periodic boundary conditions across its four sides. One example of a cell containing four streamers is shown in Fig. 26.

This setup allows us, by considering different numbers of streamers per cell, to investigate the impact of streamer density on the front propagation. We found that a denser packing of streamers leads to weaker electric fields at their tips, weaker internal fields, lower electron densities and a slower propagation. This is illustrated in Fig. 27, which displays key streamer properties for varying numbers of streamers in a cell of constant size. In (Teixeira-Gomes et al. 2023) we presented a simple one-dimensional model of streamer fronts that shows consistency with three-dimensional simulations.

4.2.2 Streamer Branching Simulated with HPC, and Validation

3D simulations can also be performed on CPUs instead of GPUs. To study streamer branching (Wang et al. 2023), about 200 simulations were performed using the Dutch supercomputer Snellius, with each simulation using 32 cores for about a day.

In these simulations, the ionizing photons were presented as discrete particles that would start ionization avalanches at random locations, with a distribution according to the classical Zheleznyak approximation for photo-ionization (Zheleznyak et al. 1982). The parameters of the simulations were chosen to closely resemble those of a lab experiment. The results on branching frequencies, lengths and angles agreed well between simulations and experiments, which validates the model, at least in the considered parameter regime. It

Fig. 26 Example simulation of a cell containing four streamers in the setup of (Teixeira-Gomes et al. 2023). ▶ The upper left panel shows the maximum of the electron density along lines aligned with the x axis. The upper right panel shows the average magnitude of the electric fields along these same lines. The lower two panels contain cuts of the electron density (left) and electric field magnitude (right) at horizontal planes indicated by the dashed lines in the upper panels. Figure reproduced from (Teixeira-Gomes et al. 2023) in agreement with the CC BY 4.0 licence (`https://creativecommons.org/licenses/by/4.0/`)

is interesting to note that the results are very sensitive to the detailed form of the Zheleznyak approximation (Wang et al. 2023).

We note that simulations and lab experiments of propagating, axially symmetric streamers already had been compared in (Li et al. 2021), with convincing results.

4.3 Streamers in Inhomogeneous and Moving Air

An inhomogeneous medium can have a strong influence on streamer evolution. If the gas is moving or if it has an inhomogeneous density or composition due to shock fronts or previous discharges, new phenomena occur. Within the SAINT project, all three types of phenomena have been studied.

4.3.1 Streamers in Unsteady Air

The study of the effects of airflow on streamer discharges is important as, in real-world scenarios like lightning strikes to wind turbine blades, the air is not stationary. A relatively recent experimental study on the effects of lateral wind on positive and negative streamer discharges showed a clear tilting of positive streamers in the direction of the wind (Vogel and Holbøll 2018). In order to understand the physical mechanism with which the airflow can affect the streamer discharges, we developed a three dimensional model which couples the dynamics of streamer discharges and the airflow (Niknezhad et al. 2021). The model uses adaptive mesh refinement, unstructured mesh, and implicit ELP (which is the Exact integration of the Linear Part of densities) time integration scheme (Beylkin et al. 1998) to overcome the challenges of simulating a discharge over a long period of time as the effect of airflow on discharges can manifest on ion-timescales (Niknezhad et al. 2021).

We designed a simulation which follows the initiation, propagation and stagnation of two successive positive streamers originating from a needle tip (length of 2 cm and width of 1 mm) with an applied voltage of 8.5 kV while being exposed to a lateral wind of 50 m s^{-1}. Figure 28 shows that the 1st streamer experiences minimal deflection during its propagation ($t < 1\mu s$). However, after the streamer stagnation the streamer channel continuously tilts in the direction of the wind over the next 50 μs. During this time the streamer channel remains continuously attached to the anode due to the ionization maintained by the flow of electrons from the streamer channel toward the anode.

The 2nd streamer then initiates within the remnants of the previous streamer channel which is now moved toward the trailing edge of the anode. After the propagation of the 2nd streamer its channel will experience a similar deflection as the 1st streamer, leading to an even more pronounced tilting in the direction of the airflow, see Fig. 29. This is in agreement with the experimental findings in (Vogel and Holbøll 2018).

In (Niknezhad et al. 2021a), we extended our study of airflow effects on streamer discharges by modeling the influence of airflow on negative coronas of Trichel type pulses (Trichel 1938). We simulated two successive negative corona pulses and investigated their behavior when exposed to a lateral wind. The simulation results showed that

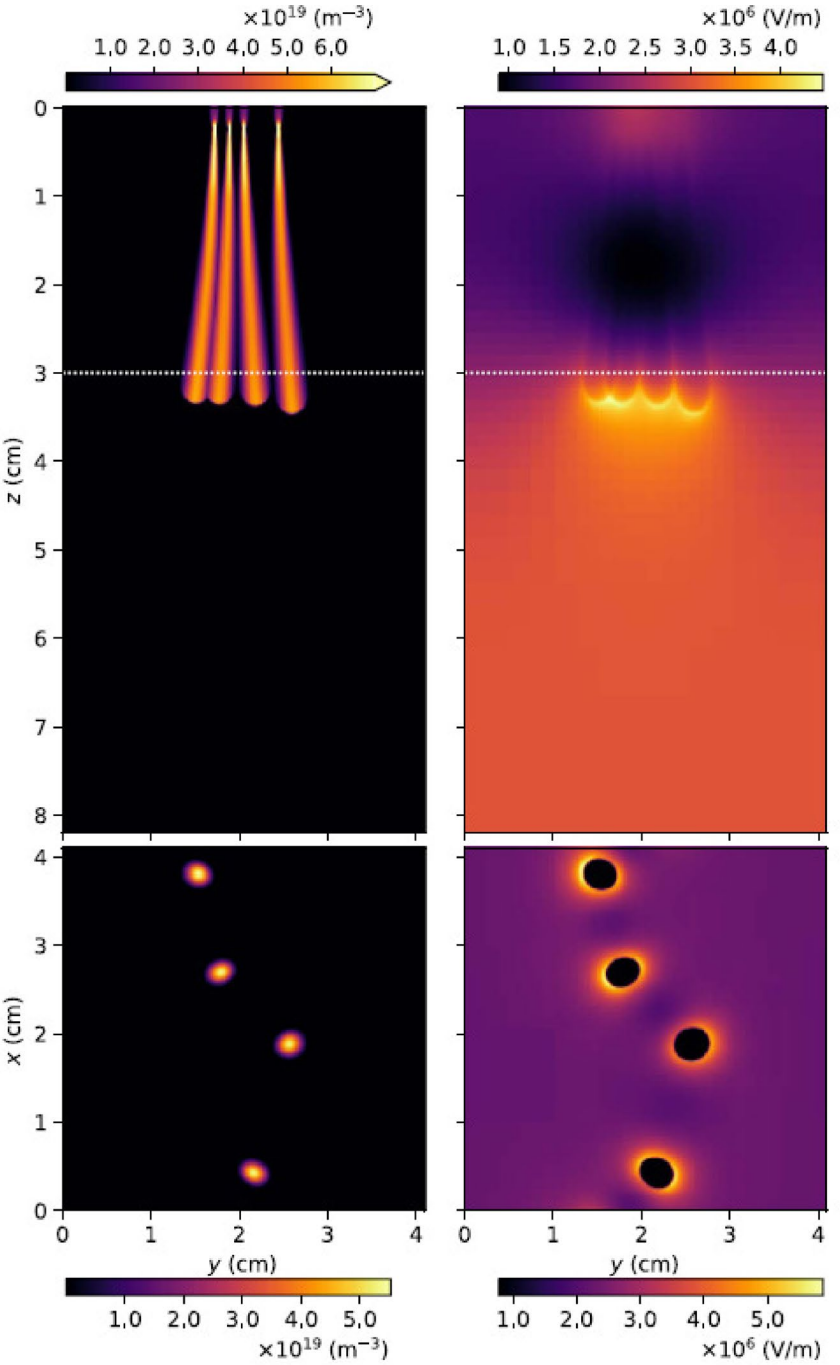
×10^19 (m^−3)
1,0 2,0 3,0 4,0 5,0 6,0
×10^6 (V/m)
1,0 1,5 2,0 2,5 3,0 3,5 4,0
z (cm)
x (cm)
y (cm)
y (cm)
1,0 2,0 3,0 4,0 5,0
×10^19 (m^−3)
1,0 2,0 3,0 4,0 5,0
×10^6 (V/m)

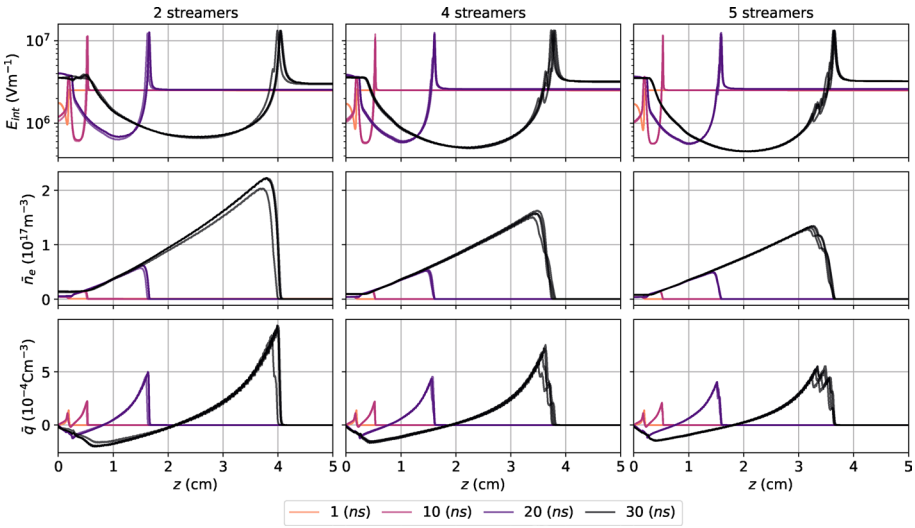

Fig. 27 Representative quantities of the evolution of a streamer front for different numbers of streamers inside a cell and at several time steps. The upper panels display a measure of the electric field inside the streamer channels; the middle and lower panels show the cross-sectionally averaged electron and space charge densities, respectively (see (Teixeira-Gomes et al. 2023) for precise definitions). The plots show that a denser packing of streamers leads to slower streamers with more strongly screened electric field and lower electron density in their interior. Figure reproduced from (Teixeira-Gomes et al. 2023) in agreement with the CC BY 4.0 licence (`https://creativecommons.org/licenses/by/4.0/`)

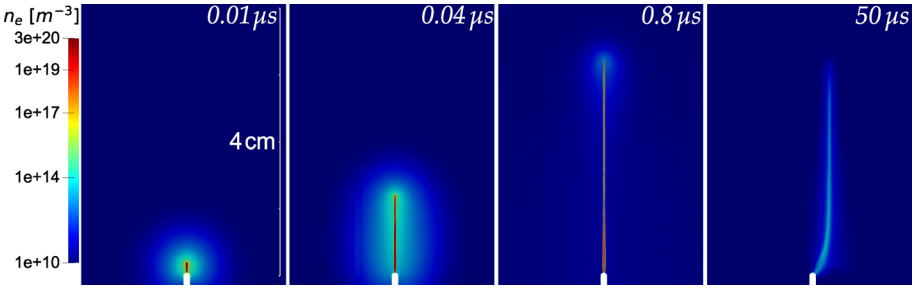

Fig. 28 Electron density n_e contour plots for the 1st streamer shown at multiple time instants. Minimal streamer channel deflection during the propagation phase. However, large deflection of the streamer channel is observed during the 50 μs post-stagnation. Figure reproduced from (Niknezhad et al. 2021)

the mechanism causing the displacement of positive streamers has negligible impact on streamers of negative polarity. The main reason is that, unlike the positive streamer case, the electrons remaining from the previous negative streamers are pushed away from the cathode toward the low electric field regions which are then removed due to the strong attachment processes. Therefore, the role played by the space charges remaining from the previous negative streamers is negligible in displacing the subsequent negative streamers. There is, however, a small displacement of the 2nd negative streamer in the direction of the wind, which is attributed to the movement of the charges while

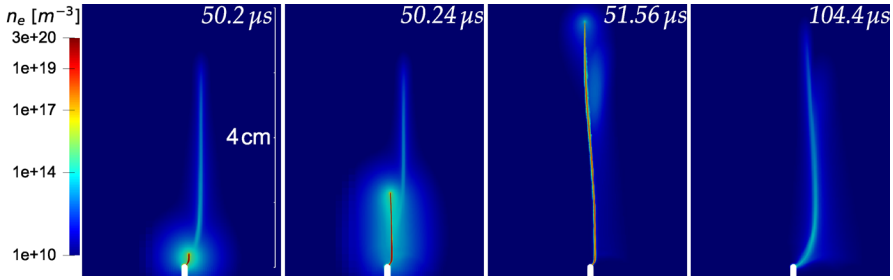

Fig. 29 The electron density n_e contour plots of the 2nd streamer at different time instants. Figure reproduced from (Niknezhad et al. 2021)

the charges are building up for the next streamer formation. These results are consistent with the experimental results reported in (Vogel and Holbøll 2018).

4.3.2 Repetitively Pulsed Streamers

A related problem appears in repetitively pulsed discharges. Repetitive voltage pulses can be a design for applications, or they can appear spontaneously due to some nonlinear charging or discharging mechanism, such as in Trichel pulses. An interesting result of the study (Malla et al. 2023) is that the outcome of repetitive pulsing depends on the time between the pulses, due to the excited and/or ionized species left over from a previous pulse.

If the temporal break between pulses is short enough, the discharge behaves as if no break had occurred, and the second streamer continues where the first one had stopped. For intermediate break durations very little light is emitted, neither from the channel nor from the tip. The channel is still so pre-ionized that it cannot support a streamer discharge with its strong field enhancement, ionization reaction and light emission, but only a rather invisible Ohmic current. And at the streamer tip not enough charge arrives in time to enhance the local field sufficiently and to restart the streamer from there. As a consequence there is hardly any discharge and light emission for intermediate break durations. For even longer break durations the conductivity disappears so far due to electron attachment and recombination that the second streamer propagates rather independently of the first one, with a similar light emission. The modeling results agree qualitatively with earlier experiments (Nijdam et al. 2014).

4.4 Modeling the Generation of Terrestrial Gamma-Ray Flashes

Based on the observation that TGFs occur before the main optical pulse of streamer and leader activity (see Fig. 15), a numerical model was built upon the following approach (Fig. 30): During a leader step, where the leader is supposed to be stationary and only streamer timescales are relevant, low-energy electrons emitted from the leader tip are accelerated in the ambient electric field and trigger the inception of negative and positive streamer coronae. Such coronae subsequently approach each other, enhance the electric field accelerating electrons into the run-away regime, finally producing TGF photons. However, since self-consistent models covering various length, time and energy scales,

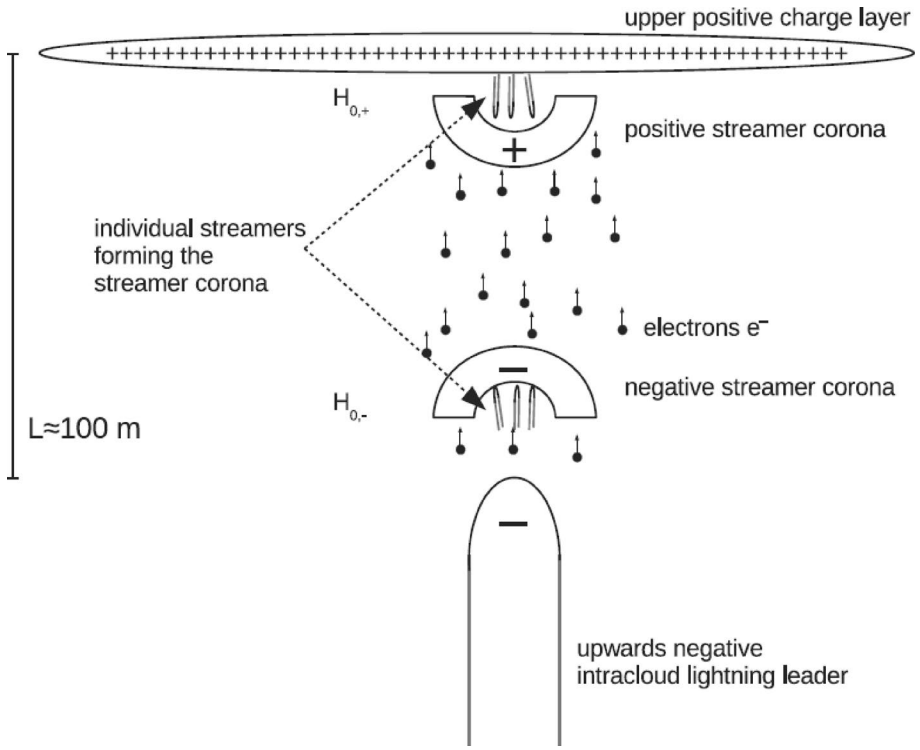

Fig. 30 Model of TGF production based on the observations presented in Sect. 3.2: During a leader step, low-energy electrons (black dots) are ejected and move between the leader tip and the upper positive charge layer (as in a thundercloud) in the direction of the indicating arrows. The accumulation of electrons incepts streamer coronae at the upper charge layer and in the vicinity of the leader tip; these coronae propagate towards each other enhancing the electric field in-between and thus accelerating electrons into the runaway regime. The length $L = 100$ m corresponds to the approximate size of a leader step. Figure adapted from (Köhn et al. 2020)

simulating the whole process from the individual electron motion to the production of TGFs, are not available, a two step approach was chosen where an electron current of 1 kA with initial electron energies of ≈ 2 eV was initiated in a field of $5E_k$ where E_k is the classic breakdown field. Once these electrons bridged the gap between the upper charge layer and the leader tip (Fig. 31a, b), a phenomenological model of the electric field of two encountering streamer coronae was applied such that the electric field in-between locally reaches values above $8E_k$ (Köhn et al. 2020) which is the threshold field for cold run-away. Figure 31c–f shows the spatial and energy distribution of the electrons and the subsequent Bremsstrahlung photons constituting TGFs. Electrons reach energies of up to 300 MeV producing photons with energies of up to 40 MeV, which is in agreement with experimental observations (Marisaldi et al. 2010). The photon energies ϵ_γ can be fitted through $\exp\left(-\epsilon_\gamma/\epsilon_{\gamma,c}\right)/\epsilon_\gamma$ with the characteristic energy $\epsilon_{\gamma,c} \approx 7$ MeV, showing a typical TGF energy distribution (Dwyer et al. 2008). These results, together with the observations presented in Sect. 3.2, indicate that the streamer-leader environment plays a crucial role in the production of TGFs.

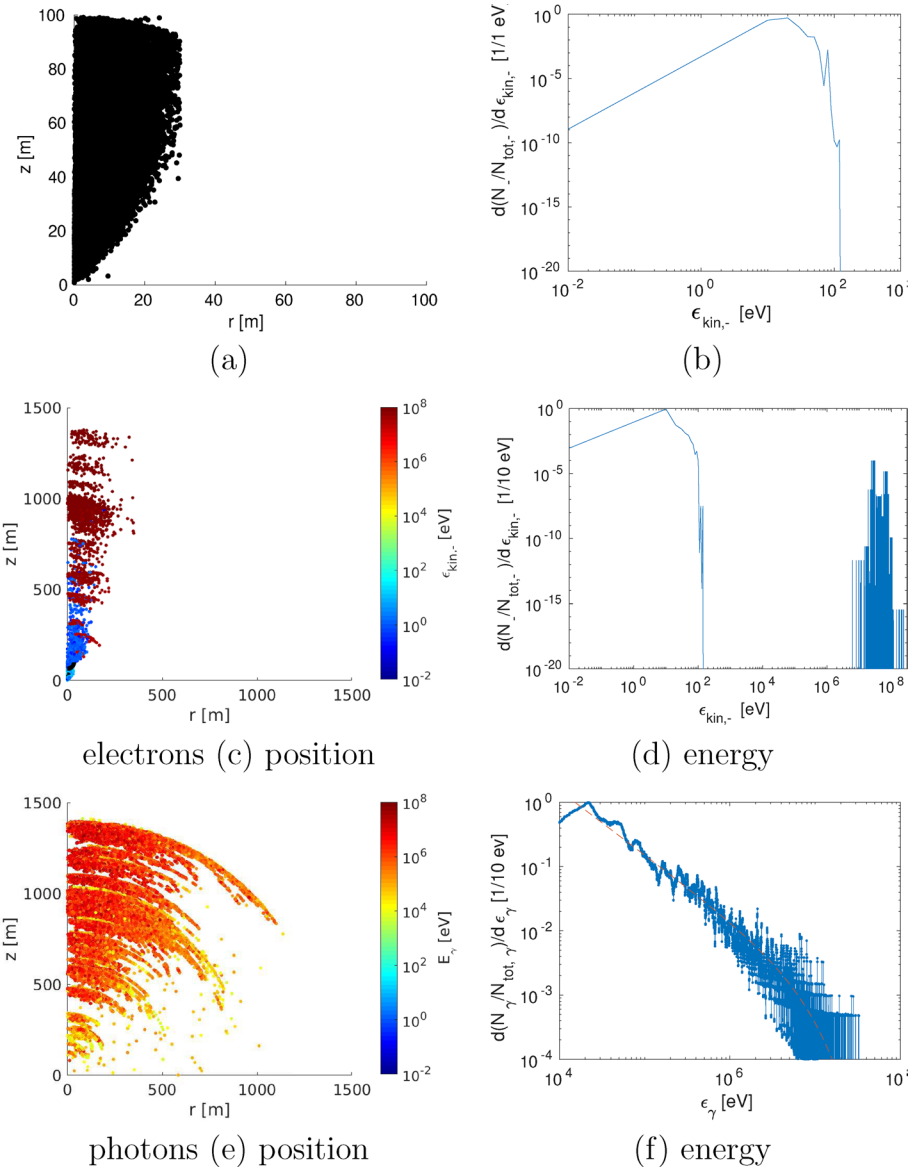

Fig. 31 **a**, **b** The spatial and energy distribution of low-energy electrons in the gap between the leader tip and the upper charge layer after $\approx 16.9\ \mu$s. **c**, **d** The spatial (energy color coded) and energy distribution of electrons after approx. 67 μs. **e**, **f** The associated spatial (energy color coded) and energy distribution of bremsstrahlung photons after the same time step. The dashed line in panel **f** indicates the fit $\exp\left(-\epsilon_\gamma/\epsilon_{\gamma,c}\right)/\epsilon_\gamma$ for the photon energy distribution where ϵ_γ is the photon energy and $\epsilon_{\gamma,c} \approx 7$ MeV is the characteristic photon energy. The energy distributions are normalized to the total number $N_{tot,-/\gamma}$ of electrons/photons. Figure adapted from (Köhn et al. 2020)

5 Experiments and Applications

In addition to ground and satellite observations as well as numerical modelling, laboratory experiments shape an environment to mimic lightning on small scales and thus to study it under controlled conditions. Within the SAINT network, determining discharge properties were approached from various angles. The general approach is to apply a voltage U at two electrodes pointing towards each other; in the case of two plate electrodes the resulting ambient electric field amounts to U/d where d is the distance between two electrodes. In the case of other geometries (such as point electrodes), the local electric field is enhanced because of the electrode curvature (e.g. see Sect. 4.3 for modelling details). The second component of such experiments are the measurement devices to monitor the quantities to be investigated. During the SAINT project, various experiments were performed. At the Technical University of Eindhoven (TU/e) a photomultiplier was used to study the inception times t_{inc} in the vicinity of electrodes (Sect. 5.1). At the Astrophysical Institute of Andalusia (CSIC), the new GALIUS spectrograph was used to perform in-situ measurements of the chemistry associated with discharges (Sect. 5.2) and record the temporal evolution of various chemical species as relevant for lightning. Finally, at Dena Desarrollos S.L. we also perform grounded rod measurements of laboratory discharges and lightning (Sect. 5.3) and determined the temporal evolution of the current, voltage, optical emission as well as of the discharge shape and investigated the streamer-leader transition more thoroughly.

5.1 Discharge Inception

5.1.1 Lightning Initiation Problem

The question of how lightning begins, remains a significant unresolved issue in the field of lightning physics (Dwyer and Uman 2014). The ambient electric field in thunderclouds typically measures no more than 0.4 MV m^{-1}, which is substantially lower than the theoretical breakdown field (E_k) of 1.5 MV m^{-1} at 500 mbar, correpsonding to the usual altitude for lightning inception (Gunn 1948; Williams 1985) (Marshall et al. 1995, 2005). For an electric discharge to initiate, two main factors are essential: electric field enhancement over a considerable distance (to ensure $E > E_k$ for a large region) and the availability of free electrons. The initiation of positive streamers can begin when the electric field around a conductor or dielectric increases, causing free electrons to move towards the charged tip or electrodes, in the opposite direction of the electric field (Mirpour et al. 2020). When these electrons reach the ionization zone, where $E > E_k$ and the electron impact ionization rate surpasses the electron attachment rate, they rapidly multiply through direct impact ionization, forming an electron avalanche. This process continues until the number of electrons in the avalanche surpasses a threshold historically defined by the "Meek criterion," leading to the transformation of the electron avalanche(s) into a streamer discharge (Loeb and Meek 1940; Meek 1940; Montijn and Ebert 2006).

5.1.2 Inception in Air Discharges

The initial electron necessary for this avalanche process may be provided by a cosmic ray ionization event, radioactivity from surrounding materials, or specific gas electron

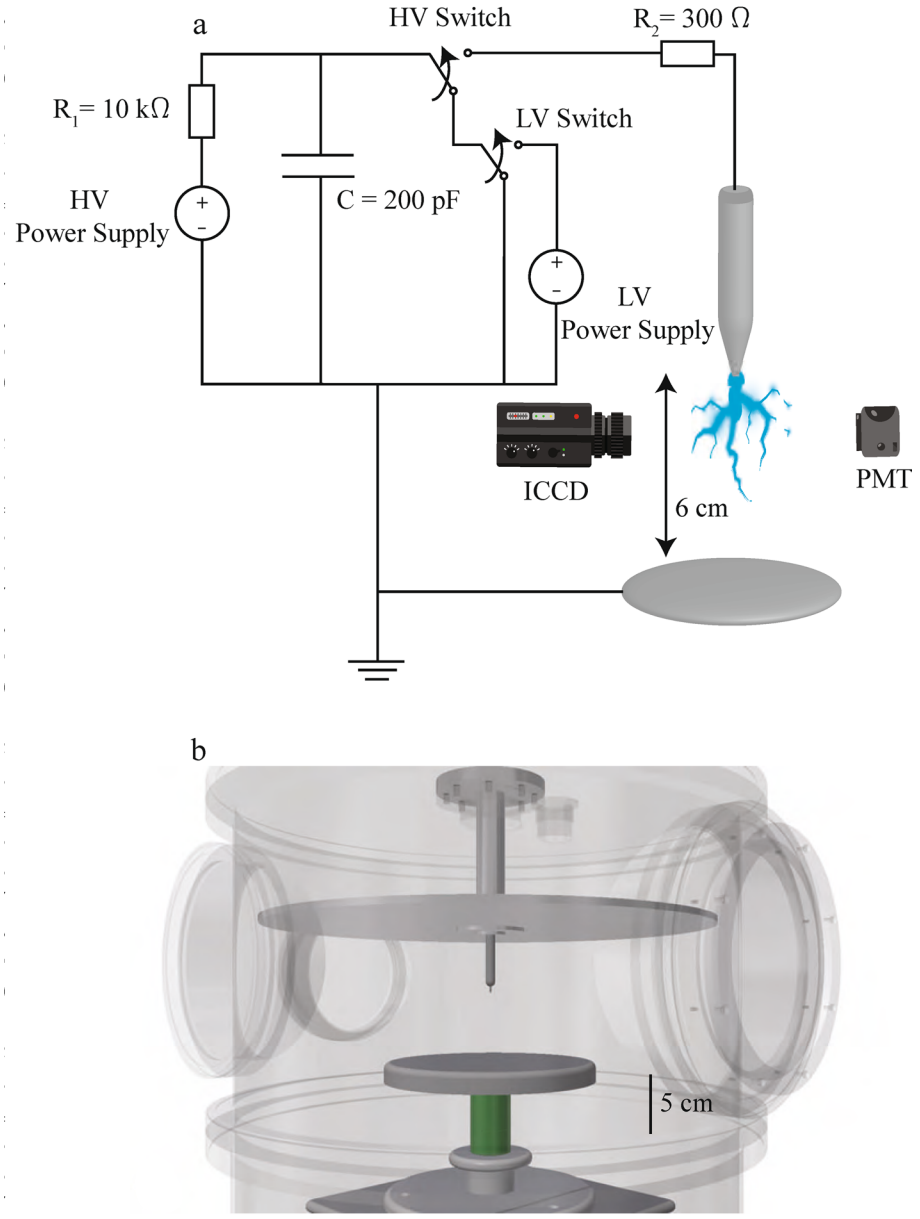

Fig. 32 **a** Schematic view of experimental setup with HV power supply connected to the anode (not to scale). **b** Schematic of experimental vessel. Figure reproduced from (Mirpour et al. 2020) in agreement with the CC BY 4.0 licence (https://creativecommons.org/licenses/by/4.0/)

sources and ion detachment processes. In the laboratory experiments performed during the lifetime of SAINT (Mirpour et al. 2020), a pin-to-plate setup in low-pressure air was used, applying repetitive high-voltage (HV) pulses, see Fig. 32 for the experimental setup. When the voltage reaches a sufficient level, the electrical breakdown

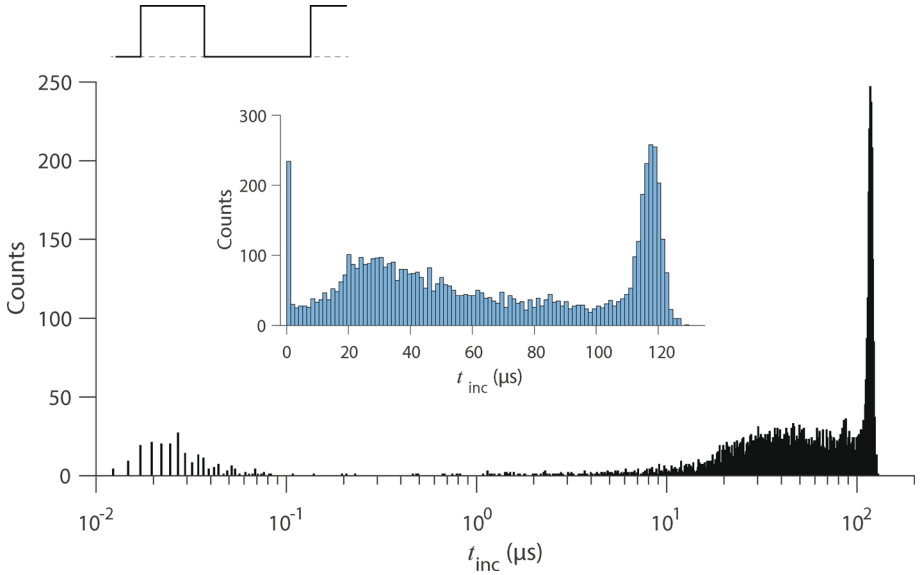

Fig. 33 Histogram of discharge inception times t_{inc} with linear (inset) and logarithmic bins for 6000 discharges in the baseline experiment. For the logarithmic plot (large) the bin size scales with log *t*, but note that for the smallest time scales most bins are empty due to sparse oscilloscope sampling (low sampling rate). The graph in the upper left corner of the figure indicates the voltage waveform, a sequence of high voltage pulses. Figure reproduced from (Mirpour et al. 2020) in agreement with the CC BY 4.0 licence (https://creativecommons.org/licenses/by/4.0/)

process begins, and if the necessary criteria are met, streamer initiation follows from the electrode tip. There is a delay between the high voltage pulse rise and the streamer initiation, primarily due to the time it takes for negative ions to migrate towards the high-electric field region and release electrons there. This time lag, measured using a photomultiplier tube (PMT), varies with operational conditions like voltage level, gas composition, and electrode distance. The experimental setup allows to measure this lag by collecting light emitted by streamers, amplified by the PMT to produce a signal on an oscilloscope. This time lag across 6000 continual pulse trains is collected and analyzed for one set of conditions, creating a histogram of discharge inception times, see Fig. 33.

The figure shows three distinct peaks at different inception times despite only one single peak representing electrons produced by cosmic ray events or electrons detached from O_2^- ions close to the ionization zone. However, these sources could not explain the longer inception times seen in the second and third peaks. A significant difference between the experimental setup and natural lightning is the use of repetitive pulses, where residual charges from previous discharges may significantly influence streamer initiation. To further investigate this, a pre-pulse at a much lower voltage than the high-voltage pulses was introduced to manipulate the position of residual charges before each discharge. By varying the pre-pulse conditions, the third peak can be shifted to earlier or later times, depending on the polarity of the voltage Mirpour et al. (2020). This adjustment demonstrates the influence and presence of residual charges in the discharge gap under repetitive pulsed conditions. Despite these insights, many questions remain

unanswered. For example, the second peak did not shift when pre-pulses were applied, suggesting it might be caused by electron detachment from neutral species.

5.1.3 Discharge Inception from Artificial Hydrometeors

Returning to the initial question of how lightning is initiated under low electric fields, a compelling hypothesis involves the role of ellipsoid hydrometeors. Due to the high dielectric permittivity of ice ($\epsilon = 90$ at low frequencies), the electric field around the tip of a

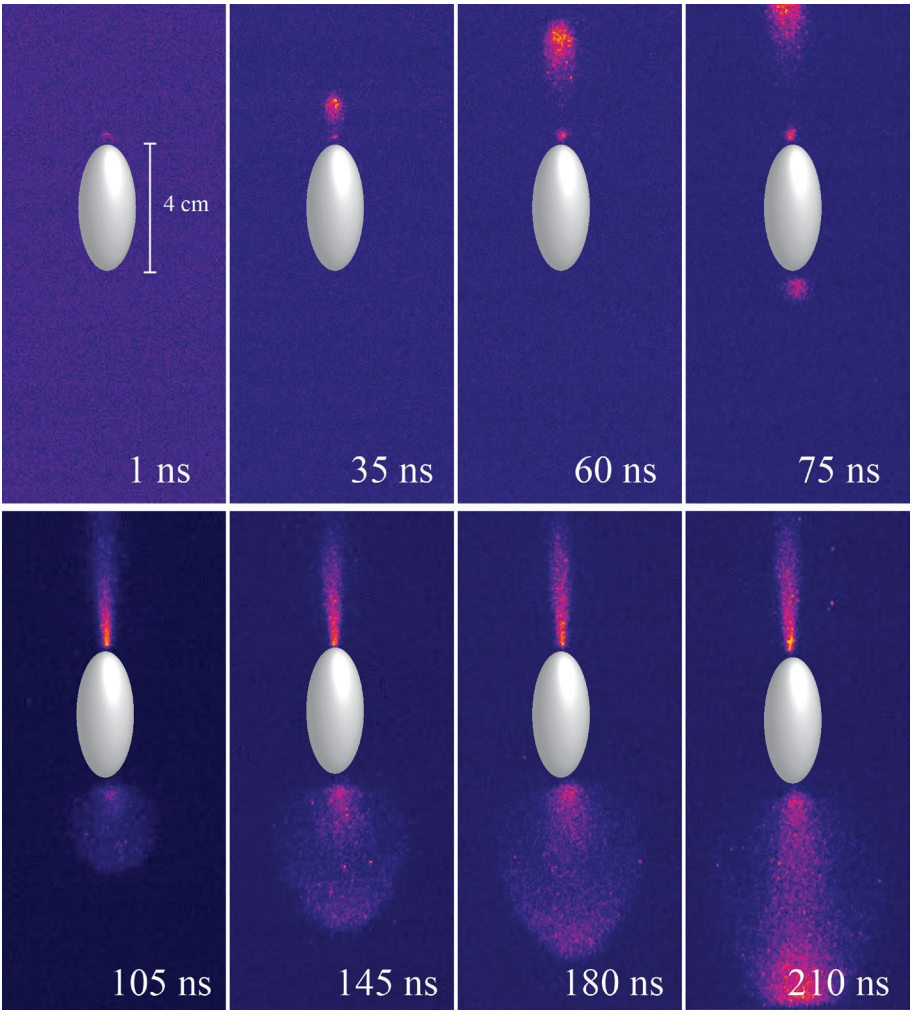

Fig. 34 Phase resolved images of bipolar discharge development from a dielectric particle with L = 4 cm and aspect ratio (minor axis/major axis) = 0.44 in 50 mbar air with a voltage of $V = 15$ kV in a gap of 15 cm. The camera gate time is 5 ns and the exposure start time with respect to the high voltage pulse is indicated in each image. Each image was taken from a different discharge event under the same conditions. Figure reproduced from (Mirpour and Nijdam 2022) in agreement with the CC BY 4.0 licence (`https://creativecommons.org/licenses/by/4.0/`)

hydrometeor could be sufficiently enhanced, potentially exceeding E_k. A numerical analysis (Peeters et al. 2022) revealed that the background electric field at the tip of a hydrometer ranges between $0.07E_k$ and $0.8E_k$ for elliptical particles with aspect ratios between 0.01 and 1. During SAINT this model was experimentally validated by suspending TiO_2 dielectric particles, which have a close dielectric profile to ice, between two parallel electrodes (Mirpour and Nijdam 2022). The results indicate that longer and sharper particles require lower background fields to initiate a discharge. Experimentally, a dielectric particle of 40 mm in length with an aspect ratio (minor axis/major axis) of 0.044 could initiate a discharge at $0.3E_k$. Furthermore, bipolar streamers develop from both the top and bottom of the hydrometer, see Fig. 34. The positive streamer typically initiates earlier than the negative streamer, due to a lower breakdown threshold. Negative streamers were observed to be thicker compared to positive streamers.

5.2 In-situ Measurements of Chemical and Physical Parameters

Laboratory experiments also allow to study the chemical and physical parameters of electric discharges in-situ. Figure 35 shows the GrAnada LIghtning Ultrafast Spectrograph (GALIUS) (Passas-Varo et al. 2019): a portable, ground-based spectrographic system intended for the spectral analysis of various electrostatic discharges. GALIUS includes a set of four interchangeable prisms covering different spectral ranges and a set of ten collector lenses. It has been designed to measure spectra of the light emitted from natural, triggered lightning, and laboratory electrostatic discharges, at recording speeds of up to 2.1 Mfps with spectral resolutions ranging from 0.29 nm to 0.76 nm. With different configurations of GALIUS, physical parameters of the lightning channel, such as electron density or gas temperature, amongst others, can be estimated.

GALIUS was first tested with short sparks (4 cm long) created by a Wimshurst machine at CSIC, Granada (Institute of Astrophysics of Andalucia). It was then moved to Barcelona to capture images of bigger laboratory electrical discharges generated by a 2.0 MV Marx generator. These discharges were generated at 800 kV with one-meter gap, by two different mechanisms: Switching impulse mode (SI) and Lightning impulse mode (LI). In the SI mode, the voltage rises to its maximum in 100 μs and then discharges, estimated peak current of 125 A. In the LI mode, the voltage immediately rises to its maximum in 0.5 μs and stays at the peak for 2-3 μs, and then it suddenly discharges; the estimated peak current is 3000 A. Spectral images of laboratory discharges

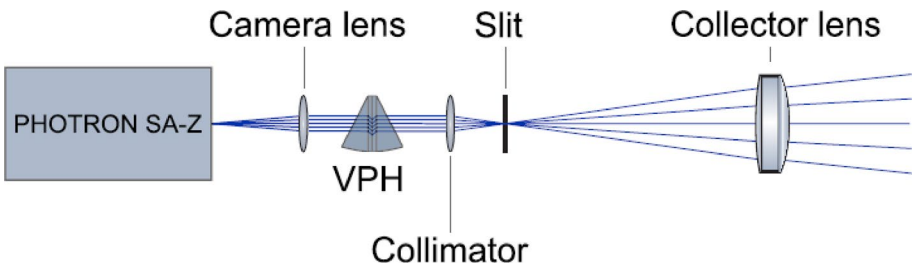

Fig. 35 Scheme of the GALIUS imaging spectrograph. VPH indicates the volume phase holographic (VPH) diffraction gratings. Figure reprinted with permission from (Passas-Varo et al. 2019) © Optical Society of America

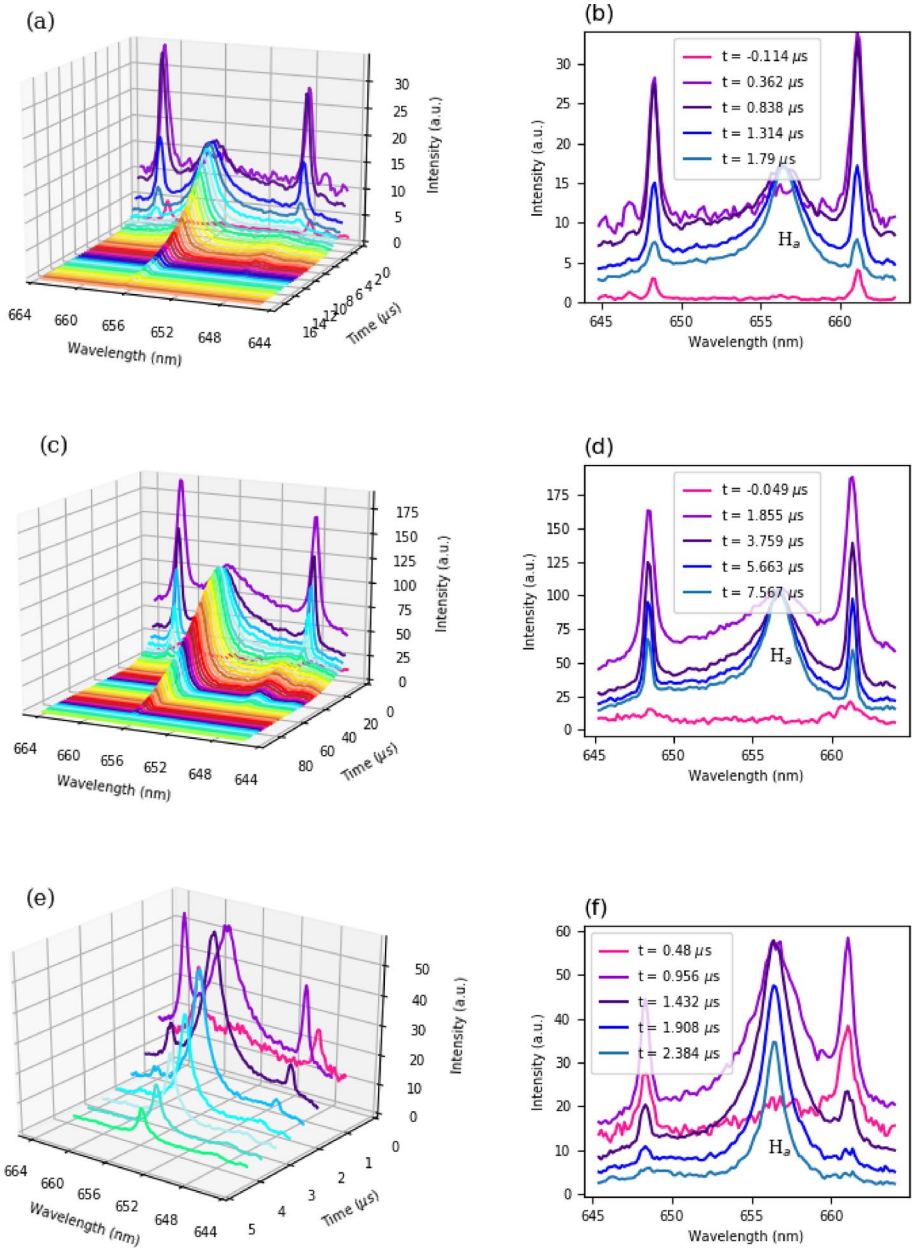

Fig. 36 Time-resolved spectra of meter long lightning-like discharges produced with the switching impulse (SI) mode (**a**, **b**) and lightning impulse (LI) mode (**c**, **d**) of a Marx generator. Panels (**e**) and (**f**) show time-resolved spectra of a 4 cm long spark produced with a small electrostatic generator. In these discharges, the peak intensities and voltages reached 0.125 kA and 0.8 MV in the SI mode, 3 kA and 0.8 MV for the LI mode, as well as 0.350 kA and −55.0 kV for the electrostatic spark. The panels in the right column show the six initial times for the SI mode (**b**) and electrostatic discharges (**f**) and six selected (not consecutive) instants in the temporal evolution for the LI mode. Figure reproduced from (Kieu et al. 2020)

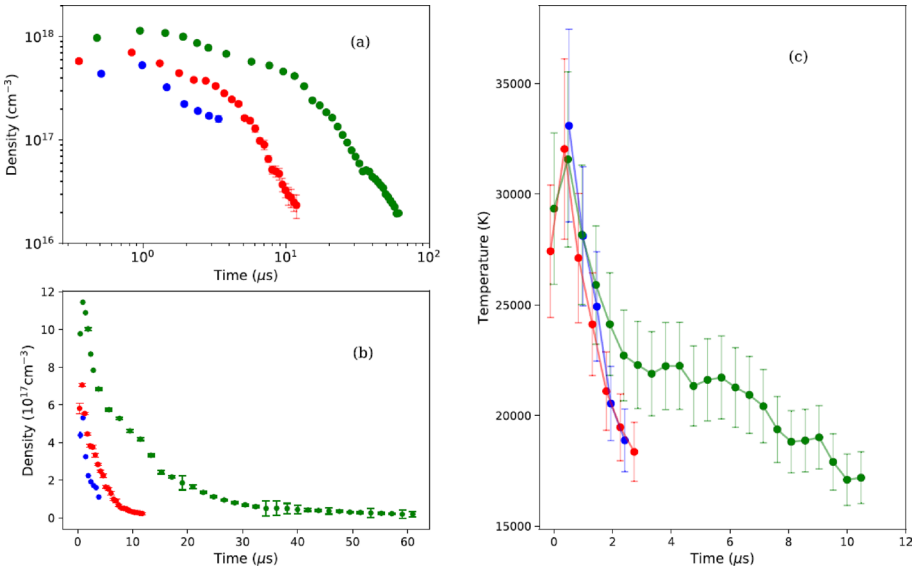

Fig. 37 Temporal evolution of the measured electron density (**a** logarithmic; **b** linear) and temperature (panel **c**) for meter long lightning-like discharges (red dots: switching impulse mode (SI); green dots: lightning impulse mode (LI)) and small spark (blue dots) discharges. Due to very weak Hα signal, the electron density could not be measured at −0.120 μs (SI) and at $t \approx 0$ (LI). Time was measured from the moment the camera was triggered from the spark, with negative values indicating the period before the trigger. Figure reproduced from (Kieu et al. 2020)

were recorded at 2.1 M frames per second (0.476 μs per frame) with an exposure time of 160 ns, providing a high spectral resolution of 0.38 nm within the visible spectral range (645-665 nm).

Figure 36 shows the time-resolved spectra of different laboratory-produced lightning-like discharges produced by different mechanisms with different scales (Kieu et al. 2020). The measured spectra were compared with synthetic spectra, demonstrating that the Boltzmann equilibrium was maintained at very early pre-trigger times. The temporal evolution of black-body radiation and self-reversion calculated from two singly ionized N II (648.20 and 661.05 nm) lines and the Hα line, revealed distinct differences between meter-long discharges and short spark discharges in their optical thickness. The optical thickness of meter-long discharges is influenced by their overpressure. However, the optical thickness of short sparks appears to change little with time.

Figure 37 shows quantitative calculations based on the time-resolved data from different laboratory discharges (Kieu et al. 2020). The gas temperature of these discharges exhibits an approximately equal peak value of ≈ 32000 K, while the peak values of electron densities vary among the different discharges. The maximum electron densities of one-meter-long discharges reach up to $\approx 10^{18}$ cm^{-3}, which are like those estimated from natural lightning. These high estimations in temperature and electron density of laboratory discharges could be attributed to the ultra-fast recording speed of the high-speed camera, allowing access to the early phases of the discharges at the sub-microsecond time scale.

In the near-ultraviolet, GALIUS was used to record time-resolved spectra at 672 kfps in the bandwidth of 380 to 450 nm. As an exmaple, Fig. 38 shows the spectrum

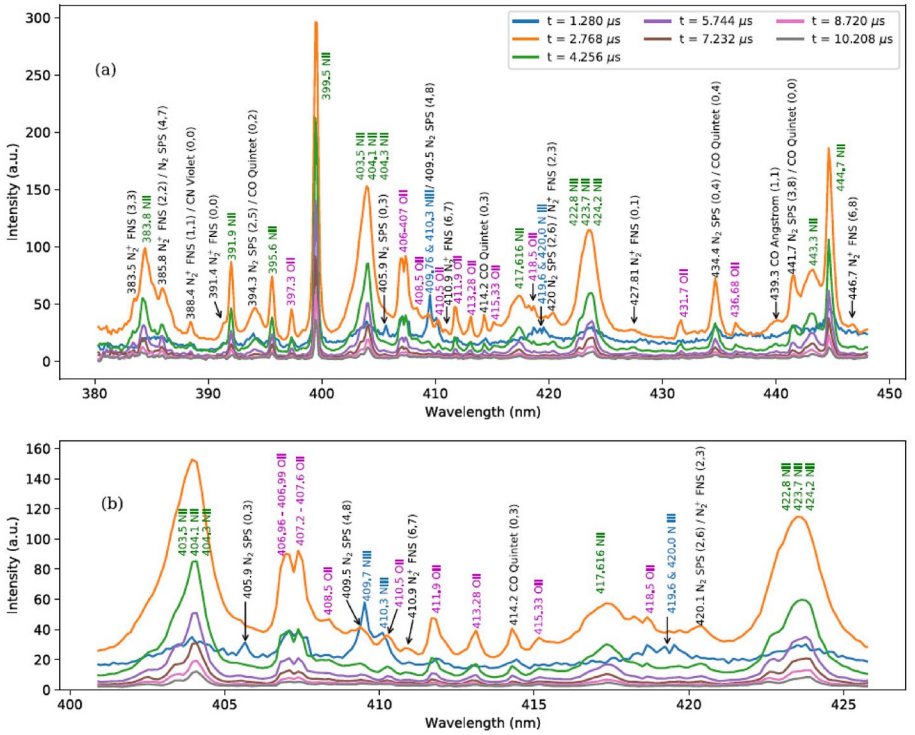

Fig. 38 The time resolved spectra (380–450 nm) of a meter long lightning-like discharge produced in the Lightning Impulse (LI) mode of a Marx generator with 800 kV. Panel **a** shows the entire spectral range. Panel **b** zooms into the bandwidth of 400–425 nm. The spectrum was recorded at 672000 fps with a spectral and time resolutions of 0.29 nm and 1.488 μs. Figure reproduced from (Kieu et al. 2021)

for discharges generated in the LI mode. It reveals the presence of early-time optical emissions associated with singly ionized nitrogen, oxygen, doubly ionized nitrogen, and several molecular species. Molecular emissions have been previously reported in studies (Salanave et al. 1962; Wallace 1960), including the CN violet transition, N_2 second positive system, and the N_2^+ first negative system. GALIUS spectra show new spectroscopic signatures from the Swan band (516.5 nm) of C_2 and several electronically excited states of CO. The detection of these molecular species can indicate the presence of milder regions around a heated channel where the gas temperature is cooler than at its center; or they may form due to the chemical activity of streamers surrounding the channel. Detecting molecular emissions does not only provide insight into the atmospheric conditions, but also opens a new door for quantifying NO production by lightning using high-sensitivity spectroscopic techniques.

GALIUS has also been used for experimental studies of the radial and temporal variation of neutral and ion spectroscopic signatures emerging from the heated channel of lightning-like discharges diagnosed at a high speed (900 kfps) (Passas-Varo et al. 2022). It was found that light emissions emanate from three regions: an inner core (up to ~ 2 mm), an external sheath (up to ~ 4 mm) featuring a sudden temperature increase, and further optical emissions forming a dim glow from 4 mm up to 16 mm. The optical emissions are initially (at < 1.11 μs) dominated by the N_2 first positive system at 660.8 nm and by the

N II ion line at 661.05 nm. Between 1.11 and 3.33 μs the optical emissions are dominated by H_α (656.3 nm) and O II ion (656.54 nm) lines. The N II ion line at 648.20 nm prevails in the outer dim glow region (9-12 mm) before 2.22 μs. Spectroscopic signals were used to experimentally derive the time dynamics of the electron density and electron/gas temperature radial profiles, which allowed the estimation of the early time overpressure pulse, electrical conductivity and concentrations of key molecular species (N_2, NO, O_2, OH, H_2, N_2O, NO_2, HO_2, O_3, and H_2O) along the radial axis of the heated air plasma channel. These populations were calculated from the overpressure pulse, assuming that they were produced from humid (50 %) air under thermal equilibrium conditions. OH is found to be the second most abundant molecular species (after NO) directly generated by heated lightning-like channels.

5.3 Grounded Rod Measurements of Laboratory Discharges and Lightning

In addition to the inception of discharges and the measurement of chemically active species, SAINT provided an investigation of the features of corona point discharges from a grounded conductive rod subject in a high background electric field (Arcanjo et al. 2021, 2023). In laboratory settings, a high voltage is applied to an upper plate in a plane-to-point experiment, with discharges observed from a grounded rod using an ultraviolet camera and a photosensor. The current measurement employs a shunt resistor, a current transformer, and a high impedance ammeter. In field experiments, a single current sensor, positioned 1.5 m above a roof, was coupled to a grounded rod at an altitude of 2525 m above sea level over a shelter in La Tossa d'Alp, near the Eagle Nest Tower, in the Spanish Pyrenees. As a result of this research, a sensor has been developed to measure corona current pulses and detect low currents related to lightning events (such as upward unconnected leaders and induced pulses) through a grounded electrode (Arcanjo et al. 2023).

Two approaches were employed in laboratory corona current measurement: a current transformer and a shunt resistor. Figure 39 illustrates the connections of these sensors to the rod within the setup, featuring a grounded conductive rod of 80 cm placed between two plates (with diameters of 1.4 m and 2.0 m) separated by 100 cm, resulting in a 20 cm gap distance. The high voltage power supply delivers up to 20 kV DC with positive or negative polarity, connected to the upper plate, while the bottom plate is

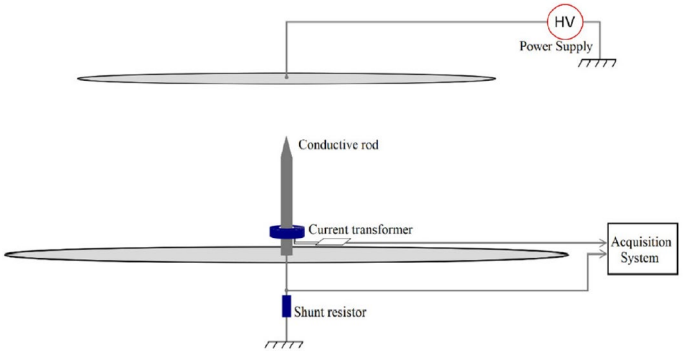

Fig. 39 Conductive sharp rod in the plane-to-point setup. Figure reproduced from (Arcanjo et al. 2021)

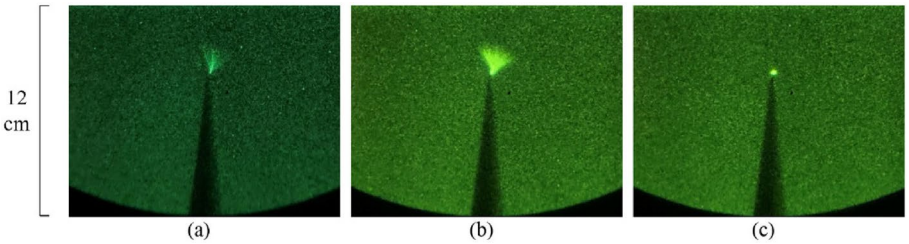

Fig. 40 Positive corona shape for different voltages: **a** -10 kV; **b** -15 kV; **c** -19 kV. Figure reproduced from (Arcanjo et al. 2021)

grounded via the resistor. This setup replicates conditions of sharp grounded structures exposed to high electric fields in the presence of charged clouds, inducing corona emissions from the rod tip.

Images of the three different stages of positive corona are presented in Fig. 40. When applying –10 kV (a), filament streamers are observed forming the corona in a conical shape. When increasing the voltage to –15 kV (b) streamers are slightly larger and more intense; however, it is possible to identify that they are formed from an onset glow at the tip. For a voltage of –19 kV (c) the streamers are barely perceptible, and the tiny glowing spot is formed on the tip of the rod. This stage (for applied voltages between around –14 kV and –19 kV) is a transition between the burst pulse stage and the glow corona stage. At –19 kV, when the corona discharge is pulseless, the glow corona is established.

In field experiments, observations indicate that lightning activity can rapidly modulate the electric field, thereby initiating, ceasing, or modifying the frequency of corona discharges. A positive correlation was noted between the frequency of positive corona pulses and the ambient electric field, with the frequency of pulses increasing as the electric field strength intensified. Moreover, higher wind speeds appeared to enhance pulse frequencies under similar electric field conditions, likely because faster wind removes some of the corona's space charge from around corona points more efficiently.

The investigation detailed in (Arcanjo et al. 2021) consolidates findings from laboratory long sparks, focusing on optical signatures at 337 nm and 777 nm. These experiments hold particular significance in supporting satellite-based lightning observations by ASIM and operational lightning imagers like GLM and the forthcoming MTG-LI. The study leverages optical measurements, current signatures, and short-time exposure images to examine the processes involved in long spark formation. Blue emissions at 337 nm are linked to streamer development and negative leader stepping, while red emissions at 777 nm predominantly correlate with stable leader propagation and surpass blue emissions. Furthermore, the study validates the relationship that the intensity of optical irradiance systematically increases with increasing electric current of individual streamer bursts.

Figure 41 illustrates the analysis of positive leader development through four experiments, presenting optical irradiances and current, at different leader-formation stages. Employing a plate-to-rod setup with negative voltage applied to the upper plate accentuates the distinctive features of positive streamer/leader propagation. Panel (a) shows the last 80 μs of an aborted leader development. The signals measured after t = –35 μs reveal the pattern of the stable leader formation, first, with a strong peak of current and emission at both lines, then with a remaining quasi-DC component of tens of milliamperes. At t = −6.5 μs, the blue signal reaches its peak and reduces substantially, the red signal, on the other hand, starts to increase consistently (stable leader development) until t = 0, when the leader is

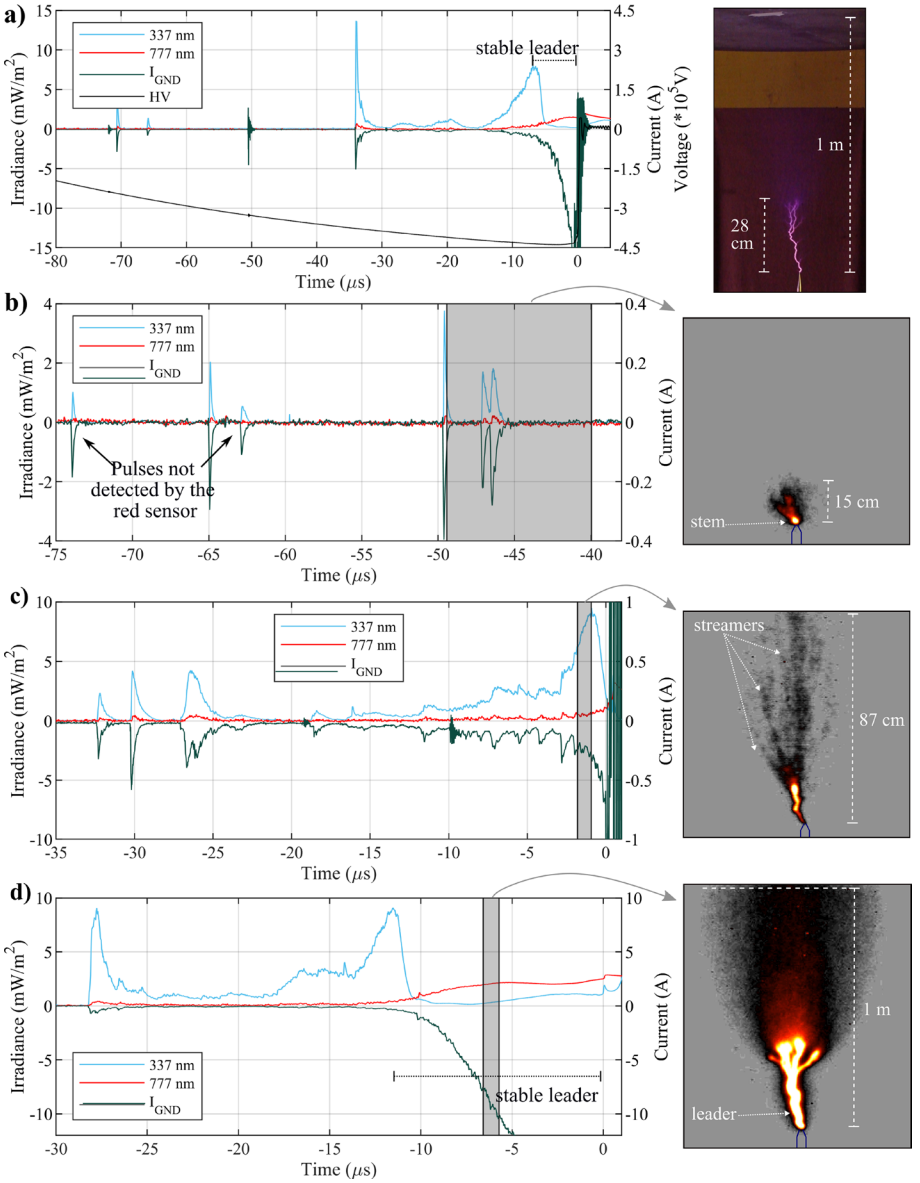

Fig. 41 Irradiance (blue and red) and current (green) measured for four different discharges. **a** Upper plate negative voltage increase, PMT measurements over 80 μs and 3-s still picture of the development of the aborted upward leader. **b** Pulses of current and irradiances during the formation of a stem with surrounding streamers in a 9.5 μs picture. **c** Streamer burst at the peak of the blue irradiance. The forming leader is observed in a 0.9-μs picture. **d** Optical signals and current signals during the stable leader development toward the upper plate. Figure reproduced from (Arcanjo et al. 2021)

aborted. In panels (b) and (c), the process of streamer-to-leader transition is enhanced, in which a number of streamers emerge from a stem connected to the grounded rod (b), and from the developing upward leader (c). A later stage of the leader development is shown

in d), where the burst of streamers in the gap is already decayed, as indicated by the low amplitude of the blue signal and the steadily rising red signal.

6 Summary, Conclusions and Outlook

The research activities and results of the SAINT (Science And INnovation with Thunderstorms) project have provided a big leap forward in our understanding of lightning and of associated phenomena such as TLEs and TGFs. The microphysics and macrophysics was approached through ground and satellite measurements as well as modelling and experiments, and we here give an overview of the SAINT's key findings as well as discuss possible future research paths.

Ground observations allowed for the first time to detect converging sprite streamers at approximately 80 km altitude over northern Spain (Sect. 2.1). These sprites were initiated through a +CG lightning stroke with a maximum current moment of 140 kA km. Firstly, downwards propagating streamers were observed. Subsequently the large electric field in their vicinity triggered the detachment of electrons from oxygen on the symmetry axes of the original streamers leading to upwards moving streamers meeting the original downward moving streamers. Similarly, sprites were also detected from the UK, which is quite uncommon, as lightning activity is less abundant and less powerful in northern latitudes. These sprites were associated with a high peak current average of +170 kA. Moreover, high-energy phenomena were observed from downwards moving lightning leaders in the Pyrenees and appeared in conjunction with VHF radiation (2.3). Measurements showed that X-rays appeared in the last millisecond before the return stroke with the most intense VHF pulses; X-rays were emitted from different branches of the descending leader indicating that high-energy emission can easily be emitted from lightning leaders.

Part of the work performed within the SAINT project used space-based observations as provided by the Astro-rivelatore Gamma a Immagini LEggero (AGILE) satellite and by the Atmosphere-Space Interaction Monitor (ASIM) mounted on the International Space Station. Both missions provided new details on lightning, luminous events above thunderstorms and terrestrial gamma-ray flashes. New data catalogues of TGFs were provided based on AGILE and ASIM data (3.1). ASIM measured approximately one TGF per day, mainly over the three main lightning "chimneys" Central/South America, Central Africa and South East Asia, and it even provided details about 14 mid-latitude events of TGFs occurring between 37° and 51° degree latitude. High energy observations from AGILE and ASIM were used to analyze the temporal evolution of TGFs relative to the occurrence of streamers and leaders. This analysis revealed that TGFs appear at the onset of the streamer and leader activity before the main optical pulse implying that TGFs are produced in the high electric fields of the leader-streamer system (3.2). ASIM also provided the first evidence of a TGF coinciding with an elve (3.3); whilst the superposed electric field of the leader-streamer system is sufficiently high to accelerate electrons to relativistic energies, this configuration also emits an electromagnetic pulse exciting the elve.

ASIM also provided new results on Blue LUminous Events (BLUEs) and on sprites above thunderstorms (3.4). Blue events become apparent through a strong signal in ASIM's "blue" photometer with little or no signal in the photometer measuring in 777.4 nm. Such events are identified as fast streamer events incepting above both developing and decaying thunderstorms. Similarly, through the simultaneous analysis of ASIM's photometers, including the measurement of UV signals - and ASIM's Camera Head Units, it was

possible to detect sprites (3.5). However, more effort is needed in the future to use ASIM data to improve our understanding of sprites.

We also performed quite a range of simulations to study the microphysics of electric discharges and - where applicable - compare them to the observations and experiments. During the SAINT project, fluid and particle models were used and extended (e.g. for the use of Graphical Processing Units) to study the propagation of single streamers (4.1) in steady and unsteady and pre-ionized air, the stagnation and fading of streamers, as well as multi-streamer phenomena in full 3D such as streamer branching and interactions and streamer coronae. Simulations both of propagating and of branching streamers agreed well with experimental results. Simulations also showed that there can be a profound effect of moving air on the inception and propagation of streamers as experimentally observed (4.3). After the inception of the first streamers from an electrode, air moves the ions on this electrode transversally to the streamer direction. Subsequently, after a brief quiescent period, a second streamer incepts from the side of the electrode due to the previously moved ions. When studying the collective behaviour of a dense streamer front (4.2), we observed that a higher streamer density leads to lower electric field enhancement and to slower propagation. The interaction of encountering streamer coronae was simulated to understand the emission of TGFs in thunderclouds (4.4). Inspired by ASIM's simultaenous lightning-TGF measurements, numerical experiments were performed simulating the acceleration of thermal electrons in the superposed electric field of approaching streamer coronae. In this setup, the acceleration to relativistic energies was observed leading to the subsequent emission of Bremsstrahlung photons constituting TGFs. The spatial and energy distributions as well as the relative timing of high-energy photon beams are compatible with previous and present (ASIM) measurements, illustrating well the fruitful study of TGFs through satellite measurements and numerical experiments.

In addition to observations and modelling, experiments investigated various aspects of electric discharges. One of the main mysteries of lightning is the inception problem (5.1). As the electric field in thunderclouds is on the order of one tenth of the breakdown field, streamer inception as a precursor of lightning seems unlikely, but according to simulations the inception is helped by the field enhancement near a hydrometeor. Experiments indeed showed that hydrometeors provide such field enhancement at their tips both in air. The discharge inception times show three distinct peaks at different inception times depending on whether free electrons originate from cosmic rays or from electron detachment. When studying discharges, both streamer coronas and hot lightning leaders, it is of interest which chemical reactions occur and which species are created. SAINT made use of GALIUS (GrAnada Lightning Ultrafast Spectrograph; Sect. 5.2) to measure the temporal evolution of various species in controlled lightning-like discharges. GALIUS measured key molecular species (N_2, NO, O_2, OH, H_2, N_2O, NO_2, HO_2, O_3 and H_2O) which might play a key role in greenhouse gas production. Similarly, laboratory measurements thoroughly illustrated the shape of discharges including the streamer corona consisting of several bursts of streamers (5.3). Two stages are visible: For low voltages (in this experiment between -10 and -15 kV), filament streamers are observed which become brighter for a higher voltage. For higher voltages, however, there is only one small bright spot, the glow corona stage.

In conclusion, the SAINT network provided the scientific community working on electric discharges, lightning and associated phenomena, with the unique opportunity to leap forward our understanding. Through ground-based measurements and satellite observations, we increased our knowledge on TLEs and TGFs, their temporal evolution and their relation to lightning discharges whilst modelling and laboratory experiments provided us with a detailed knowledge on the microphysics of discharges, TGFs and TLEs as well as on

streamer inception and plasma chemistry. These new findings provide a stepping stone for future research and can be used as a baseline for new collaborative projects.

SAINT has provided the Atmospheric Electricity community with significant development about lightning, TLEs and TGFs as well as new technology and numerical tools, which has laid the foundation for future research, accompanied by recent findings after the end of SAINT. TGFs were first reported in 1994 (Fishman et al. 1994) and the last ~ 30 years have been vibrant in TGF research with a significant push through SAINT. However, we are still missing details on gamma-ray glows (Parks et al. 1981; McCarthy and Parks 1992; Wada et al. 2019; Marisaldi et al. 2024), the emission of energetic X- and gamma-rays from thunderclouds, similar to TGFs, but lasting up to tens of minutes. Furthermore, the recent ALOFT (Airborne Lightning Observatory for FEGS and TGFs; FEGS stands for "Fly's Eye Geostationary Lightning Mapper (GLM) Simulator") mission has detected so-called flickering gamma-ray flashes (Østgaard et al. 2024) that need to be understood better.

SAINT provided details of how discharges behave in moving air which is a first approximation of how lightning might interact with the moving blades of wind turbines. This is, however, far from being fully understood, and we suggest to investigate this interaction further to solidify wind energy as a reliable option for renewable energy as a substitution for fossil energy and thus action against human-made climate change. Additionally, it is well-known that lightning creates approx. 10% of climate relevant gases (Schumann and Huntrieser 2007), but we are lacking a lot of details: what is the role of energetic emission of atmospheric chemistry, will there be more or less thunderstorms in a warmer climate and what are thus the feedback cycles between lightning and global warming? We should address these questions in order to improve our understanding of global warming.

SAINT mostly addressed lightning and associated phenomena in air, but what about other gas mixtures? In the recent years, streamer simulations have been performed for non-air atmospheres such as the atmospheres of Titan (Köhn et al. 2019) or Primordial Earth (Köhn et al. 2022); additionally, there have been a plethora of observations that indicate that lightning or TLEs exist in other bodies of our solar system (Renno et al. 2003; Vasavada and Showman 2005; Dyudina et al. 2010; Pérez-Invernón et al. 2016). With the growing interest in exoplanets and the possible connection between electric discharges and the origin of life (Miller 1953, 1955), we suggest to also study lightning in exoplanet atmospheres. Additionally, studying plasma breakdown in various gas mixtures can also be relevant for new technologies. For a few decades electric switchgears used SF_6 (Christophorou et al. 1997). However, SF_6 has a global warming potential of approx. 23500 which is thus far more relevant for global warming than CO_2 (Ray et al. 2017; Masson-Delmotte et al. 2021). Hence, we need to find gases that have similar properties to gases such as SF_6 (e.g. as insulators), but are more climate friendly. There has been some recent development, e.g. understanding streamers in C_4F_7N-CO_2 mixtures which is considered to be more environmentally friendly than the insulating gas SF_6 (Guo et al. 2023), but more research is advised to find suitable gases that compromise between technological usability and being climate friendly.

Author Contributions All authors of this review paper contributed to the science performed during SAINT. Drafting the paper was led by C.K. and T.N. Otherwise, all authors contributed equally to the paper. All authors read and approved the final manuscript.

Funding This project has received funding from the European Union's Horizon 2020 research and innovation program under the Marie Sklodowska-Curie grant agreement 722337.

C.K. has received funding from the Independent Research Fund Denmark (grant 1054-00104).

Data Availability As this is a review paper, all data and code are associated and referred to in the individual publications produced during the lifetime of SAINT. All the publications with their respective data and code statements can be accessed through `https://www.saint-h2020.eu/publications`.

Declarations

Conflict of interest The authors declare no Conflict of interest.

Ethical Approval Not applicable.

References

Abarca SF, Corbosiero KL, Galarneau TJ Jr (2010) An evaluation of the worldwide lightning location network (WWLLN) using the national lightning detection network (NLDN) as ground truth. J Geophys Res 115:18. https://doi.org/10.1029/2009JD013411

Allen DJ, Pickering KE, Bucsela E, Krotkov N, Holzworth R (2019) Lightning NO_x production in the tropics as determined using OMI NO_2 retrievals and WWLLN stroke data. J Geophys Res: Atmos 124(23):13498–13518. https://doi.org/10.1029/2018JD029824

Alpers M, Brüns C, Pillukat A (2017) METimage: an innovative multi-spectral imaging radiometer for the EUMETSAT polar system follow-on satellite mission. Proceedings Volume 10566, International Conference on Space Optics - ICSO 2008, Toulouse, France 10566:10566–1105667 https://doi.org/10.1117/12.2308292

Arcanjo M, Montanyá J, Urbani M, Lorenzo V (2021) Optical signatures associated with streamers and leaders of laboratory discharges. Geophys Res Lett 48:2021–095601. https://doi.org/10.1029/2021GL095601

Arcanjo M, Montanyá J, Urbani M, Lorenzo V (2023) Measuring low-current discharges from grounded rods under high background electric fields. Electr Power Syst Res 217:109139. https://doi.org/10.1016/j.epsr.2023.109139

Arcanjo M, Montanyá J, Urbani M, Lorenzo V, Pineda N (2021) Observations of corona point discharges from grounded rods under thunderstorms. Atmos Res 247:105238. https://doi.org/10.1016/j.atmosres.2020.105238

Babich LP (2007) Neutron generation mechanism correlated with lightning discharges. Geomag Aero 47:664–670. https://doi.org/10.1134/S0016793207050155

Babich LP, Bochkov EI, Kutsyk IM, Neubert TOC (2017) Analyses of electron runaway in front of the negative streamer channel. J Geophys Res Space Phys 122:8974–8984. https://doi.org/10.1002/2017JA023917

Bagheri B, Teunissen J (2019) The effect of the stochasticity of photoionization on 3D streamer simulations. Plasma Sour Sci Technol 28(4):045013. https://doi.org/10.1088/1361-6595/ab1331

Bagheri B, Teunissen J, Ebert U, Becker MM, Chen S, Ducasse O, Eichwald O, Loffhagen D, Luque A, Mihailova D, Plewa JM, Van Dijk J, Yousfi M (2018) Comparison of six simulation codes for positive streamers in air. Plasma Sour Sci Technol 27(9):095002. https://doi.org/10.1088/1361-6595/aad768

Bai X, Füllekrug M, Chanrion O, Soula S, Peverell A, Mashao D et al (2023) Height determination of a blue discharge observed by ASIM/MMIA on the international space station. J Geophys Res Atmos 128:2022–037460. https://doi.org/10.1029/2022JD037460

Banerjee A, Archibald AT, Maycock AC, Telford P, Abraham NL, Yang X, Braesicke P, Pyle JA (2014) Lightning NO_x, a key chemistry-climate interaction: impacts of future climate change and consequences for tropospheric oxidising capacity. Atmos Chem Phys 14:9871–9881. https://doi.org/10.5194/acp-14-9871-2014

Barrington-Leigh CP, Inan US (1999) Elves triggered by positive and negative lightning discharges. Geophys Res Lett 26:683–686. https://doi.org/10.1029/1999GL900059

Beirle S, Huntrieser H, Wagner T (2010) Direct satellite observation of lightning-produced NO_x. Atmos Chem Phys 10:10965–10986. https://doi.org/10.5194/acp-10-10965-2010

Bertram TH et al (2007) Direct measurements of the convective recycling of the upper troposphere. Science 315:816–820. https://doi.org/10.1126/science.1134548

Betz H-D et al (2009) LINET-An international lightning detection network in Europe. Atmos Res 91:564–573. https://doi.org/10.1016/j.atmosres.2008.06.012

Beylkin G, Keiser JM, Vozovoi L (1998) A new class of time discretization schemes for the solution of nonlinear PDEs. J Comput Phys 147(2):362–387. https://doi.org/10.1006/jcph.1998.6093

Bjørge-Engeland I et al (2022) Terrestrial gamma-ray flashes with accompanying Elves, detected by ASIM. J Geophys Res Atmos 127:2021–036368. https://doi.org/10.1029/2021JD036368

Bjørge-Engeland I et al. (2024) Evidence of a new population of weak terrestrial gamma-ray flashes observed from aircraft altitude. Submitted to Geophys Res Lett. 10.1029/2024GL110395

Blakeslee RJ et al (2020) Three years of the lightning imaging sensor onboard the international space station: expanded global coverage and enhanced applications. J Geophys Res: Atmos 125(16):1–20. https://doi.org/10.1029/2020JD032918

Boulos MI (1991) Thermal plasma processing. IEEE Trans Plasma Sci 19:1078–1089. https://doi.org/10.1109/27.125032

Bouwman D, Francisco H, Ebert U (2023) Estimating the properties of single positive air streamers from measurable parameters. Plasma Sour Sci Technol 32(7):075015. https://doi.org/10.1088/1361-6595/ace792

Briggs MS et al (2011) Electron-positron beams from terrestrial lightning observed with Fermi GBM. Geophys Res Lett 38:02808. https://doi.org/10.1029/2010GL046259

Briggs MS, Fishman GJ, Connaughton V, Bhat PN, Paciesas WS, Preece RD et al (2010) First results on terrestrial gamma ray flashes from the Fermi gamma-ray burst monitor. J Geophys Res 115:07323. https://doi.org/10.1029/2009JA015242

Briggs MS, Xiong S, Connaughton V, Tierney D, Fitzpatrick G, Foley S et al (2013) Terrestrial gamma-ray flashes in the Fermi era: improved observations and analysis methods. J Geophys Res 118:3805–3830. https://doi.org/10.1002/jgra.50205

Bucsela EJ, Pickering KE, Allen DJ, Holzworth RH, Krotkov NA (2019) Midlatitude lightning NO_x production efficiency inferred from OMI and WWLLN data. J Geophys Res: Atmos 124(23):13475–13497. https://doi.org/10.1029/2018JD029824

Bór J (2013) Optically perceptible characteristics of sprites observed in Central Europe in 2007–2009. J Atmos Solar-Terr Phys 92:151–177. https://doi.org/10.1016/j.jastp.2012.10.008

Bürgesser RE (2017) Assessment of the world wide lightning location network (WWLLN) detection efficiency by comparison to the lightning imaging sensor (LIS). Quart J Royal Meteor Soc 143:2809–2817. https://doi.org/10.1002/qj.3129

Carbone E, Nijdam S (2015) Thomson scattering on non-equilibrium low density plasmas: principles, practice and challenges. Plasma Phys Contr Fus 57:014026. https://doi.org/10.1088/0741-3335/57/1/014026

Carlson BE, Gjesteland T, Østgaard N (2012) Connecting the terrestrial gamma-ray flash source strength and observed fluence distributions. J Geophys Res Atmos 117:01314. https://doi.org/10.1029/2011JA017122

Chanrion O et al (2019) The modular multispectral imaging array (MMIA) of the ASIM payload on the international space station. Space Sci Rev 215:28. https://doi.org/10.1007/s11214-019-0593-y

Chanrion O, Neubert T (2010) Production of runaway electrons by negative streamer discharges. J Geophys Res 115:00–32. https://doi.org/10.1029/2009JA014774

Chanrion O, Neubert T, Mogensen A, Yair Y, Stendel M, Singh R, Siingh D (2017) Profuse activity of blue electrical discharges at the tops of thunderstorms. Geophys Res Lett 44:496–503. https://doi.org/10.1002/2016GL071311

Chen H, Xiong X, Link DO, Sun C, Chiang KV (2020) NOAA-20 visible infrared imaging radiometer suite day-night band on-orbit calibration and performance. J Appl Rem Sens 14:034516. https://doi.org/10.1117/1.JRS.14.034516

Chilingarian A et al (2010) Ground-based observations of thunderstorm-correlated fluxes of high-energy electrons, gamma rays and neutrons. Phys Rev D 82:043009. https://doi.org/10.1103/PhysRevD.82.043009

Chou J-K, Hsu R-R, Su H-T, Chen AB-C, Kuo C-L, Huang S-M, Chang S-C, Peng K-M, Wu Y-J (2018) ISUAL-observed blue luminous events: the associated sferics. J Geophys Res 123:3063–3077. https://doi.org/10.1002/2017JA024793

Christian HJ et al (2003) Global frequency and distribution of lightning as observed from space by the optical transient detector. J Geophys Res Atmos 108:1. https://doi.org/10.1029/2002JD002347

Christophorou LG, Olthoff JK, Van Brunt RJ (1997) Sulfur hexafuoride and the electric power industry. IEEE Electr Insul Mag 13:20–24. https://doi.org/10.1109/57.620514

Cooray V, Cooray G, Rubinstein M, Rachidi F (2020) Modeling compact intracloud discharge (CID) as a streamer burst. Atmosphere 11:549–575. https://doi.org/10.3390/atmos11050549

Cooray V (2003) The Lightning Flash. https://doi.org/10.1049/PBPO034E
Cummer SA, Zhai Y, Hu W, Smith DM, Lopez LI, Stanley MA (2005) Measurements and implications of the relationship between lightning and terrestrial gamma ray flashes. Geophys Res Lett 32:08811. https://doi.org/10.1029/2005GL022778
Cummins KL, Murphy MJ (2009) An overview of lightning locating systems: history, techniques, and data uses, with an in-depth look at the US NLDN. IEEE Trans Elect Comp 51:499–518. https://doi.org/10.1109/TEMC.2009.2023450
Dimitriadou K, Chanrion O, Neubert T, Protat A, Louf V, Heumesser M, Husbjerg L, Köhn C, Østgaard N, Reglero V (2022) Analysis of blue corona discharges at the top of tropical thunderstorm clouds in different phases of convection. Geophys Res Lett 49:2021–095879. https://doi.org/10.1029/2021GL095879
Dimitriadou K (2021) Analysis of Blue Corona Discharges and Lightning observed by the ASIM and GLM Space Missions. PhD thesis, Technical University of Denmark
Dwyer JR (2003) A fundamental limit on electric fields in air. Geophys Res Lett 30:2055. https://doi.org/10.1029/2003GL017781
Dwyer JR, Grefenstette BW, Smith DM (2008) High-energy electron beams launched into space by thunderstorms. Geophys Res Lett 35:02815. https://doi.org/10.1029/2007GL032430
Dwyer JR, Rassoul HK, Al-Dayeh M, Caraway L, Chrest A, Wright B, Kozak E, Jerauld J, Uman MA, Rakov V et al (2005) X-ray bursts associated with leader steps in cloud-to-ground lightning. Geophys Res Lett. https://doi.org/10.1029/2004GL021782
Dwyer JR, Smith D (2005) A comparison between Monte Carlo simulations of runawaybreakdown and terrestrial gamma-ray flash observations. Geophys Res Lett 32:22804. https://doi.org/10.1029/2005GL023848
Dwyer JR, Smith DM, Cummer SA (2012) High-energy atmospheric physics: terrestrial gamma-ray flashes and related phenomena. Space Sci Rev 173:133–196. https://doi.org/10.1007/s11214-012-9894-0
Dwyer JR, Uman MA (2014) The physics of lightning. Phys Rep 534(4):147–241. https://doi.org/10.1016/j.physrep.2013.09.004
Dyudina UA, Ingersoll AP, Ewald SP, Porco CC, Fischer G, Kurth WS, West RA (2010) Detection of visible lightning on Saturn. Geophys Res Lett 37:09205. https://doi.org/10.1029/2010GL043188
Ebert U, Nijdam S, Li C, Luque A, Briels T, Veldhuizen E (2010) Review of recent results on streamer discharges and discussion of their relevance for sprites and lightning. J Geophys Res 115:00–43. https://doi.org/10.1029/2009JA014867
Efraim A, Rosenfeld D, Holzworth R, Thornton JA (2023) A possible cause for preference of super Bolt lightning Overthe Mediterranean Sea and the Altiplano. J Geophys Res Atmos 128:2022–038254. https://doi.org/10.1029/2022JD038254
Fan XP, Zhang YJ, Zheng D, Zhang Y, Lyu WT, Liu HY, Xu LT (2018) A new method of three-dimensional location for low-frequency electric field detection array. J Geophys Res: Atmos 123(16):8792–8812. https://doi.org/10.1029/2017JD028249
Fehr T, Dotzek N, Höller H (2005) Comparison of lightning activity and radar-retrieved microphysical properties in EULINOX storms. Atmos Res 76:167–189. https://doi.org/10.1016/j.atmosres.2004.11.027
Finke U (1999) Space-time correlations of lightning distributions. Month Weath Rev 127:1850–1861
Fishman GJ et al (1994) Discovery of intense gamma-ray flashes of atmospheric origin. Science 264:1313–1316. https://doi.org/10.1126/science.264.5163.1313
Francisco H, Bagheri B, Ebert U (2021) Electrically isolated propagating streamer heads formed by strong electron attachment. Plasma Sour Sci Technol 30:025006. https://doi.org/10.1088/1361-6595/abdaa3
Francisco H, Teunissen J, Bagheri B, Ebert U (2021) Simulations of positive streamers in air in different electric fields: steady motion of solitary streamer heads and the stability field. Plasma Sour Sci Technol 30:115007. https://doi.org/10.1088/1361-6595/ac2f76
Franklin B (1752) Experiments and observations on electricity made at Philadelphia in America. Phil Trans R Soc London 47: 565
Franz RC, Nemzek RJ, Winckler JR (1990) Television image of large upward electrical discharge above a thunderstorm system. Science 249:48–51. https://doi.org/10.1126/science.249.4964.48
Fukunishi H, Takahashi Y, Sakanoi K (1996) Elves: lightning-induced transient luminous events in the lower ionosphere. Geophys Res Lett 23:2157–2160. https://doi.org/10.1029/96GL01979
Füllekrug M, Liu Z, Koh K, Mezentsev A, Pedeboy S, Soula S, Enno SE, Sugier J, Rycroft MJ (2016) Mapping lightning in the sky with a mini array. Geophys Res Lett 43(19):10448–10454. https://doi.org/10.1002/2016GL070737
Füllekrug M, Mezentsev A, Watson R, Gaffet S, Astin I, Smith N, Evans A (2015) Map of low-frequency electromagnetic noise in the sky. Geophys Res Lett 42(11):4648–4653. https://doi.org/10.1002/2015GL064142

Füllekrug M, Mareev E, Rycroft M (2006) Sprites. Elves and Intense Lightning Discharges. https://doi.org/10.1007/1-4020-4629-4

Gamerota WR, Cummer SA, Li J, Stenbaek-Nielsen HC, Haaland RK, McHarg MG (2011) Comparison of sprite initiation altitudes between observations and models. J Geophys Res 116:02317. https://doi.org/10.1029/2010JA016095

Gjesteland T, Østgaard N, Laviola S, Miglietta MM, Arnone E, Marisaldi M, Fuschino F, Collier AB, Fabró F, Montanya J (2015) Observation of intrinsically bright terrestrial gamma ray flashes from the Mediterranean basin. J Geophys Res: Atmos 120(23):12143–12156. https://doi.org/10.1002/2015JD023704

Gomez Kuri Z, Soula S, Neubert T, Mlynarczyk J, Köhn C (2021) Converging luminosity in column-sprite filaments. Geophys Res Lett 48:2020–090364. https://doi.org/10.1029/2020GL090364

Gomez Kuri Z (2021) Analysis of Transient Luminous Events from ground and space observations. PhD thesis, Université Paul Sabatier Toulouse III

Gordillo-Vázquez FJ, Pérez-Invernón FJ (2021) A review of the impact of transient luminous events on the atmospheric chemistry: past, present, and future. Atmos Res 252:105432. https://doi.org/10.1016/j.atmosres.2020.105432

Gordillo-Vázquez FJ, Pérez-Invernón FJ, Huntrieser H, Smith AK (2019) Comparison of six lightning parameterizations in CAM5 and the impact on global atmospheric chemistry. Earth Space Sci 6(12):2317–2346. https://doi.org/10.1029/2019EA000873

Graves DB (1994) Plasma Process. IEEE Trans Plasma Sci 22:31–42. https://doi.org/10.1109/27.281547

Gunn R (1948) Electric field intensity inside of natural clouds. J Appl Phys 19(5):481–484. https://doi.org/10.1063/1.1698159

Guo B, Ebert U, Teunissen J (2023) 3D particle-in-cell simulations of negative and positive streamers in C_4F_7N-CO_2 mixtures. Plasma Sour Sci Technol 32:115001. https://doi.org/10.1088/1361-6595/ad0570

Guo B, Li X, Ebert U, Teunissen J (2022) A computational study of accelerating, steady and fading negative streamers in ambient air. Plasma Sour Sci Technol 31(9):095011. https://doi.org/10.1088/1361-6595/ac8e2e

Gurevich A, Zybin K, Medvedev YV (2007) Runaway breakdown in strong electric field as a source of terrestrial gamma flashes and gamma bursts in lightning leader steps. Phys Lett A 361(1–2):119–125. https://doi.org/10.1016/j.physleta.2006.05.063

Heumesser M et al (2021) Spectral observations of optical emissions associated with terrestrial gamma-ray flashes. Geophys Res Lett 48:2020–090700. https://doi.org/10.1029/2020GL090700

Holle RL, Demetriades NWS, Nag A (2014) Lightning warnings with NLDN cloud and cloud-to-ground lightning data. International Conference on Lightning Protection (ICLP), Shanghai, China, pp 315–324. https://doi.org/10.1109/ICLP.2014.6973143

Holzworth R, McCarthy M, Brundell J, Jacobson A, Rodger C (2019) Global distribution of superbolts. J Geophys Res: Atmos 124(17–18):9996–10005. https://doi.org/10.1029/2019JD030975

Huntrieser H et al (2007) Lightning-produced NO_x over Brazil during TROCCINOX: airborne measurements in tropical and subtropical thunderstorms and the importance of mesoscale convective systems. Atmos Chem Phys 7:2987–3013. https://doi.org/10.5194/acp-7-2987-2007

Huntrieser H, Feigl C, Schlager H, Schröder F, Gerbig C, Velthoven P, Flatøy F, Théry C, Petzold A, Höller H, Schumann U (2002) Airborne measurements of NOx, tracer species, and small particles during the European lightning nitrogen oxides experiment. J Geophys Res Atmos 107:5–1524. https://doi.org/10.1029/2000JD000209

Ialongo I, Virta H, Eskes H, Hovila J, Douros J (2020) Comparison of TROPOMI/sentinel-5 precursor NO_2 observations with ground-based measurements in Helsinki. Atmos Meas Tech 13:205–218. https://doi.org/10.5194/amt-13-205-2020

Inan US, Cohen MB, Said DMRK, Smith Lopez LI (2006) Terrestrial gamma ray flashes and lightning discharges. Geophys Res Lett 33:18802. https://doi.org/10.1029/2006GL027085

Jaeglé L (2007) Pumping up surface air. Science 315:772–773. https://doi.org/10.1126/science.1138988

Karunarathna N, Marshall TC, Stolzenburg M, Karunarathne S (2015) Narrow bipolar pulse location compared to thunderstorm radar echo structure. J Geophys Res Atmos 120:11690–11706. https://doi.org/10.1002/2015JD023829

Kersten H, Deutsch H, Steffen H, Kroesen GMW, Hippler R (2001) The energy balance at substrate surfaces during plasma processing. Vacuum 63(3):385–431. https://doi.org/10.1016/S0042-207X(01)00350-5

Kieu N, Gordillo-Vázquez FJ, Passas M, Sánchez J, Pérez-Invernón FJ (2021) High-speed spectroscopy of lightning-like discharges: evidence of molecular optical emissions. J Geophys Res Atmos 126:2021–035016. https://doi.org/10.1029/2021JD035016

Kieu N, Gordillo?Vázquez FJ, Passas M, Sánchez J, Pérez?Invernón FJ, Luque A, Montanyá J, Christian H (2020) Submicrosecond spectroscopy of lightning? like discharges: exploring new time regimes. Geophys Res Lett 47: 2020–088755. https://doi.org/10.1029/2020GL088755

Koshak WJ, Solakiewicz RJ, Phanord DD, Blakeslee RJ (1994) Diffusion model for lightning radiative transfer. J Geophys Res 99:14361–14371. https://doi.org/10.1029/94JD00022

Köhn C, Chanrion O, Enghoff MB, Dujko S (2022) Streamer discharges in the atmosphere of Primordial Earth. Geophys Res Lett 49:2021–09750. https://doi.org/10.1029/2021GL097504

Köhn C, Chanrion O, Neubert T (2019) The sensitivity of sprite streamer inception on the initial electron-ion patch. J Geophys Res Space Phys 124:3083–3099. https://doi.org/10.1029/2018JA025972

Köhn C, Diniz G, Harakeh MN (2017) Production mechanisms of leptons, photons, and hadrons and their possible feedback close to lightning leaders. J Geophys Res Atmos 122:1365–1383. https://doi.org/10.1002/2016JD025445

Köhn C, Dujko S, Chanrion O, Neubert T (2019) Streamer propagation in the atmosphere of Titan and other N_2:CH_4 mixtures compared to N_2:O_2 mixtures. Icarus 333:294–305. https://doi.org/10.1016/j.icarus.2019.05.036

Köhn C, Ebert U (2015) Calculation of beams of positrons, neutrons, and protons associated with terrestrial gamma ray flashes. J Geophys Res Atmos 120:1620–1635. https://doi.org/10.1002/2014JD022229

Köhn C, Heumesser M, Chanrion O, Nishikawa K, Reglero V, Neubert T (2020) The emission of terrestrial gamma ray flashes from encountering streamer coronae associated to the breakdown of lightning leaders. Geophys Res Lett 47:2020–089749. https://doi.org/10.1029/2020GL089749

Köhn C, Heumesser H, Chanrion O, Reglero V, Østgaard N, Christian HJ, Lang TJ, Blakeslee RJ, Neubert T (2024) Employing optical lightning data to identify lightning flashes associated to terrestrial gamma-ray flashes. Bull Atmos Sci Technol 5:2. https://doi.org/10.1007/s42865-024-00065-y

Lalande P, Bondiou-Clergerie A, Laroche P (1999) Computations of the initial discharge initiation zones on aircraft or helicopter. SAE Technical Paper 1999-01-2371 https://doi.org/10.4271/1999-01-2371

Lapierre JL, Laughner JL-, Geddes JA, Koshak WJ, Cohen RC, Pusede SE (2020) Observing US regional variability in lightning NO_2 production rates. J Geophys Res: Atmos 125(5):2019–031362. https://doi.org/10.1029/2019JD031362

Li X, Dijcks S, Nijdam S, Sun A, Ebert U, Teunissen J (2021) Comparing simulations and experiments of positive streamers in air: steps toward model validation. Plasma Sour Sci Technol 30(9):095002. https://doi.org/10.1088/1361-6595/ac1b36

Li C, Ebert U, Hundsdorfer W (2009) 3D hybrid computations for streamer discharges and production of run-away electrons. J Phys D: Appl Phys 42:202003. https://doi.org/10.1088/0022-3727/42/20/202003

Li X, Guo B, Sun A, Ebert U, Teunissen J (2022) A computational study of steady and stagnating positive streamers in N_2-O_2 mixtures. Plasma Sour Sci Technol 31(6):065011. https://doi.org/10.1088/1361-6595/ac7747

Light TE, Suszcynsky DM, Kirkland MW, Jacobson AR (2001) Simulations of lightning optical waveforms as seen through clouds by satellites. J Geophys Res 106:17103–17114. https://doi.org/10.1029/2001JD900051

Lindanger A, Marisaldi M, Maiorana C, Sarria D, Albrechtsen K, Ostgaard N, Galli M, Ursi A, Labanti C, Tavani M, Pittori C, Verrecchia F (2020) The 3rd AGILE terrestrial gamma ray flash catalog. Part I: association to lightning sferics. J Geophys Res Atmos 125(11):2019–031985. https://doi.org/10.1029/2019JD031985

Lindanger A, Skeie CA, Marisaldi M, Bjørge-Engeland I, Østgaard N, Mezentsev A, Sarria D, Lehtinen N, Reglero V, Chanrion O, Neubert T (2022) Production of terrestrial gamma-ray flashes during the early stages of lightning flashes. J Geophys Res Atmos 127:2021–036305. https://doi.org/10.1029/2021JD036305

Liu F, Neubert T, Chanrion O, Lu G, Wu T, Lyu F, Lyu W, Köhn C, Li D, Zhu B, Lei J (2024) Polarity transitions of narrow bipolar events in thundercloud tops reaching the lower stratosphere. Nat Comm 15:7344. https://doi.org/10.1038/s41467-024-51705-y

Liu N, Pasko VP (2004) Effects of photoionization on propagation and branching of positive and negative streamers in sprites. J Geophys Res 109:04301. https://doi.org/10.1029/2003JA010064

Liu F, Zhu B, Lu G, Qin Z, Lei J, Peng K-M et al (2018) Observations of blue discharges associated with negative narrow bipolar events in active deep convection. Geophys Res Lett 45:2842–2851. https://doi.org/10.1002/2017GL076207

Loeb LB, Meek JM (1940) The mechanism of spark discharge in air at atmospheric pressure. J Appl Phys 11:438–47. https://doi.org/10.1063/1.1712792

Luque A, Ebert U (2009) Emergence of sprite streamers from screening-ionization waves in the lower ionosphere. Nat Geosci 2:757–760. https://doi.org/10.1038/ngeo662

Luque A, Gordillo-Vázquez FJ, Li D, Malagón-Romero A, Pérez-Invernón FJ, Schmalzried A, Soler S, Chanrion O, Heumesser M, Neubert T, Reglero V, Østgaard N (2020) Modeling lightning observations from space-based platforms (CloudScat.jl 1.0). Geosci Model Dev 13:5549–5566. https://doi.org/10.5194/gmd-13-5549-2020

López JA, Montanyà J, Velde OA, Pineda N, Salvador A, Romero D, Aranguren D, Taborda J (2019) Charge structure of two tropical thunderstorms in Colombia. J Geophys Res: Atmos 124(10):5503–5515. https://doi.org/10.1029/2018JD029188

Maiorana C, Marisaldi M, Füllekrug M, Soula S, Lapierre J, Mezentsev A, Skeie CA, Heumesser M, Chanrion O, Østgaard N, Neubert T, Reglero V (2021) Observation of terrestrial gamma-ray flashes at mid latitude. J Geophys Res Atmos 126:2020–034432. https://doi.org/10.1029/2020JD034432

Maiorana C, Marisaldi M, Lindanger A, Østgaard N, Ursi A, Sarria D, Galli M, Labanti C, Tavani M, Pittori C, Verrecchia F (2020) The 3rd AGILE terrestrial gamma-ray flashes catalog. Part II: optimized selection criteria and characteristics of the new sample. J Geophys Res Atmos 125:2019–031986. https://doi.org/10.1029/2019JD031986

Malagón-Romero A, Teunissen J, Stenbaek-Nielsen HC, McHarg MG, Ebert U, Luque A (2020) On the emergence mechanism of carrot sprites. Geophys Res Lett 47:2019–085776. https://doi.org/10.1029/2019GL085776

Malla H, Martinez A, Ebert U, Teunissen J (2023) Double-pulse streamer simulations for varying interpulse times in air. Plasma Sour Sci Technol 32(9):095006. https://doi.org/10.1088/1361-6595/acf60e

Marais EA, Jacob DJ, Choi S, Joiner J, Belmonte-Rivas M, Cohen RC, Beirle S, Murray LT, Schiferl LD, Shah V et al (2018) Nitrogen oxides in the global upper troposphere: interpreting cloud-sliced NO_2 observations from the OMI satellite instrument. Atmos Chem Phys 18(23):17017–17027. https://doi.org/10.5194/acp-18-17017-2018

Marisaldi M et al (2024) Highly dynamic gamma-ray emissions are common in tropical thunderclouds. Nature 634:57–60. https://doi.org/10.1038/s41586-024-07936-6

...Marisaldi M, Argan A, Ursi A, Gjesteland T, Fuschino F, Labanti C, Galli M, Tavani M, Pittori C, Verrecchia F, D'Amico F, Østgaard N, Mereghetti S, Campana R, Cattaneo PW, Bulgarelli A, Colafrancesco S, Dietrich S, Longo F, Gianotti F, Giommi P, Rappoldi A, Trifoglio M, Trois A (2015) Enhanced detection of terrestrial gamma-ray flashes by AGILE. Geophys Res Lett 42(21):9481–9487. https://doi.org/10.1002/2015GL066100

Marisaldi M, Fuschino F, Labanti C, Galli M, Longo F, Del Monte E (2010) Detection of terrestrial gamma ray flashes up to 40 MeV by the AGILE satellite. J Geophys Res 115:00–13. https://doi.org/10.1029/2009JA014502

Marshall TC, McCarthy MP, Rust WD (1995) Electric field magnitudes and lightning initiation in thunderstorms. J Geophys Res 100:7097–7103. https://doi.org/10.1029/95JD00020

Marshall RA, Silva CL, Pasko VP (2015) Elve doublets and compact intracloud discharges. Geophys Res Lett 42:6112–6119. https://doi.org/10.1002/2015GL064862

Marshall TC, Stolzenburg M, Maggio CR, Coleman LM, Krehbiel PR, Hamlin T, Thomas RJ, Rison W (2005) Observed electric fields associated with lightning initiation. Geophys Res Lett 32:03813. https://doi.org/10.1029/2004GL021802

Masson-Delmotte V et al. (2021) IPCC, 2021: Climate Change 2021: The Physical Science Basis. Contribution of Working Group I to the Sixth Assessment Report of the Intergovernmental Panel on Climate Change. Technical Report Cambridge University Press, Cambridge, United Kingdom and New York, NY, USA. https://doi.org/10.1017/9781009157896

Mazur V, Fisher BD, Gerlach JC (1984) Lightning strikes to an airplane in a thunderstorm. J Aircraft 21:607. https://doi.org/10.2514/3.45030

McCarthy MP, Parks GK (1992) On the modulation of X ray fluxes in thunderstorms. J Geophys Res 97:5857–5864. https://doi.org/10.1029/91JD03160

Meek JMA (1940) A theory of spark discharge. Phys Rev 57:722–728. https://doi.org/10.1103/PhysRev.57.722

Mezentsev A, Füllekrug M (2013) Mapping the radio sky with an interferometric network of low-frequency radio receivers. J Geophys Res: Atmos 118(15):8390–8398. https://doi.org/10.1002/jgrd.50671

Miller SL (1953) A production of amino acids under possible primitive earth conditions. Science 117:528–529. https://doi.org/10.1126/science.117.3046.528

Miller SL (1955) Production of some organic compounds under possible primitive earth conditions. Am Chem Soc 77:2351–2361. https://doi.org/10.1021/ja01614a001

Mirpour S, Martinez A, Teunissen J, Ebeert U, Nijdam S (2020) Distribution of inception times in repetitive pulsed discharges in synthetic air. Plasma Sour Sci Technol 29:115010. https://doi.org/10.1088/1361-6595/abb614

Mirpour S, Nijdam S (2022) Experimental investigation on streamer inception from artificial hydrometeors. Plasma Sour Sci Technol 31(10):105009. https://doi.org/10.1088/1361-6595/ac95be
Montanyà J, Fabró F, Velde O, Romero D, Solà G, Hermoso JR, Soula S, Williams ER, Pineda N (2014) Registration of X-rays at 2500 m altitude in association with lightning flashes and thunderstorms. J Geophys Res: Atmos 119(3):1492–1503. https://doi.org/10.1002/2013JD021011
Montanyà J, López JA, Morales Rodriguez CA, Velde OA, Fabró F, Pineda N, Navarro-González J, Reglero V, Neubert T, Chanrion O et al (2021) A simultaneous observation of lightning by ASIM, Colombia-lightning mapping array, GLM, and ISS-LIS. J Geophys Res: Atmos 126(6):2020–033735. https://doi.org/10.1029/2020JD033735
Montanyá J, Velde O, Williams ER (2014) Lightning discharges produced by wind turbines. J Geophys Res Atmos 119:1455–1462. https://doi.org/10.1002/2013JD020225
Montijn C, Ebert U (2006) Diffusion correction to the Raether-Meek criterion for the avalanche-to-streamer transition. J Phys D Appl Phys 39(14):2979. https://doi.org/10.1088/0022-3727/39/14/017
Morgan D, Hardwick CJ, Haigh SJ, Meakins AJ (2012) The interaction of lightning with aircraft and the challenges of lightning testing. J Aerospace Lab AL05–10:1–20
Murray LT (2016) Lightning NOx and impacts on air quality. Curr Pollut Rep 2:115–133. https://doi.org/10.1007/s40726-016-0031-7
Neubert T (2003) On sprites and their exotic kin. Science 300:747–749. https://doi.org/10.1126/science.1083006
Neubert T et al (2019) The ASIM mission on the international space station. Space Sci Rev 215:26. https://doi.org/10.1007/s11214-019-0592-z
Neubert T, Chanrion O, Heumesser M, Dimitriadou K, Husbjerg L, Rasmussen IL, Østgaard N, Reglero V (2021) Observation of the onset of a blue jet into the stratosphere. Nature 589:371–375. https://doi.org/10.1038/s41586-020-03122-6
Neubert T, Østgaard N, Reglero V, Chanrion O, Heumesser M, Dimitriadou K, Christiansen F, Budtz-Jørgensen C, Kuvvetli I, Rasmussen IL, Mezentsev A, Marisaldi M, Ullaland K, Genov G, Yang S, Kochkin P, Navarro-Gonzalez J, Connell PH, Eyles CJ (2020) A terrestrial gamma-ray flash and ionospheric ultraviolet emissions powered by lightning. Science 367:183–186. https://doi.org/10.1126/science.aax3872
Nijdam S, Takahashi E, Markosyan A, Ebert U (2014) Investigation of positive streamers by double pulse experiments, effects of repetition rate and gas mixture. Plasma Sour Sci T 23:025008. https://doi.org/10.1088/0963-0252/23/2/025008
Nijdam S, Teunissen J, Ebert U (2020) The physics of streamer discharge phenomena. Plasma Sour Sci Technol 29(10):103001. https://doi.org/10.1088/1361-6595/abaa05
Nijdam S, Wetering FMJH, Blanc R, Veldhuizen EM, Ebert U (2010) Probing photo-ionization: experiments on positive streamers in pure gases and mixtures. J Phys D: Appl Phys 43:145204. https://doi.org/10.1088/0022-3727/43/14/145204
Niknezhad M, Chanrion O, Holbøll J, Neubert T (2021) Dynamics of negative coronas in airflow. Plasma Sour Sci Technol 30:105001. https://doi.org/10.1088/1361-6595/ac24d2
Niknezhad M, Chanrion O, Holbøll J, Neubert T (2021) Underlying mechanism of the stagnation of positive streamers. Plasma Sour Sci Technol 30:115014. https://doi.org/10.1088/1361-6595/ac3214
Niknezhad M, Chanrion O, Köhn C, Holbøll J, Neubert T (2021) A three-dimensional model of streamer discharges in unsteady airflow. Plasma Sour Sci Technol 30:045012. https://doi.org/10.1088/1361-6595/abefa6
Ono R, Oda T (2008) Measurement of gas temperature and OH density in the afterglow of pulsed positive corona discharge. J Phys D: Appl Phys 41:035204. https://doi.org/10.1088/0022-3727/41/3/035204
Pan LL et al (2014) Thunderstorms enhance tropospheric ozone by wrapping and shedding stratospheric air. Geophys Res Lett 41:7785–7790. https://doi.org/10.1002/2014GL061921
Pancheshnyi SV, Starikovskiy AY (2004) Stagnation dynamics of a cathode-directed streamer discharge in air. Plasma Sour Sci Technol 13(3):1–5. https://doi.org/10.1088/0963-0252/13/3/B01
Parks GK, Mauk BH, Spiger R, Chin J (1981) X-ray enhancements detected during thunderstorm and lightning activities. Geophys Res Lett 8:1176–1179. https://doi.org/10.1029/GL008i011p01176
Passas-Varo M, Sánchez J, Kieu N, Sanchez-Blanco E, Gordillo-Vázquez FJ (2019) GALIUS: an ultrafast imaging spectrograph for the study of lightning. Appl Opt 58:8002–8006. https://doi.org/10.1364/ao.58.008002
Passas-Varo M, Gordillo-Vázquez FJ, Sánchez J, Kieu N (2022) Experimental radial profiles of early time ($< 4\ \mu$s) neutral and ion spectroscopic signatures in lightning-like discharges. J Geophys Res: Atmos 127(12): 2022–036553. https://doi.org/10.1029/2022JD036553

Pavlovich MJ, Chang H-W, Sakiyama Y, Clark DS, Graves DB (2013) Ozone correlates with antibacterial effects from indirect air dielectric barrier discharge treatment of water. J Phys D: Appl Phys 46:145202. https://doi.org/10.1088/0022-3727/46/14/145202

Pavlovich MJ, Clark DS, Graves DB (2014) Quantification of air plasma chemistry for surface disinfection. Plasma Sour Sci Technol 23:065036. https://doi.org/10.1088/0963-0252/23/6/065036

Peeters SA, Mirpour S, Köhn C, Nijdam S (2022) A model for positive Corona inception from charged ellipsoidal thundercloud hydrometeors. J Geophys Res: Atmos 127(6):2021–035505. https://doi.org/10.1029/2021JD035505

Peterson Koshak HW, Biazar A, Khan M, Wang L (2014) The NASA lightning nitrogen oxides model (LNOM): application to air quality modeling. Atmos Res 135–136:363–369. https://doi.org/10.1016/j.atmosres.2012.12.015

Peverell AG (2022) Sub-wavelength Radio Array Instrumentation and Analysis for Transmitter and Thunderstorm-related Signalss. PhD thesis, University of Bath, Department of Electronic and Electrical Engineering

Pickering KE, Bucsela E, Allen D, Ring A, Holzworth R, Krotkov N (2016) Estimates of lightning NO_x production based on OMI NO_2 observations over the Gulf of Mexico. J Geophys Res: Atmos 121(14):8668–8691. https://doi.org/10.1002/2015JD024179

Pizzuti A, Bennett A, Füllekrug M (2021) Long-term observations of Schumann resonances at Portishead (UK). Atmosphere 13(1):38. https://doi.org/10.3390/atmos13010038

Pizzuti A, Bennett A, Soula S, Amor SA, Mlynarczyk J, Füllekrug M, Pédeboy S (2022) On the relationship between lightning superbolts and TLEs in Northern Europe. Atmos Res 270:106047. https://doi.org/10.1016/j.atmosres.2022.106047

Pizzuti A, Wilkinson JM, Soula S, Mlynarczyk J, Kolmašová I, Ondřej S, Scovell R, Bennett A, Füllekrug M (2021) Signatures of large peak current lightning strokes during an unusually intense sprite-producing thunderstorm in southern England. Atmos Res 249:105357. https://doi.org/10.1016/j.atmosres.2020.105357

Price CG (2013) Lightning applications in weather and climate research. Surv Geophys 34:755–767. https://doi.org/10.1007/s10712-012-9218-7

Pérez-Invernón FJ, Gordillo-Vázquez FJ, Passas-Varo M, Neubert T, Chanrion O, Reglero V, Østgaard N (2022) Multispectral optical diagnostics of lightning from space. Remote Sens 14(9):2057. https://doi.org/10.3390/rs14092057

Pérez-Invernón FJ, Gordillo-Vázquez FJ, Velde O, Montanyá J, López Trujillo JA, Pineda N, Huntrieser H, Valks P, Loyola D, Seo S et al (2023) Lightning-produced nitrogen oxides per flash length obtained by using TROPOMI observations and the Ebro lightning mapping array. Geophys Res Lett 50(24):2023–104699. https://doi.org/10.1029/2023GL104699

Pérez-Invernón FJ, Huntrieser H, Erbertseder T, Loyola D, Valks P, Liu S, Allen DJ, Pickering KE, Bucsela EJ, Jöckel P et al (2022) Quantification of lightning-produced NO_x over the Pyrenees and the Ebro Valley by using different TROPOMI-NO_2 and cloud research products. Atmos Meas Tech Discuss 15:3329–3351. https://doi.org/10.5194/amt-15-3329-2022

Pérez-Invernón FJ, Luque A, Gordillo-Vázquez FJ (2016) Mesospheric optical signatures of possible lightning on Venus. J Geophys Res Space Phys 121:7026–7048. https://doi.org/10.1002/2016JA022886

Ray EA, Moore FL, Elkins JW, Rosenlof KH, Laube JC, Röckmann T, Marsh DR, Andrews AE (2017) Quantifcation of the SF_6 lifetime based on mesospheric loss measured in the stratospheric polar vortex. J Geophys Res Atmos 122:4626–4638. https://doi.org/10.1002/2016JD026198

Ray D, Ye P, Yu JC, Song C (2023) Recent progress in plasma-catalytic conversion of CO2 to chemicals and fuels. Catal Today 423:113973. https://doi.org/10.1016/j.cattod.2022.12.004

Renno NO, Wong A-S, Atreya SK, Pater I, Roos-Serote M (2003) Electrical discharges and broadband radio emission by Martian dust devils and dust storms. Geophys Res Lett 30:2140. https://doi.org/10.1029/2003GL017879

Rison W, Krehbiel PR, Stock MG, Edens HE, Shao X-M, Thomas RJ, Stanley MA, Zhang Y (2016) Observations of narrow bipolar events reveal how lightning is initiated in thunderstorms. Nat Comm 7:10721. https://doi.org/10.1038/ncomms10721

Rison W, Thomas RJ, Krehbiel PR, Hamlin T, Harlin J (1999) A GPS-based three-dimensional lightning mapping system: Initial observations in central New Mexico. Geophys Res Lett 26:3573–3576. https://doi.org/10.1029/1999GL010856

Rodriguez A, Stuhlmann R, Tjemkes S, Aminou DM, Stark H, Blythe P (2009) Meteosat Third Generation: mission and system concepts. Proceedings Volume 7453. Infrared spaceborne remote sensing and instrumentation XVII, San Diego, California, United States 7453:74530–17453010. https://doi.org/10.1117/12.824236

Romps DM, Seeley JT, Vollaro D, Molinari J (2014) Projected increase in lightning strikes in the United States due to global warming. Science 346:851–854. https://doi.org/10.1126/science.1259100

Salanave LE, Orville RE, Richards CN (1962) Slitless spectra of lightning in the region from 3850 to 6900 Angstroms. J Geophys Res 67(5):1877–1884. https://doi.org/10.1029/JZ067i005p01877

Sarafraz MM, Christo FC, Tran NN, Fulcheri L, Hessel V (2023) Conversion of greenhouse gases to synthetic fuel using a sustainable cyclic plasma process. Int J Hydrog Energy 48(16):6174–6191. https://doi.org/10.1016/j.ijhydene.2022.05.272

Sarajcev P, Meglic A, Goic R (2021) Lightning overvoltage protection of step-up transformer inside a nacelle of onshore new-generation wind turbines. Energies 14:332. https://doi.org/10.3390/en14020322

Sarria D et al. (2023) Observation of Long and Intense sequences of Gamma-ray Glows during the 2023 ALOFT flight campaign. Presentation at the AGU Fall Meeting AE22A-05

Schumann U, Huntrieser H (2007) The global lightning-induced nitrogen oxides source. Atmos Chem Phys 7:3823–3907. https://doi.org/10.5194/acp-7-3823-2007

Sentman DD, Wescott EM, Osborne DL, Hampton DL, Heavner MJ (1995) Preliminary results from the Sprites94 aircraft campaign: 1. Red Sprites Geophys Res Lett 22:1205–1208. https://doi.org/10.1029/95GL00583

Shah GN et al (1985) Neutron generation in lightning bolts. Nature 313:773–775. https://doi.org/10.1038/313773a0

Skeie CA, Østgaard N, Mezentsev A, Bjørge-Engeland I, Marisaldi M, Lehtinen N, Reglero V, Neubert T (2024) The temporal relationship between terrestrial gamma-ray ashes and the associated optical pulses. J Geophys Res Atmos 127:2022–037128. https://doi.org/10.1029/2022JD037128

Smith DM, Hazelton BJ, Grefenstette BW, Dwyer JR, Holzworth RH, Lay EH (2010) Terrestrial gamma ray flashes correlated to storm phase and tropopause height. J Geophys Res 115:00–49. https://doi.org/10.1029/2009JA014853

Soler S, Pérez Invernón FJ, Gordillo Vázquez FJ, Luque A, Li D, Malagón Romero A (2020) Blue optical observations of narrow bipolar events by ASIM suggest corona streamer activity in thunderstorms. J Geophys Res Atmos 125:1–13. https://doi.org/10.1029/2020JD032708

Solomon S, Rosenlof KH, Portmann RW, Daniel JS, Davis SM, Sanford TJ, Plattner G-K (2010) Contributions of stratospheric water vapor to decadal changes in the rate of global warming. Science 327:1219–1223. https://doi.org/10.1126/science.1182488

Soloviev VR, Krivtsov VM (2009) Surface barrier discharge modelling for aerodynamic applications. J Phys D Appl Phys 42(12):125208. https://doi.org/10.1088/0022-3727/42/12/125208

Spizzi P (2018) TARANIS : Myriade small satellite for TLE observation, 8 instruments challenge. 32st Annual AIAA/USU Conference on Small Satellites, pp 18–01

Starikovskaia SM (2006) Plasma assisted ignition and combustion. J Phys D Appl Phys 39:265. https://doi.org/10.1016/j.pecs.2012.05.003

Starikovskiy AY, Aleksandrov NL, Shneider MN (2021) Simulation of decelerating streamers in inhomogeneous atmosphere with implications for runaway electron generation. J Appl Phys 129(6):063301. https://doi.org/10.1063/5.0037669

Stock MG, Akita M, Krehbiel PR, Rison W, Edens HE, Kawasaki Z, Stanley MA (2014) Continuous broadband digital interferometry of lightning using a generalized cross-correlation algorithm. J Geophys Res: Atmos 119(6):3134–3165. https://doi.org/10.1002/2013JD020217

Stoller PC, Seeger M, Iordanidis AA, Naidis GV (2013) CO_2 as an arc interruption medium in gas circuit breakers. IEEE Trans Plasma Sci 41:2359–2369. https://doi.org/10.1109/TPS.2013.2259183

...Tavani M, Barbiellini G, Argan A, Bulgarelli A, Caraveo P, Chen A, Cocco V, Costa E, de Paris G, Del Monte E, di Cocco G, Donnarumma I, Feroci M, Fiorini M, Froysland T, Fuschino F, Galli M, Gianotti F, Giuliani A, Evangelista Y, Labanti C, Lapshov I, Lazzarotto F, Lipari P, Longo F, Marisaldi M, Mastropietro M, Mauri F, Mereghetti S, Morelli E, Morselli A, Pacciani L, Pellizzoni A, Perotti F, Picozza P, Pontoni C, Porrovecchio G, Prest M, Pucella G, Rapisarda M, Rossi E, Rubini A, Soffitta P, Trifoglio M, Trois A, Vallazza E, Vercellone S, Zambra A, Zanello D, Giommi P, Antonelli A, Pittori C (2008) The AGILE space mission. Nucl Inst Methods Phys Res A 588:52–62. https://doi.org/10.1016/j.nima.2008.01.023. arXiv:0807.4254

Tavani M, Marisaldi M, Labanti C, Fuschino F, Argan A, Trois A et al (2011) Terrestrial gamma-ray flashes as powerful particle accelerators. Phys Rev Lett 106:018501. https://doi.org/10.1103/PhysRevLett.106.018501

Teixeira-Gomes MB, Gordillo-Vázquez FJ, Luque A (2023) Collective dynamics of a dense streamer front. Plasma Sour Sci Technol 32:095010. https://doi.org/10.1088/1361-6595/acf730

Teunissen J (2020) Improvements for drift-diffusion plasma fluid models with explicit time integration. Plasma Sour Sci Technol 29(1):015010. https://doi.org/10.1088/1361-6595/ab6757

Teunissen J, Ebert U (2017) Simulating streamer discharges in 3D with the parallel adaptive afivo framework. J Phys D Appl Phys 50(47):474001. https://doi.org/10.1088/1361-6463/aa8faf
Teunissen J, Ebert U (2018) Afivo: a framework for quadtree/octree AMR with shared-memory parallelization and geometric multigrid methods. Comput Phys Commun. https://doi.org/10.1016/j.cpc.2018.06.018
Trichel GW (1938) The mechanism of the negative point to plane corona near onset. Phys Rev 54:1078–1084. https://doi.org/10.1103/PhysRev.54.1078
Urbani M, Montanyá J, Arcanjo M, López J (2022) Multi-stroke positive cloud-to-ground lightning sharing the same channel observed with a VHF broadband interferometer. Geophys Res Lett 49(9):2021–097272. https://doi.org/10.1029/2021GL097272
Urbani M, Montanyá J, Velde OA, López JA, Arcanjo M, Fontanes P, Romero D, Roncancio JA (2021) High-energy radiation from natural lightning observed in coincidence with a VHF broadband interferometer. J Geophys Res Atmos 126:2020–033745. https://doi.org/10.1029/2020JD033745
Vadikkeettil Y, Subramaniam Y, Murugan R, Ananthapadmanabhan PV, Mostaghimi J, Pershin L, Batiot-Dupeyrat C, Kobayashi Y (2022) Plasma assisted decomposition and reforming of greenhouse gases: a review of current status and emerging trends. Renew Sustain Energy Rev 161:112343. https://doi.org/10.1016/j.rser.2022.112343
Vasavada AR, Showman AP (2005) Jovian atmospheric dynamics: an update after Galileo and Cassini. Rep Prog Phys 68:1935–1996. https://doi.org/10.1088/0034-4885/68/8/R06
Vaughan OH, Vonnegut B (1989) Recent observations of lightning discharges from the top of a thundercloud into the clear air above. J Geophys Res 94:13179–13182. https://doi.org/10.1029/JD094iD11p13179
Velde OA, Montanyá J (2016) Statistics and variability of the altitude of elves. Geophys Res Lett 43:5467–5474. https://doi.org/10.1002/2016GL068719
Vogel S, Holbøll J (2018) Experimental evaluation of discharge characteristics in inhomogeneous fields under air flow. IEEE Trans Dielectr Electr Insul 25(2):721–728. https://doi.org/10.1109/TDEI.2018.006987
Wada Y et al (2019) Gamma-ray glow preceding downward terrestrial gamma-ray flash. Comm Phys 2:67. https://doi.org/10.1038/s42005-019-0168-y
Wallace L (1960) Note on the spectrum of lightning in the region 3670 to 4280 A. J Geophys Res 65(4):1211–1214. https://doi.org/10.1029/JZ065i004p01211
Wang Z, Dijcks S, Guo Y, Van Der Leegte M, Sun A, Ebert U, Nijdam S, Teunissen J (2023) Quantitative modeling of streamer discharge branching in air. Plasma Sour Sci Technol 32(8):085007. https://doi.org/10.1088/1361-6595/ace9fa
Wang Z, Sun A, Dujko S, Ebert U, Teunissen J (2024) 3D simulations of positive streamers in air in a strong external magnetic field. Plasma Sour Sci Technol 33(2):025007. https://doi.org/10.1088/1361-6595/ad227f
Wang Z, Sun A, Teunissen J (2022) A comparison of particle and fluid models for positive streamer discharges in air. Plasma Sour Sci Technol 31(1):015012. https://doi.org/10.1088/1361-6595/ac417b
Wescott EM, Sentman DD, Osborne DL, Hampton DL, Heavner MJ (1995) Preliminary results from the Sprites94 aircraft campaign: 2. Blue Jets Geophys Res Lett 22:1209–1212. https://doi.org/10.1029/95GL00582
Williams ER (1985) Large-scale charge separation in thunderclouds. J Geophys Res: Atmos 90(D4):6013–6025. https://doi.org/10.1029/JD090iD04p06013
Wu T, Dong W, Zhang Y, Funaki T, Yoshida S, Morimoto T, Ushio T, Kawasaki Z (2012) Discharge height of lightning narrow bipolar events. J Geophys Res 117:05119. https://doi.org/10.1029/2011JD017054
Zalhaf AS, Mansour D-EA, YH, Yang P, Darwish MMF (2022) Numerical and experimental analysis of the transient behavior of wind turbines when two blades are simultaneously struck by lightning. IEEE Trans Instr Measur 71: 9001612. https://doi.org/10.1109/TIM.2021.3132076
Zhang X, Yin YAR, Lapierre JL, Chen Q, Kuang X, Yan S, Chen J, He C, Shi R (2020) Estimates of lightning NO_x production based on high-resolution OMI NO_2 retrievals over the continental US. Atmos Meas Tech 13(4):1709–1734. https://doi.org/10.5194/amt-13-1709-2020
Zheleznyak MB, Mnatsakanian AK, Sizykh SV (1982) Photoionization of nitrogen and oxygen mixtures from a gas discharge. High Temp 20:357–62
Østgaard N et al (2019) First 10 months of TGF observations by ASIM. J Geophys Res Atmos 124:14024–14036. https://doi.org/10.1029/2019JD031214
Østgaard N et al (2019) The modular X- and gamma-ray sensor (MXGS) of the ASIM payload on the international space station. Space Sci Rev 215:23. https://doi.org/10.1007/s11214-018-0573-7
Østgaard N et al (2021) Simultaneous observations of EIP, TGF, Elve and optical lightning. J Geophys Res Atmos 126:2020–033921. https://doi.org/10.1029/2020JD033921

Østgaard N et al (2024) Flickering gamma-ray flashes, the missing link between gamma glows and TGFs. Nature 634:53–56. https://doi.org/10.1038/s41586-024-07893-0
Østgaard N et al. (2023) Airborne Lightning Observatory for FEGS and TGFs (ALOFT)
Østgaard N et al. (2023) Results from the ALOFT mission: a flight campaign for TGF and gamma-ray glow observations over Central America and the Caribbean in July 2023. Presentation at the AGU Fall Meeting AE22A-03

Authors and Affiliations

Christoph Köhn[1] · Torsten Neubert[1] · Martin Füllekrug[2] · Ute Ebert[3,4] · Sander Nijdam[4] · Olivier Chanrion[1] · Nikolai Østgaard[5] · Martino Marisaldi[5] · Serge Soula[6] · Joan Montanyà[7] · Francisco Gordillo-Vázquez[8] · Alejandro Luque[8] · Jannis Teunissen[3] · Joachim Holbøll[9] · Alec Bennett[10] · Paul Smith[10] · Victor Lorenzo[11] · Hugh J. Christian[12] · Søren F. Madsen[13] · Diana Mihailova[14] · Jean-François Boissin[15] · Stéphane Pedeboy[16] · Laure Chaumat[17] · Matthias Heumesser[1] · Krystallia Dimitriadou[1,18] · Carolina Maiorana[5] · Simon Ghilain[2] · Zaida Gomez Kuri[6] · Adam Peverell[2] · Michele Urbani[7,11] · Thi Ny Kieu[8,20] · Andy Martinez[3] · Hani Francisco[3] · Mojtaba Niknezhad[1] · Miguel B. Teixeira-Gomes[8] · Andrea Pizzuti[2,10] · Marcelo Arcanjo[11] · Shahriar Mirpour[4] · Xue Bai[2] · Victor Reglero[19]

✉ Christoph Köhn
koehn@space.dtu.dk

[1] National Space Institute (DTU Space), Technical University of Denmark, Kgs. Lyngby 2800, Denmark

[2] Centre for Space, Atmospheric and Oceanic Science, Department of Electronic and Electrical Engineering, University of Bath, Bath BA27AY, United Kingdom

[3] Multiscale Dynamics Group, Centrum Wiskunde & Informatica (CWI), 1098XG Amsterdam, The Netherlands

[4] Department of Applied Physics, Eindhoven University of Technology, 5612AZ Eindhoven, The Netherlands

[5] Birkeland Centre for Space Science, University of Bergen, 5007 Bergen, Norway

[6] Laboratoire d'Aérologie, University of Toulouse, 31062 Toulouse, France

[7] Electrical Engineering Department, Polytechnic University of Catalonia, 08034 Barcelona, Spain

[8] Instituto Astrofísica de Andalusía, CSIC, 18006 Granada, Spain

[9] DTU Elektro, Technical University of Denmark, Kgs. Lyngby 2800, Denmark

[10] Bristol Industrial and Research Associates Limited (Biral), Bristol BS20 7BL, United Kingdom

[11] Dena Desarrollos S.L. (Ingesco), 08223 Terrassa, Spain

[12] Department of Atmospheric Science, Earth System Science Center, University of Alabama, Huntsville, Alabama 35899, USA

[13] Polytec, 6740 Bramming, Denmark

[14] Plasma Matters, 5612AJ Eindhoven, The Netherlands

[15] AIRBUS, 31700 Blagnac, France

[16] Météorage, 640000 Pau, France

[17] Thales Services SAS, 31100 Toulouse, France

[18] DTU Wind and Energy Systems, Technical University of Denmark, Roskilde 4000, Denmark

[19] Image Processing Laboratory, University of Valencia, 46980 Valencia, Spain

[20] Department of Physics, Loyola University Chicago, IL 60660, Chicago, USA